Since January 2020 Elsevier has created a COVID-19 resource centre with free information in English and Mandarin on the novel coronavirus COVID-19. The COVID-19 resource centre is hosted on Elsevier Connect, the company's public news and information website.

Journal of Molecular Liquids 320 (2020) 114427

Contents lists available at ScienceDirect

Journal of Molecular Liquids

journal homepage: www.elsevier.com/locate/molliq

Review

The recent advancement of low-dimensional nanostructured materials for drug delivery and drug sensing application: A brief review

Hamidur Rahman [a], Md. Rakib Hossain [b,*], Tahmina Ferdous [a]

[a] Department of Physics, Jahangirnagar University, Savar, Dhaka 1342, Bangladesh
[b] Department of Physics, Bangabandhu Sheikh Mujibur Rahman Science and Technology University, Gopalganj 8100, Bangladesh

ARTICLE INFO

Article history:
Received 26 July 2020
Received in revised form 17 September 2020
Accepted 23 September 2020
Available online 30 September 2020

Keywords:
Drug delivery
Drug sensing
Review
Graphene
Boron nitride
DFT

ABSTRACT

In this review article, we have presented a detailed analysis of the recent advancement of quantum mechanical calculations in the applications of the low-dimensional nanomaterials (LDNs) into biomedical fields like biosensors and drug delivery systems development. Biosensors play an essential role for many communities, e.g. law enforcing agencies to sense illicit drugs, medical communities to remove overdosed medications from the human and animal body etc. Besides, drug delivery systems are theoretically being proposed for many years and experimentally found to deliver the drug to the targeted sites by reducing the harmful side effects significantly. In current COVID-19 pandemic, biosensors can play significant roles, e.g. to remove experimental drugs during the human trials if they show any unwanted adverse effect etc. where the drug delivery systems can be potentially applied to reduce the side effects. But before proceeding to these noble and expensive translational research works, advanced theoretical calculations can provide the possible outcomes with considerable accuracy. Hence in this review article, we have analyzed how theoretical calculations can be used to investigate LDNs as potential biosensor devices or drug delivery systems. We have also made a very brief discussion on the properties of biosensors or drug delivery systems which should be investigated for the biomedical applications and how to calculate them theoretically. Finally, we have made a detailed analysis of a large number of recently published research works where theoretical calculations were used to propose different LDNs for bio-sensing and drug delivery applications.

Contents

1. Introduction . . . 2
2. Basic properties investigated for drug delivery and sensing study . . . 4
   2.1. Structural properties . . . 4
      2.1.1. Geometry optimization . . . 4
      2.1.2. IR spectroscopy and imaginary frequencies . . . 4
      2.1.3. Cohesive energy . . . 5
   2.2. Spectroscopic properties . . . 6
      2.2.1. UV–vis spectroscopy . . . 6
      2.2.2. NMR spectroscopy . . . 6
   2.3. Adsorption properties analysis . . . 6
      2.3.1. Adsorption energy . . . 6
      2.3.2. Adsorbate-adsorbent distance . . . 6
   2.4. Thermodynamical parameter analysis . . . 6
      2.4.1. Change in Gibbs free energy . . . 6
      2.4.2. Change in enthalpy . . . 6
      2.4.3. Change in entropy . . . 7

* Corresponding author.
E-mail address: rakibphy_r@bsmrstu.edu.bd (M.R. Hossain).

https://doi.org/10.1016/j.molliq.2020.114427
0167-7322/

2.5. Frontier molecular orbitals analysis . . . 7
2.5.1. HOMO and LUMO energy . . . 7
2.5.2. Density of States (DOS) Spectrum. . . . 7
2.5.3. Fermi level energy and work function . . . 7
2.6. Global reactivity parameters . . . 7
2.6.1. Global hardness. . . . 7
2.6.2. Global softness . . . 7
2.6.3. Chemical potential . . . 7
2.6.4. Electrophilicity . . . 7
2.6.5. Electronegativity . . . 7
2.7. Charge transfer analysis . . . 7
2.7.1. NBO and Mulliken charge transfer . . . 7
2.7.2. AIM analysis . . . 8
2.7.3. Molecular electrostatic potential . . . 8
2.7.4. Change in fractional charge . . . 8
2.7.5. Dipole moment . . . 8
2.8. Effect of solvents . . . 8
2.8.1. Solvation energy . . . 8
2.9. Drug release mechanism . . . 8
2.9.1. Recovery time . . . 8
3. Carbon-based LDNs for drug delivery and sensing applications . . . 8
3.1. Graphene and functionalized graphene nanosheet . . . 8
3.2. Single and multi-walled carbon nanotube . . . 11
3.3. Carbon fullerene . . . 14
3.4. Miscellaneous carbon-based LDNs for drug delivery and sensing applications . . . 16
3.4.1. Graphene oxide . . . 16
3.4.2. Graphyne and graphdiyne . . . 17
3.4.3. BC_3 and BCN . . . 17
4. Boron-based LDNs for drug delivery and sensing applications . . . 17
4.1. Hexagonal boron nitride nanosheet . . . 17
4.2. Boron nitride nanotube . . . 19
4.3. Boron nitride nanocage . . . 20
4.4. Quasi-planar boron nanoclusters . . . 22
5. Miscellaneous LDNs for drug delivery and sensing applications . . . 24
5.1. Metal oxide nanostructures . . . 24
5.2. Al and Ga nitride nanostructures . . . 24
5.3. Gold and silver nanoparticles . . . 25
5.4. Phosphorene nanosheet . . . 26
6. Conclusion . . . 27
CRediT authorship contribution statement . . . 27
Declaration of competing interest. . . . 27
Acknowledgment . . . 27
References . . . 27

1. Introduction

From the 1959 lecture, “There's Plenty of Room at the Bottom”, by the Nobel laureate Richard Feynman [1] to the 1985's first experimental discovery of the C_{60} buckminsterfullerene lead by another Nobel laureate Harry Kroto [2], 21st-century communities have observed unstoppable integrity of nanomaterials with daily life in the last few decades. The extensive applications of nanomaterials include in almost all major scientific and commercial fields including semiconductor technologies [3–7], energy storage device [8–12], biological research [13–19], aerospace industries [20–22], constructions [23–26], foods [27–29], textiles [30–32], cosmetics [33–35] etc. These wide ranges of applications were made possible due to the availability of many different kinds of nanomaterials with various novel properties. For example, while the single layer of a two-dimensional (2D) hexagonal network of carbon atoms, graphene [36], and its allotrope carbon nanotube (CNT) [37] are some of the hardest materials known so far with an elastic modulus in terapascal (TPa) range, another hexagonal 2D nanosheet of boron and nitrogen atoms, hexagonal boron nitride (BN) and it's allotrope boron nitride nanotubes (BNNT) doesn't exhibit as much mechanical strength as graphene and CNT. But while graphene performs as a zero bandgap semiconductor, BN works as a wide bandgap semiconductor with a bandgap ~5.5 eV which enables it showing more superior optical properties and thermal stabilities than that of the graphene [38]. Besides these nanomaterials with boron and carbon atoms, there is a wide range of promising 2D nanomaterials were proposed or synthesized like silicene [39], phosphorene [40], germanene [41], stanene [42] etc. Despite, these alluring properties and applications of nanomaterials, over the years, nanomaterials were claimed to have toxicity and detrimental effects on nature, along with the fast-growing applications which induce a possibility of outweighing its benefit to the harmful effects [43,44]. However, many individual research groups [45] and government officials [46] then came with the necessary policy on the usages of nanomaterials to limit its harmful effects on the environment. In addition to that the biocompatibility of the nanomaterials became a great concern for the scientist to apply these novel nanomaterials into the biomedical applications. Interestingly, most of the low-dimensional nanomaterials (LDNs) including Graphene [47], CNTs [48,49], carbon fullerenes [50], Borophene [51], boron nanotube [52], boron fullerenes etc. were experimentally reported to have biocompatibility hence is safe to be used to develop biosensors and drug or vaccine delivery.

The application of the biosensors is increasing day by day in the various communities with many different purposes. For example, it is crucial to detect illicit drugs for the law enforcement agency whereas medical communities need drug sensors to detect and remove an

overdose of a drug (as it is shown in Fig. 1) which may lead to a deadly threat. While these drugs or biomolecules can be detected using many laboratory techniques including chromatography, mass spectroscopy, infrared (IR) and Fourier-transformed IR (FT-IR) spectroscopy etc., for a fast response and mass applications electrochemical sensors play a vital role. An electrochemical sensor usually converts the data of a physical reaction between the biomolecule and the sensor surface into a detectable electronic signal as it is displayed in the Fig. 2 [53]. Basically, most of these electrochemical sensors are consists of a receptor where the interaction of the biomolecules takes place and a transducer which converts these data into electrochemical signal and finally, an amplifier to amplify the signal into a detectable one. Over the last few decades, LDNs, especially 2D nanomaterials, received immense attention to the scientific community for electrochemical drug sensors as they offer many advantages in the field of drug sensing and four most important of them were pointed out by R. Boroujerdi et al. [54]. Firstly, as 2D nanomaterials are a single layer of atoms known as nanosheets, in these nanosheets electrons are allowed to flow more freely than 3D structures without any inter-layer interaction of electrons which increase the sensitivity of these 2D nanomaterials towards the drugs. Secondly, as we have seen in case of the graphene, 2D nanomaterials are some of the hardest known materials with an excellent mechanical strength which allows them to develop some of the most enduring sensors. Thirdly, the optical transparency of the 2D nanomaterials enables them to develop transparent and flexible wearable optical sensors. Finally, the negligible thickness of the 2D nanomaterials lead them to a very high surface to weight ratio than any other bulk materials, and this specific property of 2D nanomaterials helps them to interact with the drug with a greater surface area with greater sensitivity. Application of these fascinating properties of 2D nanomaterials was observed in many research works, including a recent investigation on the detection of nucleic acids and several other biomolecules by M. T. Hwang et al. [55]. It was found that the nucleic acids and other biomolecules with a structure in millimetre range showed an ultra-sensitivity towards the field-effect transistor coated with a monolayer of deformed graphene by increasing the local conductivity noticeably. Besides, core-shell nanoparticles incorporated boron nitride nanosheets (BNNS) were used to develop a sensor for the etoposide anticancer drug by A. Özkan et al. which showed very high sensitivity with the detection limit (LOD) of 0.00025 ng/mL whereas the linearity range was observed as 0.001–1.00 ng/mL [56]. The sensor was also highly reusable with the recovery percentage ranging as 99.30%–100.72% with a relative standard deviation <1.00. W. Zhang et al. also fabricated a biosensor based on graphene film to detect microcystin-LR which showed a very low LOD of 2.3 ng/L and it is much lower than 1 μg/L which was the limit of microcystin-LR in water sources stated in the provisional guidelines by the World Health Organization [57]. These three research works from the last three years are just some of many more recent research works done with LDNs in the search for a biosensor.

Besides the application of LDNs as drug and biomolecule sensors, their biocompatibility leads them to another crucial biomedical use, drug delivery systems. The drug delivery systems play an essential role in the pharmaceutical field by reducing the severe adverse effects of the various drug, especially chemotherapeutic anticancer drugs, by delivering the drugs to the targeted cell area. Earlier in 2020, Xibo Pei and his co-workers used polyethylene glycol attached graphene oxide (pGO) nanosheet as a dual-drug delivery system for antitumor drugs cisplatin (Pt) and doxorubicin (DOX) [58]. In vivo data from their work confirmed that compared to the toxicity of free Pt and DOX drugs itself, pGO-Pt/DOX dual-drug delivery system displayed a significantly reduced toxicity. Also, in vitro data from their study confirmed most prominent cell apoptosis and necrosis for pGO-Pt/DOX system compared to the free drugs and showed a higher growth inhibition property. The graphene and GO nanosheets were further used as a drug delivery system for many other anticancer drugs including β-lapachone [59], fluorouracil [60], camptothecin [61] etc. and many other biological drugs including plasmid DNA [62–64], siRNA [65–67], proteins [68–70] etc. Other than the graphene nanosheets (GNS), E. Czarniewska and his team found that the OH functionalized BN (BN-OH-n) nanosheets showed very low cytotoxicity in both in vivo and in vitro hence BNNSs can be applied in the platform like bio-imaging and drug delivery [71]. Furthermore, hollow BN spheres with anticancer drug paclitaxel were observed to suppress the tumour growth significantly with an increased prostate cancer cell apoptosis and decreasing cell viability [72]. Another allotrope of BN, BNNT functionalized with mesoporous silica was also found to perform as a potential drug delivery system for another anticancer drug DOX to treat prostate cancer by increasing cancer cell killing ability [73]. Other than these GNS and BN allotropes, other nanomaterials, e.g. metal-organic frameworks [74], phosphorene [75], gold nanoparticle [76] etc. displayed their ability to carry many drugs by reducing adverse effects with lower cytotoxicity.

While investigating the capability of a nanomaterial to perform as a biosensor or drug delivery system using experimental instrumentation provides with a reliable result, it often comes with the high cost and should be executed with a very low risk of failure. Hence to minimize the risk, before proceeding to these expensive experiments, a cost-effective and less time-consuming solution can be a theoretical investigation on the desired properties of the materials through computer

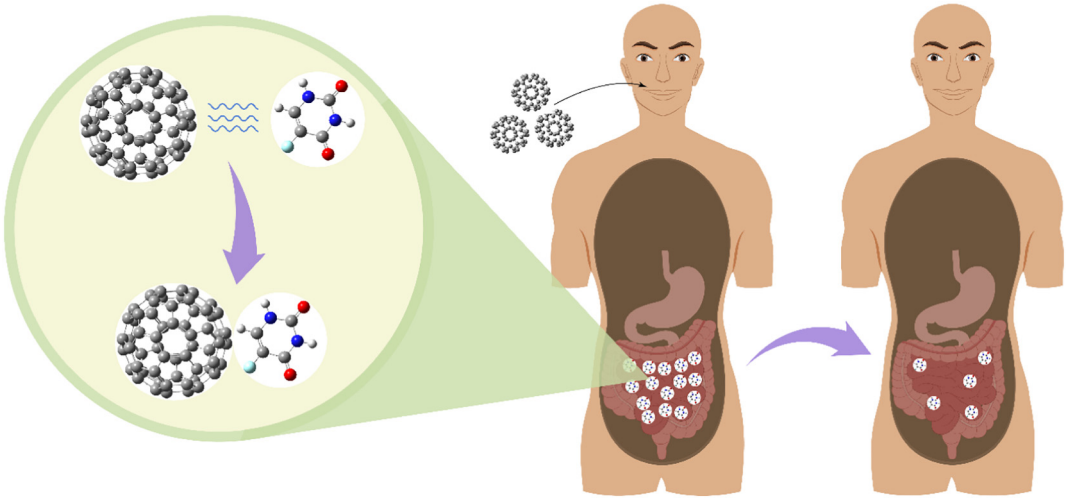

Fig. 1. Application of nanomaterials as a drug sensor to remove the drug from the human body which causes side effects.

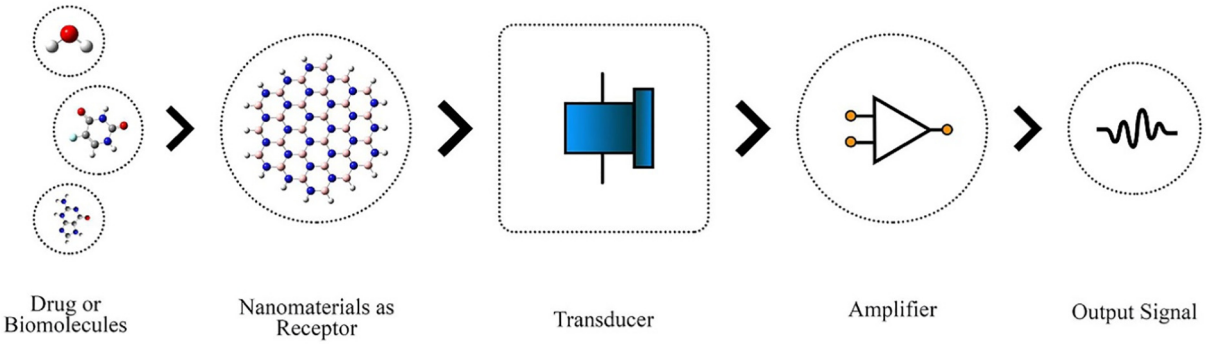

Fig. 2. Basic working methods of a simple electrochemical biosensor device.

simulations. From Shrodinger equation to describe a quantum mechanical system, theoretical calculations evolved dramatically with a lot of advanced theory like Molecular Dynamics (MD), Density Functional Theory (DFT) etc. to describe the properties of a system from quantum mechanical scale with more accuracy. Hence, first-principles calculations became more reliable over the years on predicting various properties of a material with a close resemblance to the experimental outcome. Besides, with a fast calculation power of the modern computers, first-principles calculations based computer simulations which also provides a facility to investigate a lot of quantum mechanical information about the system, got a more convincing solution for many researchers to investigate their proposed systems, including biological systems, theoretically at the first place. For example, on the investigation of in vitro antileishmanial activity of azo-benzene functionalized conventional conducting polymers, Neetika Singh and his research group observed that the theoretical calculations predicted different vibrational nodes of various bondings of the polymers with a deviation of <1% from the experimental result, e.g. the vibrational spectrum peak for N═N stretching of benzene diazonium salt was observed as 2434 cm^{-1} experimentally while it was found as 2416 cm^{-1} theoretically using DFT-B3LYP/6–311G level of theory with a deviation of only 0.74% and the similar kind of result was observed for all other vibrational modes of benzene diazonium salt, poly (aniline-azobenzene), poly(1-naphthylamine-azobenzene), poly (luminol-azobenzene), and poly (*o*-phenylenediamine-azobenzene) [78]. The resemblance of the FT-IR spectrum, predicted by DFT/B3LYP theory, with the experimental observation, was also followed by several copper complexes which were investigated for their potential anticancer activity [79]. In another study, A. D. Bani-Yaseen et al. observed that DFT-B3LYP/6-31 + G(d) level of theory predicted the UV–Vis spectrum peak with just a 10 nm deviation from the experimental observation for another azo-bonded prodrug sulfasalazine (SSZ) in water medium which is shown in Fig. 4 [77]. The theory has also predicted the precise nature of the molecular orbitals involved in the interaction between the SSZ and the medium. However, DFT theory with mPW1PW91 functional showed more close correspondence to the experimental data than B3LYP functional in case of the chemical shifts for colchicine in chloroform and DMSO investigated by the high field NMR spectroscopy [80]. Hence it is crucial to choose the functionals and basis sets selectively, in case of the first-principles calculations through a computer simulation package. Besides spectroscopic resemblance, DFT theory also predicted the reactivity and reaction mechanism successfully with accordance to the experimental observations [81]. The DFT theory was also applied by M. Darvish Ganji et al. to observe the drug release mechanism using CNT [82]. Furthermore, they have also observed the interaction energy of −12.88 kcal/mol in case of the interaction of benzene molecules with the graphene surface where it was observed as −13.6 kcal/mol experimentally. Due to these conveniences with the experimental results, first-principles calculations hold a potential application to explore various biosensor devices and drug delivery systems at the first place in a short time with a reduced cost (Fig. 3).

Finally, considering a significant increase in the drug adsorption related work in the last 30 years from Fig. 5, herein we have made a comprehensive review on the recent advancement of first-principles calculation on the applications of LDNs in the biomedical fields including drug sensors and drug delivery. We have analyzed the properties which can be investigated through the first-principles calculations and application of those properties in search for promising drug sensors and drug delivery systems for different kind of drugs, especially the anticancer drugs. Furthermore, we have explored the adverse effects of the drugs and several specific properties of the nanostructures, which provides it with an advantage to perform as a drug sensor or delivery system. Finally, we have analyzed a wide range of research works that were reported in the last few years searching for promising drug sensors or delivery systems using first-principles calculations.

2. Basic properties investigated for drug delivery and sensing study

The quantum mechanical calculations through many available computer simulation packages allow researchers to calculate a wide range of information to explore the potential application of the material in biomedical fields like drug sensor and drug delivery. In this section, we will make a brief discussion on the properties of the drug sensors and drug delivery systems which can be calculated theoretically using computer simulation packages.

2.1. Structural properties

2.1.1. Geometry optimization

The first thing first-principles calculations allows researchers is to optimize and relax their structures into the global minimum energy using many existing quantum mechanical theories like DFT, MD etc. with their respective exchange correlational functional basis sets. From the optimized geometry, it is possible to calculate the bond length and bond angle between the constituent atoms in the structures. These are essential parameters to investigate from which the interaction between the drug molecules and respective adsorbents can be confirmed, and their type of interactions can be identified.

2.1.2. IR spectroscopy and imaginary frequencies

The different vibrational mode of the constituting atoms of a material can be observed through the IR spectroscopy. As it denotes every individual vibrational mode of a material, it is often used to identify the material hence works as a fingerprint of the material [83]. By investigating the imaginary frequencies in the IR spectrum, researchers also achieve the information about the stability of the structures and the possibility of finding them into nature or synthesizing them into the laboratory. If any imaginary frequency for a vibrational mode in the

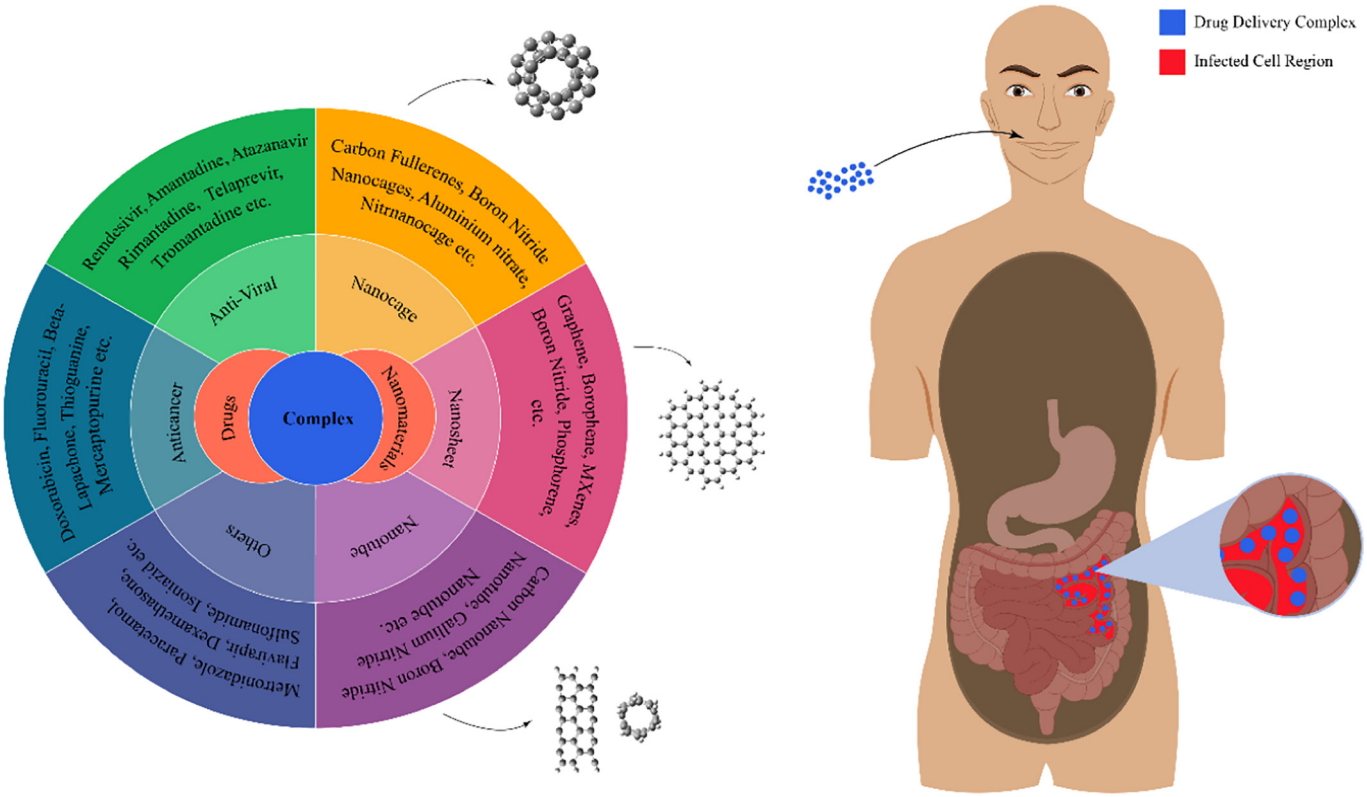

Fig. 3. Formation of a drug delivery complex to deliver the drug to a targeted infected region.

structure is observed from the theoretical calculations, there will be a minimal possibility to find that material into nature as the naturally existing materials can not possess any imaginary frequencies.

2.1.3. Cohesive energy

To investigate the structural stability of a nanostructure system, the cohesive energy (E_{Coh}) of nanostructures can be calculated as [84]:

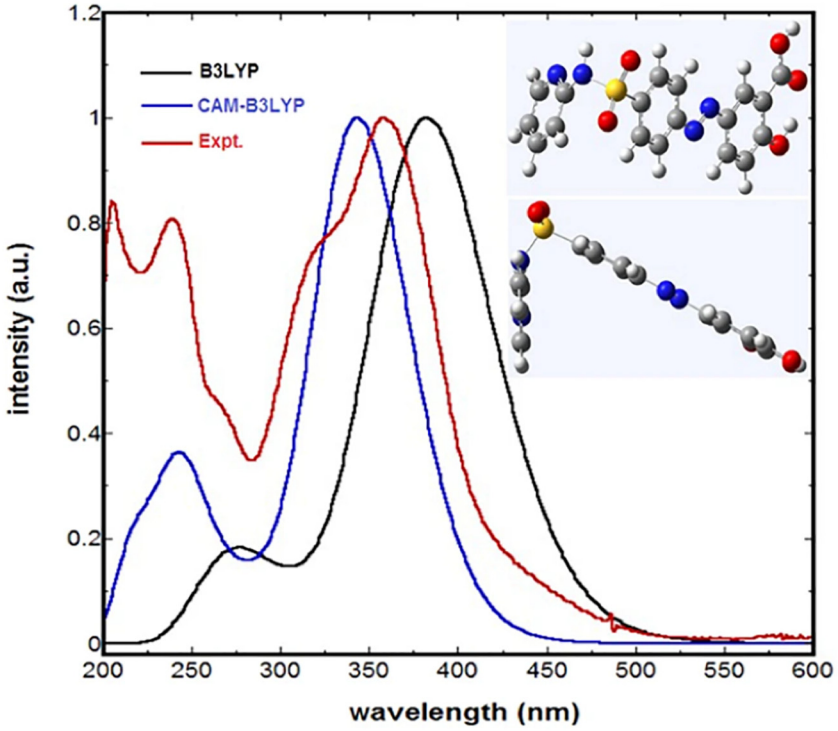

Fig. 4. Comparison between the normalized experimental and DFT simulated absorption spectra of SSZ in water. Reproduced with permission from ref. [77]. Copyright Springer Nature, 2019.

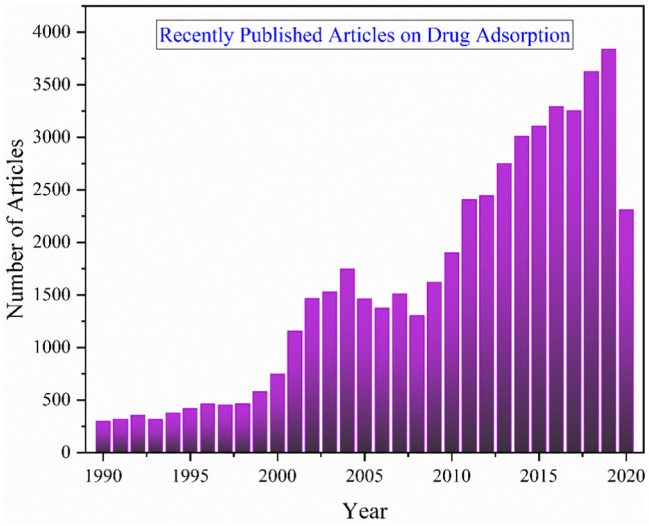

Fig. 5. Inclination of the drug adsorption related published works in the last 30 years. Data was obtained from Scopus with keyword search "Drug" in the title and "Adsorption" in the abstract.

$$E_{Coh} = \frac{1}{n}(E_{nanostructure} - xE_a - yE_b)$$

where n is the total number of constituent's atoms of the nanostructure, a and b represents the different constituent atoms of the nanostructure and E_a and E_b respectively represents their energies with x and y be the total number of them in the nanostructure.

2.2. Spectroscopic properties

2.2.1. UV–vis spectroscopy

UV–Vis spectrum usually provides researchers with information about the range of wavelength the material will absorb. The spectrum is also associated with the electronic bandgap of the material where a broader spectrum represents a wider bandgap of the material. Besides, it is also useful to investigate the interaction of a biomolecule or drugs with the adsorbent material as an introduction of the new energy states usually creates a noticeable change in the spectrum [85]. Furthermore, the right shift of the spectrum or simply redshift due to the drug adsorption indicates with a decrease in the bandgap with an increase in the conductivity of the sensor material and an enhanced sensitivity towards the drug molecule [86].

2.2.2. NMR spectroscopy

The nuclear magnetic resonance (NMR) usually allows researchers to investigate the magnetic field around an atomic nucleus. However, it is further applied extensively in structural biology to study the structure and dynamics of a biological sample. In drug sensing and drug delivery applications, NMR can also be used to investigate the chemical shift due to the interaction of an adsorbate molecule with an adsorbent [80].

2.3. Adsorption properties analysis

2.3.1. Adsorption energy

To investigate the adsorption process between the adsorbent and an adsorbate molecule, one of the most reliable and often used method is to examine the adsorption energy (E_{ads}) due to the adsorption which can be calculated as [87],

$$E_{ads} = E_{complex} - (E_{adsorbent} + E_{adsorbate})$$

where $E_{complex}$ represents the energy of adsorbate adsorbed adsorbent nanostructures and both $E_{adsorbent}$ and $E_{adsorbate}$ represents the isolated energy of the adsorbent and adsorbate, respectively.

Here a negative value for the adsorption energy represents a stable adsorption process, whereas the positive value for the adsorption energy represents no adsorption process. Besides, if the adsorption energy value is <1 eV, then the adsorption process is considered as weak physisorption, and no chemical interaction can be found between the adsorbate and adsorbent [88]. But if the adsorption energy exceeds 1 eV, then a strong chemical interaction is considered to have occurred between the adsorbate and adsorbent, and the adsorption process is then levelled as chemisorption. Hence, more negative the value of adsorption energy gets, more strongly the system is considered to be bounded, representing a higher stable system. So, for the drug delivery and drug sensor devices, the adsorption process between the drug molecules and adsorbents are expected to have a negative value for the adsorption energy where in case of drug delivery systems the adsorbent is required to make a strong interaction with the drug molecule. But in the drug sensor devices, weak physisorption is desired as the strong chemical interactions often lead to a higher recovery time which is not suitable for the drug sensor device.

2.3.2. Adsorbate-adsorbent distance

Several important information about the adsorption can also be found from the minimum distance between the adsorbate and adsorbent. A smaller distance between the adsorbate and absorbent often lead to a higher charge transfer between the adsorbent and the adsorbate molecules. Hence the sensitivity of the adsorbent materials towards the adsorbate molecules can be understood which plays an important role in a drug sensor device development [89]. Several studies also claimed that a smaller adsorbent-adsorbate distance leads to a stronger interaction between and provides them with higher stability [90].

2.4. Thermodynamical parameter analysis

2.4.1. Change in Gibbs free energy

To investigate the thermodynamical nature of the interaction, first-principles calculations allows calculating the change in the Gibbs free energy (ΔG) using [91],

$$\Delta G = G_{Complex} - (G_{adsorbent} + G_{adsorbate})$$

where G represents the sum of electronic and thermal free energies.

From the definition of the Gibbs free energy, a negative change in the Gibbs free energy represents a spontaneous interaction between the adsorbate molecule and adsorbent hence a negative change in desired in case of both drug delivery and drug sensor devices.

2.4.2. Change in enthalpy

The change in enthalpy (ΔH) can be calculated from [91],

$$\Delta H = H_{Complex} - (H_{adsorbent} + H_{adsorbate})$$

where H represents the sum of electronic and thermal enthalpies.

A positive change in the enthalpy labels the reaction between the adsorbent and adsorbate as an endothermic reaction, whereas the negative changes in the change of enthalpy lead to an exothermic reaction.

2.4.3. Change in entropy

Finally, the change in entropy (ΔS) can be calculated using,

$$\Delta S = \frac{\Delta H - \Delta G}{T}$$

where T is the considered temperature depending on the systems.

In most of the cases, the changes in entropy become negative due to the adsorption of a drug molecule by an adsorbent material which is because of the constrained movement of the structures due to their newly formed intermolecular bondings.

2.5. Frontier molecular orbitals analysis

2.5.1. HOMO and LUMO energy

The HOMO energy (E_{HOMO}) represents the energy state of the highest occupied molecular orbital (HOMO) whereas the LUMO energy (E_{LUMO}) stands for the energy state of the lowest unoccupied molecular orbital (LUMO). These are significant properties for a drug sensor or drug delivery systems as the difference between the HOMO and LUMO energy, which is often expressed as H-L energy gap (E_g), represents the conductive nature of the system where the conduction electron population (N) can be defined as [92],

$$N = AT^{\frac{3}{2}} \exp\left(\frac{-E_g}{2KT}\right)$$

where $E_g = E_{LUMO} - E_{HOMO}$.

Hence, by definition, a smaller H-L energy gap represents a higher conductivity which is desired for a drug sensor device. Therefore, to inspect the sensitivity of the adsorbent towards the adsorbate, change in the H-L energy gap due to the adsorption plays an important role. For a drug sensor, if the H-L energy gap decreases significantly due to the adsorption of the drug on the nanostructure, then the nanostructure is considered to be sensitive towards the drug. This increase in the conductivity produces a detectable electrochemical signal from which the adsorption process can be confirmed, and the drug can be detected.

2.5.2. Density of States (DOS) Spectrum

Besides just the HOMO and LUMO orbital, first-principles calculations allow investigating all possible states for a given energy range by allowing to calculate the DOS spectrum. Hence the H-L energy gap can also be investigated from the DOS spectrum. Another vital application of DOS spectrum for the drug sensor devices is that the interaction between the drug and the adsorbent can also be confirmed from the alteration of the DOS spectrum due to the adsorption of the drug molecule.

2.5.3. Fermi level energy and work function

The Fermi level energy (E_{FL}) of a nanostructure can be calculated as [93]:

$$E_{FL} = \frac{E_{HOMO} + E_{LUMO}}{2}$$

Besides, the negative value of the Fermi level energy represents the work function (φ) of a system. Mathematically [92],

$$\varphi = -E_{FL}$$

The work function is again connected with the current density (j) by the following formula [92],

$$j = AT^2 \exp\left(\frac{-\varphi}{KT}\right)$$

This introduces another type of work function based drug sensors which works based on the change in work function rather than the change in H-L energy gap.

2.6. Global reactivity parameters

2.6.1. Global hardness

The resistance of a structure towards the deformation can be investigated from the global chemical hardness (η), which can be calculated from [94]:

$$\eta = \frac{E_{LUMO} - E_{HOMO}}{2}$$

Hence, a higher value for the global hardness indicates higher chemical stability for the structure with reduced chemical reactivity.

2.6.2. Global softness

The global softness (S) has an inversely proportional relationship with the global hardness which can be expressed as [94],

$$S = \frac{1}{2\eta}$$

Hence, opposite to the global hardness, an increase in the global softness indicates an increase in the chemical reactivity with the reduced chemical stability of the structure.

2.6.3. Chemical potential

Using the Koopmans' theorem, the chemical potential (μ) can be calculated as [95]:

$$\mu = -\frac{E_{HOMO} + E_{LUMO}}{2}$$

The chemical potential also can be used to determine the stability of the investigated structures besides its another potential application to determine the direction of electron transfer from the adsorbate to adsorbent [91].

2.6.4. Electrophilicity

The electrophilicity index (ω) from Parr et al. also can be calculated using the formula [96]:

$$\omega = \frac{\mu^2}{2\eta}$$

The electrophilicity can also be used to investigate the structural stability, reactivity and toxicity of a nanostructure where, similar to the global softness, an increasing value the electrophilicity index also indicates an increase in the chemical reactivity [97].

2.6.5. Electronegativity

The negative value of the chemical potential is known as the electronegativity (χ) of the structure and can be calculated as,

$$\chi = -\mu$$

The electronegativity can be applied to determine the direction of the flow of electrons in a chemical system where the electrons move towards the higher electronegative region from a lower one [98].

2.7. Charge transfer analysis

2.7.1. NBO and Mulliken charge transfer

To investigate the charge transfer between the adsorbate molecules and the adsorbent, the Natural Bond Orbital (NBO) based charge transfer and the original basis function-based Mulliken charge transfer can be calculated from theoretical calculations using computer simulations. These investigations of the charge transfer play an essential role to the development of a drug sensor device by observing if the adsorbent

nanostructures are capable of making a detectable electrochemical signal on the presence of a drug molecule.

2.7.2. AIM analysis

To understand the charge transfer between the adsorbate and adsorbent more extensively, the quantum mechanical Atoms in Molecule (AIM) analysis can be studied where the charge transfer between the adsorbate and adsorbent atoms can be observed from the bonded paths and the bond critical points (BCP), an appearance of which can confirm the charge transfer between the adsorbate and adsorbent atoms. The type of interaction can also be understood from AIM analysis using several other parameters including the electron density at BCP (ρ_b) and its Laplacian ($\nabla^2\rho_b$), kinetic electron energy density (G_b), potential electron energy density (V_b), and the total electron energy density (H_b) which is the sum of kinetic and potential electron energy density [99]. A closed-shell interaction can be confirmed from the positive value of the H_b where the negative value represents a shared interactions. Besides, if the negative ratio of the kinetic electron energy density to the potential electron energy density ($-G_b/V_b$) is >1 then the interaction is considered to be non-covalent and electrostatic in nature where $-G_b/V_b$ <1 represent a covalent nature of the interaction. Furthermore, at the BCP, if both $\nabla^2\rho_b$ and H_b becomes negative, the interaction is considered as a strong covalent interaction following by weak electrostatic interaction for the positive value of both $\nabla^2\rho_b$ and H_b [100]. But if the $\nabla^2\rho_b$ becomes positive and H_b remains negative, then the interaction can be labeled as a partial covalent and partial electrostatic interaction in nature.

2.7.3. Molecular electrostatic potential

The molecular electrostatic potential (MEP) map represents the regions where a positive test charge can be attracted or repelled. The positive electrostatic potential region, which is often coloured as blue in the MEP map represents the regions with low electron density where a positive charge gets repelled by the atomic nuclei. Furthermore, the negative electrostatic region is coloured as red in the MEP map, which represents the region with higher electron density where a positive test charge can be attracted by the atomic nuclei. The interaction of a drug molecule with the adsorbent usually alters the electron density in the system hence an interaction can be detected from this alteration in the MEP map which can further be used in the drug sensor device development.

2.7.4. Change in fractional charge

It is also possible to determine the direction of the charge flowing through the adsorbate and adsorbent from the calculation of the change in fractional charge (ΔN) using Pearson's method [101]:

$$\Delta N = \frac{\mu_{adsorbent} - \mu_{adsorbate}}{\eta_{adsorbent} + \eta_{adsorbate}}$$

where μ and η represent the global chemical potential and chemical hardness, respectively.

In this case, if the value for ΔN appears to be negative, then it can be concluded that the charge will flow towards the adsorbent from the adsorbate where a positive value will indicate the charge transfer to the adsorbate from the adsorbent.

2.7.5. Dipole moment

The dissolvability of the nanostructures into a polar medium like water etc. can be investigated using dipole moment (DM) which plays an integral part for drug delivery devices. An increasing DM represents a higher charge asymmetry for the structures which is desired in case of the drug delivery systems so that they can attract more random electrons and dissolve into the polar mediums.

2.8. Effect of solvents

Besides vacuum, theoretical calculations allow calculating the properties of nanostructures in many other mediums, e.g. water, acid, methanol etc. which plays a crucial role on investigating the behaviour of the drug sensors and drug delivery systems in many different targeted environments. For example, it is crucial to examine the performance of an anticancer drug delivery systems in a low pH cancerous cell region for a better understanding to the drug release performance of the nanostructures in the targeted region.

2.8.1. Solvation energy

The solubility and stability of the nanostructures in any solvent medium can be further investigated in terms of the solvation energy. For example, negative solvation energy of a nanostructure in a solvent medium represents spontaneous solvation and higher stability of that nanostructure in that solvent [102]. Hence for the drug delivery application, the solvation energy is essential to be negative in the polar solvent mediums like water etc. The solvation energy can be calculated from,

$$\Delta E_{Solvation} = E_{solvent} - E_{gas}$$

where $E_{solvent}$ represents the total energy of the structure in the solvent medium and E_{gas} represents the energy of the structure in the gaseous medium.

2.9. Drug release mechanism

In both drug delivery and drug sensor devices, the drug release mechanism plays a crucial to study the efficiency of the device. This can be observed from the interaction of the drug molecule with the adsorbent in the targeted environment. For example, if the adsorption energy of an anticancer drug on a nanostructure decreases or become positive in the low pH cancerous cell environment, the nanostructure is considered to desorb and release the drug ideally in a low pH environment.

2.9.1. Recovery time

The required time for a complex system to return to its initial state by releasing the drug molecule can be investigated from the recovery time (τ) [103] which can be calculated from,

$$\tau = \nu_0^{-1} \exp\left(\frac{-E_{ads}}{KT}\right)$$

where for vacuum ultra-violet condition $\nu_0 = 3 \times 10^{14}\, s^{-1}/10^{16}\, s^{-1}/10^{12}\, s^{-1}$.

For sensor applications, less recovery time is crucial to release the drug quickly for which a less negative value for the adsorption energy is also required. Hence weak physisorption of the drug molecule with the nanostructure is suitable for the drug sensor applications.

3. Carbon-based LDNs for drug delivery and sensing applications

3.1. Graphene and functionalized graphene nanosheet

Graphene is a 2D single-layer hexagonal network of carbon atoms bonded with SP^2 hybridization. This honeycomb shaped allotrope of carbon along with its zero bandgap, exceptional hardness and other superior structural, electronic, and optical properties lead scientists to apply this material into many diverse fields like solar cells, gas sensor, biosensors, drug delivery system etc. [104–108]. After the first synthesis of graphene by Novoselov et al., from the University of Manchester using the scotch tape method [109], several synthesis methods like exfoliation of natural graphite [110], chemical vapour deposition (CVD)

[111], reduction of graphene oxide (GO) [112] etc. showed promising future in the graphene fabrication industry. Though the method relating to the reduction of GO into GNS provides excellent cost-effectiveness, CVD can offer a large area on the GNSs. The experimental C—C bond length of the graphene was observed as 1.42–1.44 Å [113] with several other superior properties like very high strength with the value of Young's modulus of 1 TPa [36], the high thermal conductivity of 5000 W/mK [114], the electrical conductivity of 5600 S/m [115], and high carrier mobility at the room temperature as 200,000 cm^2/Vs for carrier densities below 5×10^9 cm^2 [116]. Besides these unique properties, the biocompatibility and reduced cytotoxicity of GNSs made itself a promising candidate for the drug sensor and delivery applications [117,118]. But pristine GNS shows weak interaction towards many drugs and amino acids which can be significantly enhanced by altering its properties with impurity atom doping. Besides doping, the hexagonal ring of the graphene was also modified into a pentagonal and heptagonal ring to create a new type of nanomaterial named as phagraphene which shows promising applications in the drug delivery applications [119]. Besides, the theoretical calculations with GNS showed significant similarity with experimental results, e.g. in Fig. 6 we have optimized graphene quantum dot (GQD) using DFT with B3LYP/6-31G (d,p) level of theory which showed comparable bond length, bond angles etc. with the experimental observations. Thus the research on the theoretical implementation of pristine, doped or functionalized graphene in the field of drug delivery and drug sensor become very popular in recent years.

β-lapachone (β-lap), a potential chemotherapeutic anti-cancer agent, possess an excellent value as it selectively kills or stops the growth of various tumour cells responsible for pancreas, prostate head and neck cancers [120–122]. β-lap, containing naphthoquinone fused to a methylated hydropyran moiety, was originally isolated from a South American tree named Lapacho. To carry this anti-cancer agent into the cancerous cell, the feasibility of using pristine and metal-doped (Pt, Au) graphene was investigated by Zahra Khodadadi et al. by a first-principles investigation [123]. They observed the adsorption properties of β-lap into pure GNS first, and then it's dipole moment to investigate the solubility into a polar medium like water. Pristine graphene had a C—C bond length of 1.42 Å with a bond angle of 120° and SP^2 hybridization. But these properties were further modified by decorating metal atoms (Pt, Au) into the GNS. The Pt—C and Au—C bond length for Pt and Au decorated GNSs were increased to 2.25 Å and 2.47 Å respectively with a variation in the SP^2 hybridization as the bond angles decrease to 75° and 66° respectively. But these modifications into the structural properties enhanced the adsorption properties of β-lap into the Pt and Au decorated graphene and their solvation properties into polar mediums. The adsorption energies of Pt and Au decorated graphene was increased as −40.82 kcal/mol and −38.28 kcal/mol which was −21.22 kcal/mol for pristine graphene. Hence it can be understood that the stability of the graphene was enhanced due to the metal doping. Further, the dipole moment of the β-lap adsorbed graphene was increased by 22.26 and 22.69 debye by Pt and Au doping respectively while it was only 11.86 debye for the pristine GNS. Hence, β-lap was expected to dissolve into the polar medium more efficiently with an increased reactivity. So, it can be concluded that the metal-doped graphene performs better as a β-lap drug carrier rather than pristine graphene itself.

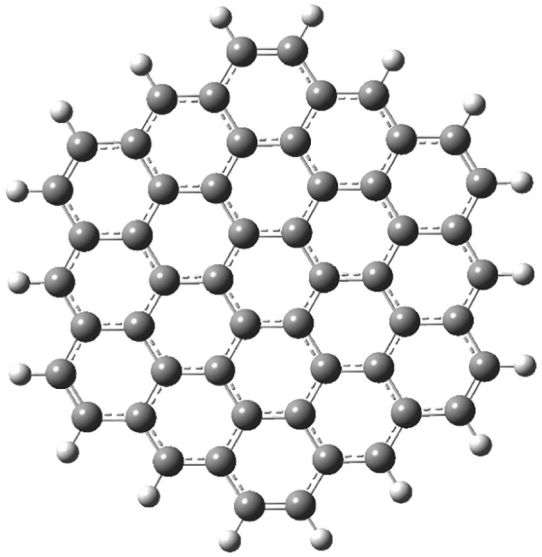

Fig. 6. Relaxed GQD nanostructure with DFT-B3LYP/6-31G (d,p) level of theory.

Doxorubicin, another chemotherapeutic drug for several cancer treatments, comes with high toxicity which causes many physical difficulties like hypertension and even a heart failure [124–126]. M. Z. Tonel et al., made an investigation on the adsorption of doxorubicin on GNS using DFT theory with GGA-PBE functional applied in the SIESTA code to decrease the side effects of the drug [127]. They have found the binding energy of the doxorubicin with the pristine graphene can be as high as 11.30 kcal/mol with an adsorbate-adsorbent distance of 2.50 Å. However, this small adsorbate-adsorbent distance allowed a charge transfer of −0.20e between them. But depending on the orientation of the doxorubicin, the binding energy can drop down to 2.99 kcal/mol with an adsorbate-adsorbent distance of 2.87 Å. So, depending on the most stable orientation, they have reported stable adsorption of doxorubicin drug on GNSs which were previously inconspicuous for carbon-based nanomaterial in many experimental and theoretical studies [128–130].

Aluminium (Al) doped nanostructures were reported to adsorb 5-fluorouracil (FU), an anti-cancer drug for gastrointestinal, stomach etc. cancer treatment, strongly adsorption with an enhanced drug loading capacity [131,132]. To bring this research further, M. Vatanparast et al., theoretically studied AlN and BN doped GQD, another low toxic structure with high biocompatibility, as an efficient nanomaterial for the FU drug delivery [133]. Supporting the literature, the AlN doped GQDs showed some strong adsorption to the FU with a noticeable adsorption energy of - 47.29 kcal/mol for AlN-FU GQD structure. In their work, they have worked with $C_{42}H_{18}$ GQD whose central ring was further replaced by B—N, B—P, Al—N and Al—P bonds. Besides high adsorption energy for the AlN-FU GQD structure, negative values for the Gibbs free energies of all other doped structures confirmed the spontaneous adsorption of FU with adsorption energies higher than that of the pristine GQD. Further restriction to the translation degree of freedom lead to a decrease in the entropy with predicted exothermic adsorption with negative values for the change in enthalpy. These confirmed the ability of the pristine and doped GQDs to load the FU drug. Finally, an increase in the dipole moment up to 18.846 debye for AlN-FU GQD, highest among the investigated structures, represents AlN doped GQD's better solubility to the polar medium and enhanced reactivity towards FU drug made itself a potential candidate to carry FU to the target sites.

A prodrug of 5-fluorouracil, Tegafur (TG) which has a very short biological half-life with the inability to overcome multidrug resistance of the cancer cells requires efficient transportation to the target area [134,135]. Hence M. Shahabi et al., investigated the performance of pristine and functionalized (–OH, —O, –CO, and –COOH) GNSs, to overcome the low solubility of GNS in a polar medium like water, as a capable tegafur drug carrier [136]. The functionalization of the GNS modified the adsorption process of the tegafur towards the structures significantly with a maximum value of the adsorption energy as −24.85 kcal/mol for G-CO/TG along with a minimum of −16.01 kcal/mol for G-COOH/TG structure. The solvation energy of the G-COOH/TG structure was also found as −38.57 kcal/mol with a −59.27 kcal/mol of interaction energy. Besides G-COOH, G-OH also showed very strong adsorption towards the tegafur with a remarkable adsorption energy of −23.31 kcal/mol and solvation energy, and interaction energy of −38.12, −58.15 kcal/mol respectively. Though the dipole moment of

the pristine GNS is zero but increases significantly with the functionalization and hits as high as 12.80 debye for the tegafur adsorbed G-CO structure. On the other side, the energy gap was reduced to as low as 3.69 eV for the tegafur adsorbed CO functionalized GNS while it was 5.68 eV for the pristine GNS nanosheet. These indicated the batter reactivity of the TG adsorbed functionalized GNS sheet with a higher polarity towards a polar medium like water which was further supported by the global parameters like chemical potential, global hardness, electrophilicity investigations.

As it can be observed from Fig. 7 that many anti-cancer drugs have structures akin to the nucleobases as the vital role of these drugs is to slow the growth rate of cancer cells by interfering their DNA synthesis [137]. This led C. Rungnim et al., to investigate the adsorption properties, along with edge effect of the GNSs, of three nucleobases with similar structures like anti-cancer drugs, mercaptopurine, thioguanine, and fluorouracil, on a graphene flake considering the weak dispersion forces caused by Van der Waals interaction [138]. The lack of accuracy of many GGA functional with DFT due to their underestimation of π–π interaction lead Rungnim et al., to use several functional like M06-2X, MP2, CCSD(T) etc. [139]. To validate their theoretical model, they have first investigated the adsorption properties of nucleobase uracil and then the anti-cancer drug akin to the uracil, fluorouracil, on the benzene ring. It was observed that the O on uracil and fluorouracil pointing to the benzene ring, and uracil/fluorouracil parallel to the benzene ring has better stability than any other investigated orientations. For O pointing to the Benzene ring, benzene/uracil and benzene/fluorouracil configurations have adsorption energies as high as −7.85 kcal/mol and −8.10 kcal/mol respectively which becomes −7.37 kcal/mol, and −8.25 kcal/mol respective for uracil/fluorouracil parallel to the benzene ring. A favourable result from the meta GGA based M06-2X functional led them to study the adsorption behaviour of the nucleobases towards the C_{24}, C_{54}, and C_{96} GNSs. They have observed an edge effect which gradually decreased with the increased size of the graphene nanoclusters. Less edge effect was observed in case of the adsorption of the nucleobases in the middle of the carbon clusters and depending on the alignment and position this effect can reduce the adsorption energies by <5 kcal/mol. Further, the edge effect of C_{96} is almost as much as C_{54} lead them to adsorb mercaptopurine, thioguanine, and fluorouracil anti-cancer drugs in a parallel position with different alignments in the C_{54} nanosheet. Finally, the adsorption energies of fluorouracil, mercaptopurine, and thioguanine were found around −15.5, −16, and −20 kcal/mol respectively made C_{54} a promising candidate for the delivery of these drugs.

Adenine, another nucleobase with a structure akin to many drugs and biomolecule, showed enhanced adsorption properties on the Ni decorated GNSs compared to the pristine GNS which was observed on an investigation made by S. Gholami et al., [140]. For a plane alignment of adenine to the pristine graphene surface, the adsorption energy was found as −5.66 kcal/mol with a graphene-adenine distance of 4.10 Å and a charge transfer of −0.01e (Mulliken) only. The adsorption energy was dramatically increased to a maximum of −44.50 kcal/mol with an adsorbate-adsorbent distance of 1.90 Å, and a charge transfer of +0.062e (Mulliken) in the Ni decorated GNS, where Ni was adsorbed above the hexagonal ring of graphene with a strong chemical interaction of −126.00 kcal/mol. Adsorption of the adenine on the Ni decorated graphene also decreased the bandgap and Fermi level of the structure to 2.152 eV and −2.991 eV respectively from a value of 2.416 eV and −3.179 eV for Ni-G itself. Though the pristine graphene showed a weak interaction towards the pristine GNS, decorating it with a Ni atom increased its interaction significantly. Hence the Ni decorated graphene can be considered as a potential candidate for delivery of the drugs with structures similar to the adenine.

Furthermore, the adsorption of guanine nucleobase was investigated by A. S. Rad et al., on pristine and Al-doped graphene (AlG) using DFT theory with B3LYP hybrid functional and 6-31G basis set [141]. It was observed that the doping of Al to the pristine GNS significantly alters the adsorption properties towards guanine. For pristine GNS, the adsorption energy of guanine was observed only as −1.34 kcal/mol with an adsorbate-adsorbent distance of 3.62 Å. This allowed them to transfer a little amount of charge of −0.02e (based on Mulliken charge transfer analysis), or −0.01e (based on natural population analysis) between adsorbate and the adsorbent. This was significantly enhanced by the doping of Al atom to the pristine GNS. For a specific orientation of guanine, O atom from guanine above Al atom from AlG, the adsorption energy increased as much as −45.10 kcal/mol with an adsorbate-adsorbent distance of 1.88 Å only which allows them to transfer +0.208e (Mulliken) amount of charge. For other orientations the adsorption energies were observed as −42.73, −41.66, −22.61, −9.94 kcal/mol with an adsorbate-adsorbate distance of 2.01 Å, 2.02 Å, 2.10 Å, and 2.20 Å respectively. Furthermore, along with the adsorption energy and charge transfer, the dipole moment of the AlG structures was also enhanced significantly with a maximum of 14.22

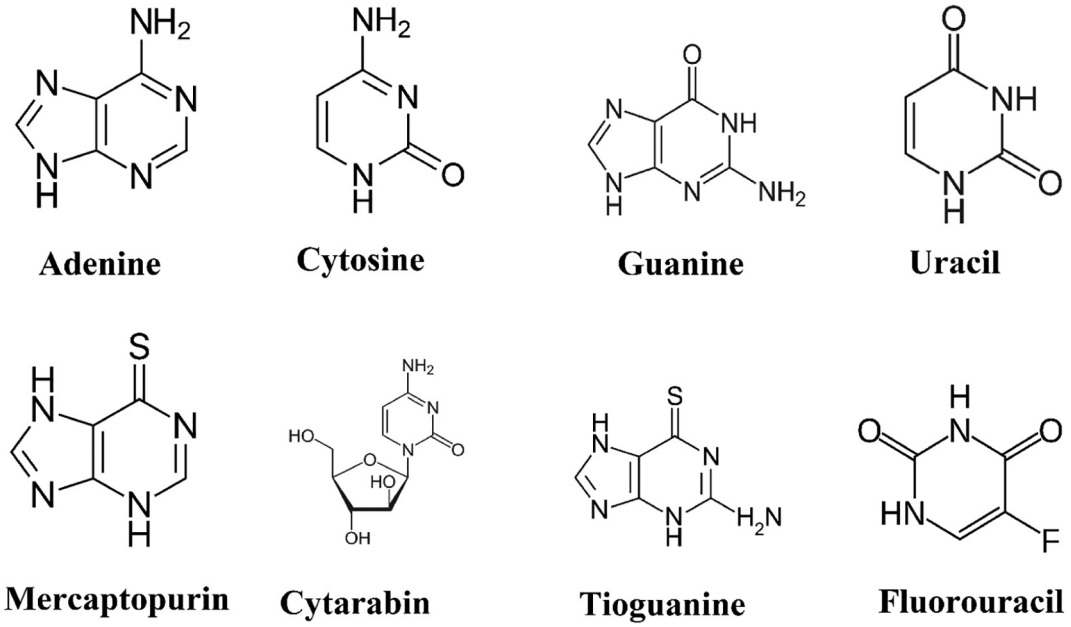

Fig. 7. Several anti-cancer drugs designed with similar structures to the various nucleic bases.

debye. This excellent modification in the adsorption energy, charge transfer and dipole moment made AlG nanostructure a suitable adsorbent or sensor for the guanine.

Other than the anti-cancer drugs, graphene was also reported to work as a drug delivery vehicle for 4-Aminopyridine or dalfampridine, often marketed as Ampyra with a chemical name of $C_5H_4N\text{-}NH_2$, helps to overcome walking difficulties for the adults by increasing nerve signal conduction through blocking the potassium channels on it [142,143]. But Ampyra has several side effects like headaches, dizziness, nausea, insomnia etc. and an increased dose of it can also cause seizures [144]. To reduce the possibility of a seizure, Najme Dastani et al. proposed pristine and functionalized GNS (f-GNS) for the transportation of Ampyra using quantum mechanical calculations [130]. They choose the DFT theory with M06-2X functional and 6-31G (d, p) basis set to optimize the structures due to its excellent agreement with the experiment. For GNS, they observed C—C bond length as 1.416 Å while it was found as 1.421 Å experimentally [145]. This encouraged them to study several f-GNS (G-COOH, G-CO, G-OH, and G-O) with the same functional and basis set. They have studied several essential properties like adsorption energies, HOMO-LUMO energy gaps, chemical potential, dipole moment and several global parameters for both gaseous and aqueous phase. It was found that the dipole moment in the aqueous phase rose to 22.53 debye from a maximum of 2.836 debye in the gaseous phase. For the functionalized GNSs this dramatic change on the dipole moment was continued and was found as high as 46.03 debye for G-COOH/Ampyra complex. Finally, the highest negative adsorption energies of −7.64 kcal/mol for G-COOH/Ampyra complex among the pristine GNS and f-GNS in the aqueous phase made G-COOH the best candidate for the transportation of Ampyra drug. This was further supported by the lowest value for the energy gap as 0.822 eV, global hardness as 0.411 eV and the highest value for the change in global electrophilicity as 16.946 eV.

Besides the application of graphene as a potential sensor for the drugs and nucleobases, to understand the interaction of graphene with other biomolecules, the adsorption properties of amino acids on the GNSs were also reported using first-principles investigations. B. Saha et al. investigated the interaction of four amino acids (alanine, serine, phenylalanine and tyrosine) into pristine and B and/or N doped functionalized (-OH, -NH_2, -COOH) GNSs [146]. It was observed that the functionalized GNSs interacted with the amino acids with interaction energy ranging from 7.17 to 19.1 kcal/mol depending on the adsorbent structures and dopants. Furthermore, though the doping of B and/or N atoms changed the adsorption properties of amino acids to the –OH and NH_2 functionalized graphene, it hardly affected the –COOH functionalized GNS. On another dispersion corrected DFT study, H. T. Larijani et al., investigated the adsorption of several amino acids (glycine, histidine and phenylalanine) on pristine, defected and oxidized GNSs [147]. They have found that every interaction of the amino acids with the monolayer GNSs was physisorption and the GNSs is a potential candidate for the bio-related applications.

Properties like high electrical conductivity, polarity, and basicity of nitrogen-containing graphene lead J. H. Chen et al., to investigate the interaction of several amino acids with three types of nitrogen functional known as pyridinic N, pyrrolic N, and graphitic N [148]. In their investigation with DFT theory along with PBE functional, they have used nitrogen-doped 2D GNSs along with pristine GNS with hexagonal vacancy. The DFT theory with PBE functional gave the C—C bond length as precise as 1.423 Å for the pristine GNS. Among three types of interaction between the amino acids and the substrates, the side chains perpendicular to the substrates was used as it was most energetically favourable. Due to the adsorption of the several amino acids arginine, histidine, aspartic acid, asparagine, and tyrosine, to the pristine GNS, the adsorption energy was found as low as −1.19 kcal/mol for the Aspartic acid with a maximum as −2.40 kcal/mol for the Arginine adsorption. But these values for the adsorption energies increased dramatically in case of the nitrogen atoms doping. For four nitrogen-doped Pyridinic 4 N, this was found as high as −14.82 kcal/mol for histidine with a minimum of −10.74 kcal/mol for the Arginine adsorption. This was again reduced in case of the hydrogenated nitrogen-doped structure disproportionally and finally for hydrogenated pyrrolic N it ranges between −2.56 kcal/mol to −3.87 kcal/mol. Despite this low adsorption values for the hydrogenated structures, it increased dramatically again in case of a hydrogenated N-edge. For hydrogenated pyrrolic N-edge, it went as high as −14.18 kcal/mol for Arginine with a minimum value of −4.84 kcal/mol for Tyrosine adsorption. Hence it was concluded that a Pyridinic N nanosheet with a hydrogenated N-edge works best for the adsorption of amino acids.

The modification of the hexagonal ring of the GNS into the pentagonal and heptagonal ring made a noble kind of nanosheet known as phagraphene is also studied as a potential drug delivery nanomaterial for adrucil by R. Bagheri et al., [149]. The small adsorption energy of −2.9 kcal/mol for phagraphene made it incompatible for the adrucil drug delivery. However, the adsorption energies increased dramatically to the −6.8, −41.8, and −14.0 kcal/mol due to the doping of B, Al and Si atoms respectively. However, noticeable change in the electronic properties of B doped phagraphene made it unsuitable for adrucil drug delivery and despite having enormous adsorption energy, Al-doped phagraphene showed a considerable response time of 4.09×10^{18} s. Hence the Si-doped graphene with a moderate adsorption energy of −14.0 kcal/mol with a short response time of 0.02 s, was predicted to be a potential drug delivery system for adrucil drug.

3.2. Single and multi-walled carbon nanotube

CNT is an allotrope of carbon made by a hexagonal network of carbon atoms which is cylindrically rolled up into a tubular shape. Ever since its discovery, numerous research works were done on its various unique properties including exceptional mechanical strength, electrical, optical, and thermal properties etc. [150–154]. Similar to the GNS, the SP^2 hybridized carbon-carbon bond of CNT lead it to one of the strongest material with Young's modulus of 1200 GPa and a tensile strength ranging from 50 GPa to 200 GPa [37]. The density of the CNT was observed experimentally as large as ~1.09 g/cm^3 with a low room temperature resistivity of ~2 mΩ-cm [155]. The thermal conductivity of CNT was predicted as high as ~6600 W/mK at room temperature along with an electrical conductivity ranging from 100 to 10^6 S-cm^{-1} [156,157].

CNT can be classified in many subclasses but most simply into two, single-walled CNT (SWCNT) and multi-walled CNT (MWCNT). Where the SWCNT is a single layer of graphene, MWCNT is a multi-layer of graphene rolled up cylindrically into a tubular shape as it is shown in Fig. 8 [158]. Now, based on the chiral vector C_h defined as $C_h = na + mb$ (where n and m are the integer number of steps along the unit vectors a and b) and chiral angle, θ ($where\ 0^0 \le \theta \le 30^0$), defined as the rolling angle between the graphene and axis of the tube, CNT can be further classified into three chiralities as zigzag ($\theta = 0^0, n \ne 0, and\ m = 0$), armchair ($\theta = 30^0, and\ n = m$), and chiral ($0^0 < \theta < 30^0\ and\ n \ne m$) [159].

After the first synthesis of CNT through arc-discharge method [150], over the years CNT was reported to be synthesized using many techniques including chemical vapour deposition (CVD) [160], laser ablation [161], plasma jet [162] and many more [163–166]. Though the arc-discharge method reports growth of SWCNT with 80% purity and laser ablation method with 90%, CVD with 30–50% purity still widely used due to its cost-effective solution for the mass production [158,167].

This wide range of methods to synthesize CNT along with a wide range of structural variation and unique properties led CNT to be applied in many fields like aerospace industry [168], electronics [169], energy harvesters [170], gas sensors [171], biosensors [172], drug delivery [173] etc. Among these widespread applications of CNT, our particular interest is in its adsorption ability of biomolecules (both for sensing and delivery purpose) as it offers biocompatibility in this field and has the ability to penetrate cells along with excellent stability, high reliability, faster response time, high adsorption strength towards the bio-

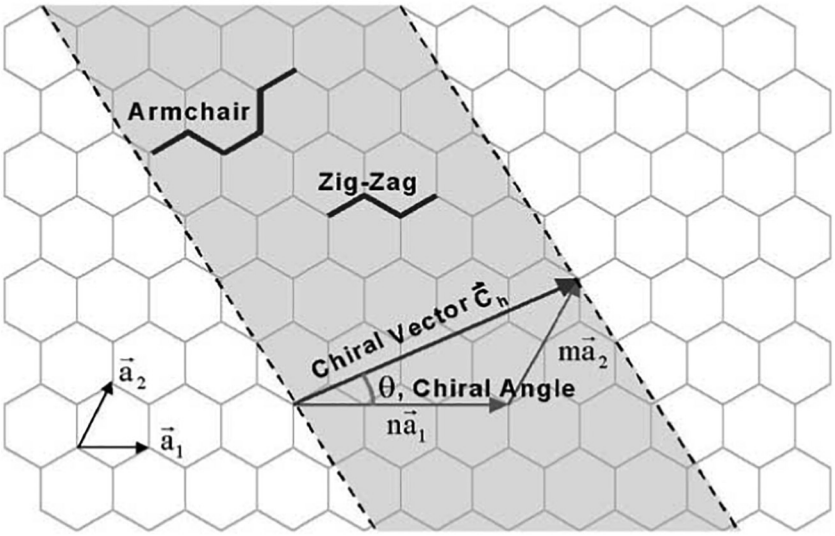

Fig. 8. Schematic diagram of various kind of CNT made by rolling up 2D graphene sheet. Reproduced with permission from ref. [159]. Copyright Elsevier Science Ltd., 2001.

molecules etc. [174]. Starting from small bio-molecules like glucose sensing [175], CNT can be used to sense and deliver several therapeutics, anaesthetic, anti-depression etc. drugs to the human body [176]. To acquire the desired sensing and drug delivery performance, sometimes CNT is required to be doped or fictionalized by impurity atoms, and several studies have successfully reported enhanced performance towards biosensors and drug delivery due to the functionalization and doping to CNT [177–179]. Finally, due to the recent advancement on the accuracy of computer simulation methods with approximation theory like DFT, e.g. a theoretically optimized SWCNT is shown in Fig. 9, numerous research works were put forward on investigating CNT as an efficient system for the bio-molecule sensing and drug delivery. In this section, we aim to review recent research work exploring the bio-molecule sensing and drug delivery efficiency of the CNT.

A first-principles study conducted by H. Shaki et al. reported the adsorption of the penicillamine (PCA), an anti-cancer drug with several vital side effects, on the pristine and functionalized SWCNT [180]. Considering the dispersion terms, for pristine SWCNT the PCA drug make weak physisorption with a maximum adsorption energy of −3.18 kcal/mol and an adsorbent-adsorbate distance of 3.251 Å. But this interaction was further enhanced by adding an extra –COOH functional group to the pristine SWCNT. With –COOH functionalized SWCNT (f-SWCNT), the maximum adsorption energy of PCA towards f-SWCNT was observed as high as −11.22 kcal/mol for a particular orientation of PCA with a maximum dipole moment of 6.993 debye and an energy gap of 1.311 eV. Thus, this study reveals that the –COOH f-SWCNT performs better the PCA drug delivery system, whereas all interactions were exothermic and stable with negative adsorption energies. These results were further compared with the MD simulations, which successfully supported the result obtained from the DFT investigations.

Isonicotinic acid hydrazide (INH), simply known as Isoniazid, is a prodrug for the treatment of the infectious disease tuberculosis (TB) caused by *Mycobacterium tuberculosis* (MTB) bacteria [181]. As INH drug often comes with side effects like peripheral neuropathy, nausea, aplastic anaemia etc. N. Saikia et al. proposed SWCNT as a drug carrier to the target area [182]. As the Si doping in the CNT is less reported in the literature than the B/N doping, better electronic properties of Si lead them to use Si-doped SWCNT to carry the INH drug using DFT theory and molecular docking [84,183]. In a Van der Waals interaction corrected investigation it was found that INH parallel to the (5, 5) SWCNT have better stability with more adsorption energy of 15.59 kcal/mol compared to the perpendicular alignment of the INH with (5, 5) SWCNT with an adsorption energy of 13.65 kcal/mol. Though the adsorbate-adsorbent distance of 3.13 Å was unchanged for both parallel and perpendicular alignment, electronic band gap decreased in the perpendicular alignment slightly to 0.592 eV compared to 0.676 eV for parallel alignment. For covalent functionalization of INH to the (5, 5) SWCNT, the adsorption energy was drastically increased to 68.31 kcal/mol with a change in the INH-(5, 5) SWCNT distance of 1.75 Å and a change in bandgap as 0.405 eV. The quantum descriptors also reported an increase in the reactivity due to the covalent functionalization of INH. Hence, (5, 5) SWCNT have a potential future as a drug delivery system for isoniazid drug.

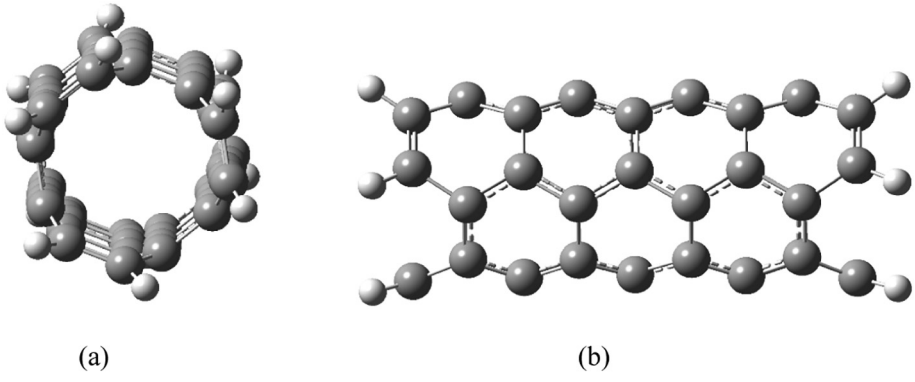

Fig. 9. Optimized 3 × 3 single-walled carbon nanotube (SWCNT) nanostructure with DFT-B3LYP/6-31G (d,p) level of theory. (a) Top view (b) side view.

2′,2′-Difluoro-deoxycytidine (dFdC) or simply know as Gemcitabine is a popular therapeutic option to treat numerous cancers including breast cancer, pancreatic cancer and non-small cell lung cancer [184–187]. It comes with relatively fewer side effects but as severe as fatal pulmonary toxicity and acute lung injury [188,189]. This lead H. Moradnia et al., to investigate the pyrrolidine functionalized (8, 0) SWCNT (f-SWCNT) as an efficient drug delivery system for gemcitabine drug using DFT theory with M062X functional and 6-31G (d,p) basis set [190]. In water solution, for a particular orientation 'Complex E', the gemcitabine was adsorbed towards f-SWCNT with an adsorption energy of −11.15 kcal/mol and a dipole moment of 26.354 Debye with a minimum adsorbate-adsorbent distance of 1.866 Å. For another orientation Complex A, the adsorption energy was slightly decreased to −10.23 kcal/mol but with an increase in the dipole moment to 32.212 Debye. The energy gap of the Complex A and E was observed as 1.501 eV and 1.406 eV respectively. The global hardness of the structures ranges between 0.673 eV to 0.750 eV where the electrophilicity had a range between 9.443 eV to 9.910 eV. These findings lead them to declare the f-SWCNT as a potential drug delivery system for the gemcitabine which was further confirmed through the AIM, NBO, and DOS analysis.

Flutamide, an anticancer drug with chemical name 4′-Nitro-3′-trifluoromethyl-isobutyranilide is a widely used drug to treat prostate cancer often comes with side effects like severe gynecomastia, liver toxicity etc. [191–193]. To transfer this drug directly to the cancerous cell, to minimize the side effects, M. Kamel et al., analyzed the potential of (5, 5) SWCNT for efficient delivery of flutamide drug, and how co-solvents like ethanol affects the interaction between the flutamide drug and (5, 5) SWCNT [98]. In the water solution for a particular orientation labeled as Configuration 3, the most negative adsorption energy value was observed with a minimum adsorbate-adsorbent distance and highest value for dipole moment. The values were −1.43 kcal/mol, 3.000 Å, and 10.417 debye, respectively. So the flutamide drug made physisorption towards the SWCNT, and the nature of the interaction was exothermic. The values of solvation energy indicated a spontaneous solvation with a range of −14.40 to −17.43 kcal/mol and the least value was for the Configuration 3. A spontaneous flow of electron was observed from the adsorbent to the adsorbate with positive values of 0.435 eV and 1.619 eV for the charge transfers (ΔN) and the energy change of the acceptor ($\Delta E_{B(A)}$). Finally, from the MD simulations, it was found that the addition of ethanol with 0.5 M concentration increases the stability of the simulation system. However, another study lead by this group, M. Kamel et al., investigated the COOH functionalized SWCNT to use as a drug carrier for flutamide drug [194]. In that study, they have found that the flutamide drug can be adsorbed in the SWCNT with a maximum adsorption energy of −5.38 kcal/mol in the water solvent where the dipole moment of the structure was found as 10.93 debye with a bandgap of 1.28 eV. The same COOH functionalized SWCNT was used to investigate the carmustine drug delivery ability by the same group but this time lead by R. Khorram [195]. The performance was almost similar as for flutamide drug with a maximum adsorption energy of −4.65 kcal/mol along with a dipole moment of 3.312 debye, the energy gap of 1.302 eV, and interaction energy of −27.98 kcal/mol.

An oral drug, Metformin (MF), is used as a first-line medication to treat type 2 diabetes especially patient with breast cancer, prostate cancer, and pancreatic cancer [196–198]. To minimize the side effects, M. S. Hoseininezhad-Namin et al., investigated pristine, Si and Al-doped (5, 5) SWCNTs as a promising MF drug carrier [199]. Weak physisorption of MF towards pristine (5, 5) SWCNT was observed with an adsorbate-adsorbent distance of 3.69 Å, charge transfer of 0.002e (NBO analysis), and adsorption energies of −1.61 kcal/mol (B3LYP) and −7.61 kcal/mol (ωB97XD) where an increment in the adsorption energy through ωB97XD functional clearly indicated the role of dispersion in the adsorption of MF drug towards the pristine SWCNT. However, doping the SWCNT with Si and Al significantly increased the adsorption energy of MF to −38.74 kcal/mol and −48.66 kcal/mol, respectively in the solvent phase. The reactivity of the MF-doped SWCNT configurations also increased in the solvent phase with an increment to the dipole moment to 22.84 debye and 20.03 debye for the MF adsorbed Si and Al doped SWCNTs respectively when it was only 6.60 debye for the adsorption of MF towards pristine SWCNT. This increment in the reactivity was further supported by the global reactivity descriptors like chemical potential, global hardness and softness, and electrophilicity. Hence Si doped SWCNT with a moderately high adsorption energy but with lowest band gap as 1.40 eV and highest reactivity in the solvation phase made itself most promising candidate for the MF drug delivery between pristine, Si and Al doped (5, 5) SWCNT.

A theoretical investigation using DFT theory with B3LYP hybrid functional and 6-311G (d, p) basis set, was made on the Ca doped (5, 5) SWCNT to inspect its ability to perform as a drug carrier for atropine drug delivery [200]. Atropine is a drug taken by an injection to the muscle to treat several types of nerve agent and also performs as an antipode to the several poisonings [201]. Atropine drug was adsorbed by Ca-SWCNT with adsorption energy of −36.07 kcal/mol for D-atropine, and −41.87 kcal/mol for L-atropine with a dipole moment of 22.7 and 22.1 debye respectively. The HOMO-LUMO energy gap was observed around 1.70 eV for both structures with a charge transfer of around +0.13e from the atropine to the Ca-SWCNT, which was confirmed by the NBO analysis. The solubility of the Atrophine+Ca-SWCNT in the water medium was established through the negative solvent energy with a value of −22.97 kcal/mol for D-atropine and −24.21 kcal/mol for L-atropine. Hence the Ca-SWCNT was predicted as a potential drug carrier for the atropine drug.

Ketamine, an *N*-methyl-Daspartate (NMDA) receptor antagonist, is clinically often used as an anaesthetic with limited use as an analgesic, anti-depression and anti-inflammatory drug, comes with numerous side effects like psychoactive effects, peripheral effects and neurotoxicity [202]. So, the urgency of rapid determination of ketamine lead R. Zhiani et al., to investigate SWCNT and COOH, $CONHCH_3$ functionalized SWCNT as a sensor to detect ketamine in the gaseous medium along with several other polar mediums [203]. It was found that the adsorption of ketamine in functionalized SWCNT causes a change in the bond length of C—O, N—H and C═O groups noticeably. Further, binding energy in the gaseous medium was observed as −22.94 kcal/mol and −25.61 kcal/mol for COOH and $CONHCH_3$ functionalized SWCNT. This value for binding energy was further increased as −32.13, −31.98, and −32.11 kcal/mol in chloroform, methanol, and water medium respectively for COOH functionalized SWCNT and became −31.07, −31.34, and −31.84 kcal/mol respectively for $CONHCH_3$ functionalized SWCNT. Furthermore, negative values for the change in enthalpy and Gibbs free energies indicated spontaneous exothermic adsorption of ketamine in the functionalized SWCNT. The response of SWCNT to the ketamine was finally confirmed through the noticeable change in Fermi energy to the positive values. Finally, though the COOH functionalized SWCNT responses better to the ketamine in the gaseous phase, $CONHCH_3$ shows slightly better response towards ketamine in other medium like chloroform, methanol and water.

Another anti-inflammatory and analgesic, ibuprofen (IBP), comes with several side effects like indigestion, nausea, vomiting etc. [204,205]. Hence C. Parlak et al., made a first-principles investigation using DFT theory along with B3LYP/M062X functional 6-31G(d) basis set and on the adsorption properties of IBP into Si-doped SWCNT and fullerene [206]. The literature on the accuracy of M062X functional to calculate the adsorption energies but the overestimation of the bandgap lead them to use B3LYP hybrid functional for bandgap calculations [207,208]. After the correction of basis set superposition error (BSSE), for a specific alignment of IBP where the O atom of (C—O) group of IBP was placed above Si atom to the CNT, the adsorption energy was observed as −16.73 kcal/mol with an adsorbate-adsorbent distance of

1.89 Å and bandgap 1.412 eV. Furthermore, due to the adsorption of IBP, the work-function of Si-doped SWCNT increased by 17.43% with a change in the Fermi energy level from −3.591 to −2.965 eV. Thus strong chemisorption with a change in the Fermi energy constitutes SWCNT a potential sensor for IBP drug detection.

Besides the SWCNT as a drug sensor and delivery system, multi-walled CNT (MWCNT) was also investigated as the potential drug sensor for several drugs. D. Shahabi et al. investigated several pristine and sulfur-doped SWCNT along with several MWCNT (Double-walled and Triple-walled CNT) as potential drug sensor for the fluoxetine (FX), a widely used antidepressant drug [209]. It was observed that sulfur atom slightly affected the adsorption processes of FX towards the SWCNT where for most stable structure, (8, 8) sulfur-doped SWCNT, the adsorption energy in the gas (liquid) phase was observed as −51.56 (−40.58) kcal/mol while the FX drug was adsorbed inside the sulfur-doped SWCNT, and only −8.77 kcal/mol while the FX was adsorbed in the outside of the sulfur-doped SWCNT. Further to reduce time consumption, molecular docking study was initiated instead of DFT to investigate the adsorption behaviour of FX towards systems with a large number of electrons like from (8, 8) SWCNT to (20,20) SWCNT, double-walled CNT, triple-walled CNT. It was found that the stability was decreased from (8, 8) SWCNT with an increase in the chirality and the most stable structure, (8, 8) SWCNT, had adsorption energy of −21.41 kcal/mol while the FX drug was adsorbed inside the (8, 8) SWCNT. The stability was increased slightly for the double and triple-walled CNT and the adsorption energies was found as −22.97 kcal/mol and −22.99 kcal/mol for (8, 8) double-walled and (8, 8) triple-walled CNT while the FX drug was adsorbed inside the CNT. However, another study lead by C. P. Sousa et al., reported that the acetaminophen drug was also adsorbed inside an MWCNT more favourably than external surface [210]. Also, the functionalization of the MWCNT with polyethyleneimine polymer enhanced the stability of the acetaminophen adsorbed f-MWCNT complex with an adsorption energy of −195 kcal/mol while it was −183 kcal/mol for the adsorption of acetaminophen towards the pristine MWCNT. So, it was observed that both acetaminophen and fluoxetine could be sensed strongly with the MWCNT.

Other than directly the drug molecule itself, CNT was theoretically investigated to perform as an efficient sensor for several other molecules like bio-molecules, amino acids and lactic acid. The adsorption of five small bio-molecules CO, H_2O NO, SO and PO towards the SWCNT was reported by Y. Xu et al., through the vibrational spectrum analysis using DFT with GGA-PBE level of theory [211]. In another study, M. Yoosefian et al. investigated ability of the Pd doped SWCNT to adsorb an amino acid, histidine, using DFT and HF theory with B3LYP hybrid functional [212]. They reported strong chemisorption of the histidine towards the Pd-SWCNT with a maximum adsorption energy of −419.93 kcal with an adsorbent-adsorbate distance of 2.336 Å. Finally, the interaction of 2-hydroxypropanoic acid or simply know as lactic acid (LA) with SWCNT with different chirality was observed with a DFT-D study from A. N. Chermahini et al. [213]. In their research, they have found that LA interacts more with (4, 4) SWCNT than other SWCNT with higher chirality with an adsorbate-adsorbent distance of 2.226 Å and maximum adsorption energy of −13.39 kcal/mol in the gas phase and −11.13 kcal/mol in the solvent phase. The solvation energy for LA adsorbed (4, 4) SWCNT was observed as −27.02 kcal/mol with an H-L energy gap of 0.455 eV. Hence the (4, 4) SWCNT can work as a potential adsorbent for the LA. So, it can be concluded that the SWCNT can perform as a potential adsorbent for amino acids, lactic acid and biomolecules.

3.3. Carbon fullerene

Akin to graphene and CNT another sp^2 hybridized allotrope of carbon atoms with closed 2D structure, fullerene, got eminent attention on the field of biosensor and drug delivery application recently. Fullerene was observed in the literature as early as in 1965 from H. P. Schultz where he predicted a new possible topological structure of $C_{60}H_{60}$ with truncated icosahedron shape with 60 vertices until the first prediction of C_{60} fullerene came from E. Osawa in 1970 [214,215]. Finally, in 1985, H. Kroto et al. unintentionally observed the C_{60} fullerene while they were performing an experiment by vaporizing the carbon atom from a solid graphite surface into a high-density helium flow to understand the mechanism of long carbon chain formations in star and space [2]. As shown in Fig. 10, the C_{60} fullerene is consists of 12 pentagons along with 20 hexagons like a soccer ball where pentagons cannot be adjacent as each of them is surrounded by five hexagons. With a fixed number of 12 pentagons, fullerenes can be found with variable hexagons, and the closest stable one to C_{60} fullerene is C_{70} fullerene with 12 pentagons and 25 hexagons. Though C_{60} is claimed to be the smallest stable fullerene structures, C_{20} unstable fullerene structure was reported to be stabilized in several ways, including metal doping [216–218].

Due to the mass commercial production of C_{60} fullerene, there is a wide range of methods available to synthesize it. After the discovery of C_{60} fullerene from H. Kroto et al., the first macroscopic production of C_{60} was reported by W. Krätschmer et al. in 1990 from electric arc heating of pure graphitic carbon soot in a helium atmosphere of around 100 Torr [219]. Following by the method of W. Krätschmer et al., C_{60} was further produced by H. Ajie et al. in 1991 from the evaporation of carbon rods but this time by heating it resistively [220]. Later in 1992, growth of fullerenes was reported from R. F. Bunshah et al. by electron beam evaporation and sputtering of graphite [221], further in 1994, extraction of C_{60} ion beam was reported from S. Chuanchen et al. from a hollow cathode ion source [222], and many more methods were used including the usage of low-pressure diffusion flame from P. Hebgen et al. [223], arc discharge method from M. Caraman et al. [224]. Besides this wide range of synthesis, due to their unique physical [225], electrical [226], optical [227] and chemical properties [228] of fullerenes lead them to many fields with potential applications in ion storage [229], photovoltaics [230], sensors [231], supercapacitors [232] etc. Despite fullerene's insolubility to the water which was further settled by functionalizing or doping with impurity atoms, it is soluble in a wide range of common solvents in room temperature, and 47 of them were reported R. S. Ruoff et al. for C_{60} fullerene back in 1993 [233]. Hence, moderated solubility in the polar mediums along with several other enchanted properties like hydrophobicity, biocompatibility [50] etc. made fullerenes one of the front liner in the biological applications like antibacterial activity [234], antiviral activity [235], drug delivery [236], drug sensing [237] etc. In this section, we aim to review the recent scientific reports on the drug delivery and sensing application of carbon fullerenes which were made by the first-principles investigation.

As several drugs require interaction with DNA and RNA, these drugs sometimes have a structure like DNA and RNA nucleobases which made the investigations on the adsorption properties of the nucleobases towards an adsorbent so crucial in drug delivery application. So, following the trend, A. S. Rad made the first-principles investigation using DFT theory on the adsorption properties of a purine derivative nucleobase, Adenine, on the Cr and Ni-doped C_{20} fullerene [238]. Considering the dispersion forces and exchange-correlation energies, all structures were optimized using meta-hybrid functional ωB97XD and a GGA functional Perdew–Burke–Ernzerhof (PBE) respectively along with 6-31G (d, p) basis set which is widely used to investigate the drug delivery systems. Chemisorption of the adenine nucleobase towards the both Cr and Ni-doped C_{20} fullerenes were reported with negative adsorption energies as high as −48.99 and −47.94 kcal/mol respectively with a charge transfer of 0.136e and 0.127e between the adenine and respective doped structure observed from NBO analysis. However, the adsorption process of adenine was spontaneous and exothermic in both Cr and Ni-doped structures with negative values for change in enthalpy (ΔH) and Gibbs free energy (ΔG) ranging −45.10 to −47.49 and −31.69 to −33.82 kcal/mol respectively for various orientation of adenine in the

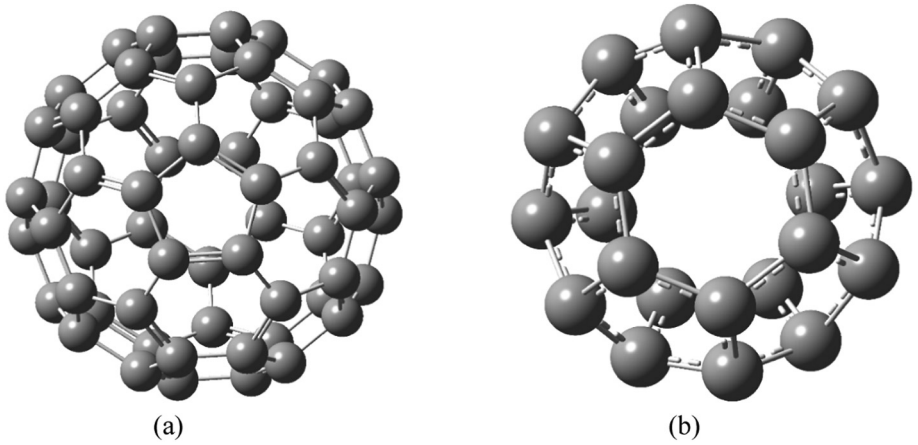

Fig. 10. (a) C_{60} and (b) C_{24} fullerene nanostructures optimized using DFT theory with B3LYP hybrid exchange correlational functional and 6-31G, 6-31G (d,p) basis sets respectively.

top of Cr and Ni-doped fullerenes. An increase in the dipole moment was observed as high as 11.8 and 10.1 Debye for the adsorption of adenine on Cr and Ni-doped C_{20} fullerenes. Finally, a variation of Fermi levels and H-L energy gaps were observed as −3.852 to −4.606 eV and 5.402 to 5.888 eV respectively for the investigated structures. These adsorption properties of Cr and Ni-doped C_{20} fullerenes made themselves a promising medium for adenine adsorption.

Besides the report from M. Vatanparast et al. on the delivery of 5-fluorouracil (FU) drug using AlN and BN doped GQD [133], another first-principles investigation was made by A. Hosseinian et al., on the interaction of FU with C_{24} fullerene using DFT theory with dispersion corrected B3LYP-D functional and 6-31G* basis set [239]. A very weak interaction of FU was observed towards the pristine C_{24} fullerene with a maximum adsorption energy of −3.2 kcal/mol along with a H-L energy gap of 1.86 eV and an inferior charge transfer of 0.008e (from NBO analysis). This interaction was further enhanced by doping a B atom to the fullerene structure. For B doped C_{24} fullerene the adsorption energy of FU was observed as high as −27.2 kcal/mol with a decreased bandgap of 1.54 eV along with a significantly increased charge transfer of 0.209e (from NBO analysis). Finally, they have reported a successful release of the FU drug to the low pH (<6) targeted area with a cancerous cell.

Similar to the adsorption behaviour of FU towards C_{24} fullerene, Y. Gökpek et al., observed a weak physisorption interaction between 4-phenylpyridine (4-phpy) and pristine C_{60} fullerene while the adsorption energy was increased significantly due to the doping of C_{60} fullerene with B or Si [240]. The dispersion corrected (with M062X functional) DFT study found that 4-phpy was adsorbed on a pristine C_{60} with an adsorption energy of −6.69 kcal/mol in the water phase where this value was significantly increased to −41.65 and −50.31 kcal/mol for B and Si-doped C_{60} fullerenes (BC_{59} and SiC_{59}) respectively. The solvation energy of 4-phpy was also increased to −7.72 and −13.19 eV for BC_{59} and SiC_{59} structures respectively while it was only −4.65 eV for pristine C_{60} fullerene. The H-L energy gap was decreased from 4.506 eV for 4-phpy-C_{60} to 3.582 and 3.584 eV for the 4-phpy-BC_{59} and 4-phpy-SiC_{59} respectively with an NBO charge transfer of −0.454e and −0.655e respectively. These adsorption properties of 4-phpy with pristine and B or Si-doped C_{60} fullerenes was slightly diminished in the gaseous phase. Observing these enhanced properties for the 4-phpy-BC_{59} and 4-phpy-SiC_{59} systems led them to conclude BC_{59} and SiC_{59} as potential structures to carry 4-phpy into drug delivery applications.

The SiC_{59} system was again subjected to study by M. Moradi et al., but this time accompanied by AlC_{59} to investigate their interactions with Phenylpropanolamine (PPA) drug [241]. PPA is used as a most used decongestant and also marked as a potentially hazardous drug due to its side effects like hypertension, cardiovascular side effects including a potential risk of hemorrhagic stroke [242–244]. Similar to 4-phpy, PPA had weak physisorption with pristine C_{60} fullerene structure with an adsorption energy of −0.1 kcal/mol with a 23.8% decrease in the H-L energy gap to 2.24 eV. This interaction was significantly enhanced due to the doping of C_{60} with Al atom, where the adsorption energy of PPA was increased to −73.9 kcal/mol with an 8.6% decrease to the bandgap to 1.58 eV. But the most stable structure to adsorb PPA was found as Si-doped C_{60} structure with the highest adsorption energy of −86.0 kcal/mol with a significant 30.3% drop in the energy gap to 1.56 eV. This fall in the bandgap increased the electrical conductivity of PPA-SiC_{59} complex, which made SiC_{59} structure most sensitive towards the PPA detection. But in another study lead by A. S. Ghasemi et al., the Al-doped C_{60} fullerene showed a promising behaviour to detect and carry penicillamine drug which is commonly used to treat Wilson's disease and rheumatoid arthritis [245–247]. Al—C_{60} adsorbed penicillamine with an adsorption energy of −41.83 kcal/mol but increasing the dipole moment to as high as 18.63 debye and decreasing the work function as low as 3.89 eV. This increase in the reactivity was further confirmed by the global reactivity descriptors where the ionization potential along with the electrophilicity and global hardness decreased with an increase in the global softness for the Al—C_{60} complex.

The rising importance on the detection of the illicit drug to the medical community and law enforcing agency lead S. Bashiri et al., to investigate pristine and several doped C_{60} fullerenes for its sensing ability to a central nervous system (CNS) stimulant, amphetamine (AA) which is medically used to treat attention deficit hyperactivity disorder but is a habit-forming and highly potential drug for abuse [154,248,249]. The pristine C_{60} fullerene showed a good sensitivity towards the AA drug with a low bandgap of 1.91 eV and a work function of 4.60 eV but with weak physisorption with an adsorption energy of −1.2 kcal/mol. Doping the fullerene with B, Al, Ga, Si, and Ge significantly increased the adsorption energy whereas the most stable structure was Al—C_{60} with adsorption energy as high as −65.6 kcal/mol while it was −59.2 and −47.1 for Ga and B doped C_{60} fullerenes respectively. But the most promising performance was found from Si and Ge doped C_{60} fullerenes with a moderate adsorption energy of −50.0 and −38.6 kcal/mol but with a 22.7% and 24.9% reduction to the work function down to 3.94 eV for both case. Hence Si and Ge doped C_{60} fullerenes were concluded as a potential sensor for the AA drug detection. C. Parlak et al. further studied these structures for a drug sensor and carrier for antiviral drug amantadine, which is used to treat or prevent influenza-A, Parkinson's disease but comes with side effects like corneal edema [250–252]. All doped structures showed a promising performance as a sensor and carrier for the amantadine drug with adsorption energies ranging around −28 to −51 kcal/mol which was further increased in the water solution and energy gap around 2 eV which was further reduced in the water solution.

Besides doping an adsorbent with impurity atoms, a noticeable change in the adsorption properties can be found due to the solvents, different isomers of the adsorbate drugs etc. which was further analyzed by O. Ergürhan et al., in their investigation on the interaction of hydroquinone (HQ) with pristine and doped C60 fullerenes [253] (Table 1).

It was observed that the isomerism of HQ played a negligible role in the adsorption properties as the values for adsorption energies, energy gap etc. were almost same for cis and trans isomers of HQ, however as always doping altered the adsorption properties significantly. The low adsorption energy (BSSE corrected) as −3.22 kcal/mol of HQ-cis towards C_{60} fullerene increased significantly to −13.71 and −18.41 kcal/mol for B and Si-doped C_{60} fullerenes respectively. In the water solution, these adsorption energies became −2.62, −16.05 and −25.10 kcal/mol for pristine, B, and Si-doped C_{60} fullerenes. Although low adsorption energy was observed due to the adsorption HQ-cis towards pristine C_{60} fullerene, a sharp 25.89% drop in the energy gap was observed while this drop was 10.64% and 0.74% for B and Si-doped C_{60} fullerenes respectively. But in the water solution, a less reduction of 13.16% in the energy gap was observed for pristine C_{60} fullerene while a higher reduction of 14.05% and 6.08% was observed for the BC_{59}-HQ and SiC_{59}-HQ complexes. The effect of basis set in the calculation significantly altered the values for adsorption energies but with an ambiguous pattern. While ccpvdz basis set estimated 40.99% larger value for the adsorption energy for C_{60}- HQ structure compared to the 6-31G (d) basis set, in case of BC_{59}-HQ and SiC_{59}-HQ it overestimated 2.41% and underestimated 5.81% respectively. This clearly showed that it is crucial to choose basis sets wisely to study the interaction HQ with C_{60} fullerenes.

Earlier in this work, we have discussed the SWCNT as a drug delivery system for isoniazid (INH), and ibuprofen (IBP) which was reported by N. Saikia et al. [182] and C. Parlak et al. [206], the interaction of INH and IBH were further studied for the various carbon fullerenes too. M. Li et al. reported Si-doped C_{70} fullerene as an efficient INH sensor between pristine, Si, and Al-doped C_{70} fullerenes [266]. INH was weakly adsorbed towards the pristine C_{70} fullerenes with an adsorption energy of −1.3 kcal/mol, but for Al and Si-doped C_{70} fullerenes, it increased to −67.9 and −51.3 kcal/mol, respectively. Despite having enormous adsorption energy for INH, Al—C_{70} suffers from sensing INH with a negligible change in the bandgap and work function which was unlikely to the Si—C_{70} structure with a significant decrease in the bandgap from 2.24 to 1.12 eV. In other work, M. K. Hazrati et al. made a significant change in the C_{60} fullerene with doping its carbon atoms with 15 B and 15 N atoms which constituted $C_{30}B_{15}N_{15}$ heterofullerene, and it sensed and adsorbed INH drug significantly [255]. For interaction between the $-NH_2$ head of INH drug and a B atom of $C_{30}B_{15}N_{15}$ heterofullerene, the adsorption energy was observed as −21.95 kcal/mol with a significant decrease of 13.54% to the bandgap which became 0.83 eV. For a drug delivery system of IBP drug E. Alipour et al. modified C_{60} fullerene by substituting its five carbon atoms by 4 N atoms and one TM atoms between Fe, Co, and Ni which formed TMN_4C_{55} system [254]. While NiN_4C_{55} was reported to have a higher sensitivity towards IBP drug, NiN_4C_{55}, CoN_4C_{55}, and FeN_4C_{55} adsorbed IBP with acceptable adsorption energies of −23.11, −17.81, and −18.07 kcal/mol, respectively including −13.14 kcal/mol for the pristine C_{60} fullerene hence was considered potential systems for the IBP drug delivery.

Besides drug delivery and drug sensor, C_{60} fullerenes were also studied by M. F. Kaya et al. to perform as a sensor for the phenylalanine (PHE) amino acid, a high concentration of which in the blood can lead to mental retardation [256,267,268]. Using M062X/6-31G (d) level of theory, the maximum binding energy of the PHE towards pristine C_{60} fullerene, AlC_{59} and, SiC_{59} was calculated as −5.97, −52.15, and −36.07 kcal/mol respectively in the gas phase, except pristine C_{60} which was further increased to −5.24, −60.09, and −48.70 kcal/mol respectively in the water solvent phase. The doping of Al and Si atoms reduces the bandgap of the structures significantly. For Phe-C_{60} the bandgap in the gas(water) phase was observed as 4.50 (7.42) eV which dropped down as much as 3.05 (3.11) and 3.68 (3.54) eV for the Al and Si-doped C_{60} fullerenes with an NBO charge transfer of −0.976e and −0.954 from N atom of PHE to the Al and Si atoms of the adsorbent respectively. Due to the alternation in the adsorption properties of PHE towards AlC_{59} and, SiC_{59} made them a potential sensor for the PHE amino acid while pristine C_{60} suffered from weak adsorption.

3.4. Miscellaneous carbon-based LDNs for drug delivery and sensing applications

3.4.1. Graphene oxide

Currently, a popular method to synthesis the graphene is to reduce the GO into GNS [112]. But the synthesis of the GO was dated back to 1859 when B. C. Brodie reported the first synthesis of GO during his investigation on the various properties of graphite [269]. This Brodie synthesis method along with a slightly improved model from L. Staudenmaier in 1898 was mostly used to synthesis until another improved model was proposed by W. S. Hummers and R. E. Offeman in 1958 by oxidizing the graphite with a water-free mixture of potassium permanganate ($KMnO_4$), sodium nitrate ($NaNO_3$), and concentrated sulfuric acid (H_2SO_4) which is popularly known as the Hummers method and is one of the most popular methods to synthesis GO till now [270,271]. Based on these methods till now there is an unambiguity on the exact structure of GO, but this nonconductive hydrophilic allotrope of carbon lead it to be applied extensively in biomedical and therapeutic applications including the drug delivery and sensing [272,273].

Pristine GO was found to be a potential drug delivery system for sumatriptan (STT), a medicine used to treat migraine headaches [260]. The dispersion corrected DFT study lead by Z. Jafari et al. found that GO adsorbed STT drug with acceptable adsorption energy to be used as a drug delivery system while the drug was reported to induce many chest symptoms [274]. In the water phase, the STT drug was adsorbed with an adsorption energy of −10.59 kcal/mol to GO with a dipole moment of 10.22 debye and solvation energy of −34.24 kcal/mol. The observed H-L energy gap of STT as 5.0385 eV was further reduced to 0.2599 eV for STT-GO while it was 0.2536 eV for GO. A −0.17e charge transfer was observed from GO to STT with a Fermi energy level of −3.9158 eV. These interactions were further supported by the global reactivity descriptors where global hardness was increased to 0.1299 eV with a decrease to the global softness and the electrophilicity to 3.8491 eV^{-1} and 59.0201 eV respectively. This result from the interaction of STT drug with GO leads them to conclude GO as a potential carrier for the STT drug.

Like other allotropes of carbon, GO was further reported as a potential drug system for several anticancer drugs. Z. Hasanzade et al. made a DFT investigation on the interaction of ellipticine (EPT) anticancer drug with pristine GO nanosheet (GONS) and observed the effects of pH and solvents on the interaction using various solvents, e.g. water, ethanol and dimethyl sulfoxide (DMSO) [262]. In the gaseous environment, the EPT drug was adsorbed with a maximum adsorption energy of −28.04 kcal/mol where the maximum rise in the dipole moment was observed as 9.454 debye. In the water phase, a significant decrease in the adsorption energy was observed with a maximum of −22.11 kcal/mol along with a considerable increase in the dipole moment to 15.537 debye where EPT was dissolved with solvation energy ranging from −21.91 to −24.55 kcal/mol for different orientation of EPT. The effects of DMSO and ethanol was almost comparable with water as the adsorption energy and dipole moment were ranged between −16.30 to −22.21 kcal/mol and 10.052 to 15.364 debye for DMSO. In contrast, for ethanol, it was −16.44 to −22.41 kcal/mol and 9.883 to 15.014 debye, respectively. As EPT failed to alter the E_g of GONS, it may not work as a sensor for EPT. Still, it can be a potential drug delivery system which was further supported by the interaction of EPT with GONS in low pH regions as cancerous cells were reported to be slightly acidic.

For another anticancer drug doxorubicin (DOX) delivery, P. Gong et al. decorated GO with fluorine (FGO) to enhance the drug release mechanism in low pH regions [275]. However, a high DOX loading capacity was observed for the water-soluble FGO where non-covalent bonds were dominated in the loading and release mechanism of DOX hence made FGO a promising candidate for the DOX delivery. In their other work, they reported the synthesis of FGO with amino-polyethylene glycol and reported its potential use in the DOX and another anticancer drug camptothecin delivery [261].

3.4.2. Graphyne and graphdiyne

Besides the purely sp^2 hybridized GNS, another sp. and sp^2 hybridized allotrope of carbon, graphyne was also studied for medical applications using first-principles calculations. The graphyne nanosheet (GpNS) was reported as a potential drug carrier for anticancer drug 5-fluorouracil (5-FU) and quercetin [90]. In the surface of GpNS, the most stable interaction of 5-FU was observed with an adsorption energy of −14.87 kcal/mol where quercetin was adsorbed with −17.59 kcal/mol. A charge transfer of 0.580e and 0.741e was observed for between the GpNS and, 5-FU and quercetin respectively with a maximum drop of 63.64% and 69.09% in the energy gap lead to 0.20 eV and 0.17 eV respectively. With the increasing reactivity observed from the quantum reactivity descriptors, an increase in the adsorbent-adsorbate distance due to the protonation ensured the ability of GpNS to deliver 5-FU and quercetin to the target cancerous cell. GpNS was also investigated as a sensor to sense the cytosine and guanine nucleobases [265]. GpNS adsorbed the cytosine and guanine with an adsorption energy of −14.69 and −14.27 kcal/mol with a significant amount of 34.03% and 53.47% reduction in the H-L energy gap, respectively. This reduction in the bandgap indicated the increase in the electrical conductivity due to the adsorption of the nucleobases to the GpNS ensured the cytosine and guanine sensing ability of the GpNS.

Another graphyne like structure with carbon atoms is graphdiyne was reported to be synthesized by Guoxing Li et al. in 2010 by a cross-coupling reaction using hexaethynylbenzene on the copper surface [276]. Graphdiyne was also subjected to study as a potential drug delivery system for anticancer drugs. The interaction of two anticancer drugs sorafenib (STB) and regorafenib (RTB) with graphdiyne nanosheet (GdNS) was investigated by U. Srimathi et al. using DFT theory with GGA based PBE functional [263]. STB that is used to treat thyroid [277] and kidney cancer [278] often come with several side-effects like alopecia, arthralgia, hypertension etc. [279–281] whereas RTB is used to treat liver and colorectal cancer [282,283] but sometimes comes with deadly side effects with severe liver damage [284]. STB was adsorbed by the GdNS with a maximum adsorption energy of −15.22 kcal/mol with solvation energy of −40.31 kcal/mol and Eg of 0.46 eV when for RTB these values were observed as −14.78 kcal/mol, −29.61 kcal/mol and 0.34 eV. A further alteration in the band structure was observed due to the adsorption of STB and RTB. Finally, in the low pH regions similar to the cancer cells regions, the bond length between the GdNS and STB, RTB increased noticeably, which ensured the drug release in the low pH regions. Another anticancer drug, flutamide (FLU), which was reported to make weak physisorption on CNT, a study by V. Nagarajan et al. revealed strong chemisorption of FLU drug with the graphdiyne nanotube (GdNT) [264]. In the most stable interaction, FLU was adsorbed by the GdNT with an adsorption energy of −18.31 kcal/mol and solvation energy of −29.59 kcal/mol along with a 56.49% reduction to the energy gap to 0.238 eV which lead to a charge transfer of 0.228e between the FLU and GdNT. Due to the interaction of the FLU with GdNT, the chemical potential and global hardness decreased with an increase in the electrophilicity, which indicated the enhancement in the reactivity of the structures. While the minimum adsorbent-adsorbate distance was observed as 1.33 Å, this was raised up to 2.34 Å for lowering the pH by protonation, which ensured the drug release capability of GdNS in slightly acidic cancerous cell environment. Hence, GdNS was concluded as a potential FLU drug delivery system.

The interaction of several other drugs like azathioprine, mesalamine, and hyoscyamine to be delivered to the targeted area using GdNT was also reported by the same group [285]. In a first-principles investigation using dispersion corrected DFT theory showed that the GdNT strongly adsorbed the azathioprine drug with an adsorption energy of −24.88 kcal/mol in its most stable position whereas the mesalamine and hyoscyamine were adsorbed with an adsorption energy of −22.09 and −29.59 kcal/mol respectively with solvation energy ranging from −116.82 to −117.82 kcal/mol. Though a 33.08% decrease in the energy gap to 0.089 eV was observed for the azathioprine drug adsorption on GdNT, it further dropped to 0.026 and 0.028 eV respectively for the mesalamine, and hyoscyamine with 80.45% and 78.95% decrease respectively. The reactivity of the structures was also studied using quantum reactivity descriptors. Finally, a significant increase in the adsorbent-adsorbate bond length in the lower pH region ensured the drug release at the targeted site.

3.4.3. BC_3 and BCN

The interaction of BCl_3 with C_6H_6 benzene at a very high temperature of 800° C created a new type of graphite-like nanosheet but less stable than graphite known as BC_3, a theoretically relaxed structure of which is displayed on Fig. 11 [286,287]. This BC_3 nanosheet (NS) and nanotube (NT) was further studied by A. R. Moosavi-zare et al. to sense an illicit CNS stimulant amphetamine (AA) which was also reported to be adsorbed by pristine and Si, Ge doped C_{60} fullerenes [248,257]. It was observed that the BC_3 NT adsorbed AA more strongly than the BC_3 NT with an adsorption energy of −15.5 kcal/mol where it was −10.7 kcal/mol for the BC_3 NS. Despite stable adsorption, BC_3 NS and NT were not considered as a sensible sensor for AA drug as a very poor decrease of 3.1% and 5.1% in the energy gap was observed. This was surmounted by doping BC_3 with a Si atom which reduced the energy gap by 26.6% and 58.7% for BC_3 NS and NT respectively in case of AA adsorption. Besides the Si-doped BC_3 NS and NT was found to adsorb AA drug more strongly with an adsorption energy of −21.3 and −24.5 kcal/mol respectively. Despite this most stable and sensible for AA drug, Si-doped BC_3 NT suffers from a considerable recovery time of 87.5 s where it was only 0.4 s for Si-doped BC_3NS. Hence Si-doped BC_3 NS was considered as a potential sensor to sense the amphetamine drug.

BC_3NT was further modified into BC_2N NT to work as a sensor for β-keto-amphetamine or simply cathinone (CT) [258]. Akin to the pristine BC_3 NS and NT, BC_2N NT also suffers from a reduction in the energy gap by only 3% while it adsorbed CT with adsorption energy as high as −14.6 kcal/mol. Though Al-doped BC_2N NT solved the problem with a 41.5% reduction in the energy gap with a very strong adsorption of CT drug with an adsorption energy of −43.9 kcal/mol, it suffers from a considerable recovery time. Besides, Si-doped BC_2N NT had a recovery time of 0.27 s and was considered as most sensible to the CT with a 55.8% decrease in the energy gap due to the adsorption of CT with an adsorption energy of −15.7 kcal/mol. Finally, the interaction of an amino acid glycine with BC_2N NT was also reported by A. Soltani et al. [259]. Glycine made strong chemisorption with the sidewall of BC_2N NT with a dipole moment ranging from 15.35 to 37.40 debye for different orientations resulting an increased reactivity due to the adsorption of glycine which was further verified from the global reactivity parameter analysis.

4. Boron-based LDNs for drug delivery and sensing applications

4.1. Hexagonal boron nitride nanosheet

Another graphene alike 2D nanosheet, BNNS made of boron and nitrogen atoms, is alternatively known as “White Graphene” due white colour and graphene-like sp^2 bonded hexagonal honeycomb structure with D_{6h} symmetry as shown in Fig. 12. The BNNS is highly popular for its higher thermal and chemical stability compared to graphene

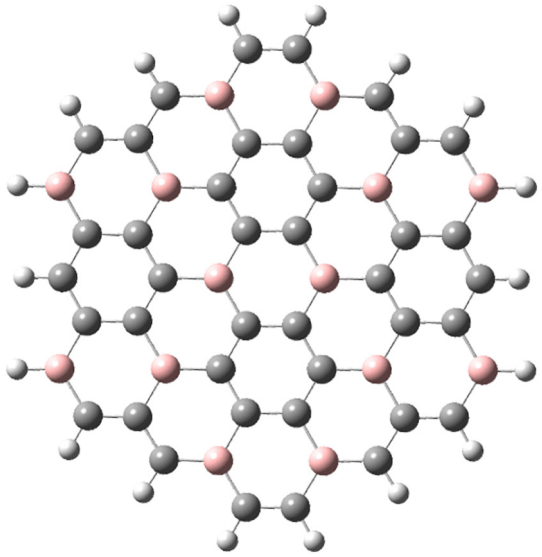

Fig. 11. BC_3 nanostructure optimized using DFT theory with B3LYP hybrid exchange correlational functional and 6-31G basis set.

while it has a very high melting point e.g. the hexagonal BNNS (BNNS) platelets showed thermal stability up to ~1000 °C in an investigation made by N. Kostoglou et al. [289]. The thermal conductivity of the BNNS is also comparable to the graphene as the thermal conductivity for the BN nanoribbon is observed as ~1700–2000 W m^{-1} K^{-1} at the room temperature [290]. On the other hand, while graphene works as a zero bandgap semiconductor material, with a large bandgap of ~5.5 eV BNNS works as an insulator or wide bandgap semiconductor material which help BNNS to exhibit several unique optical properties [38]. Besides, the BNNS can be synthesized with the large surface using numerous methods including the popular CVD methods for a large scale production [291–293]. These alluring properties and sufficiently available synthesis methods made BNNS to be applied as a catalyst [294,295], dielectric material [296,297], high temperature application [298], UV photodetector [299], energy storage device [300], sensor [301–304] etc. Finally, the biocompatibility of BNNS

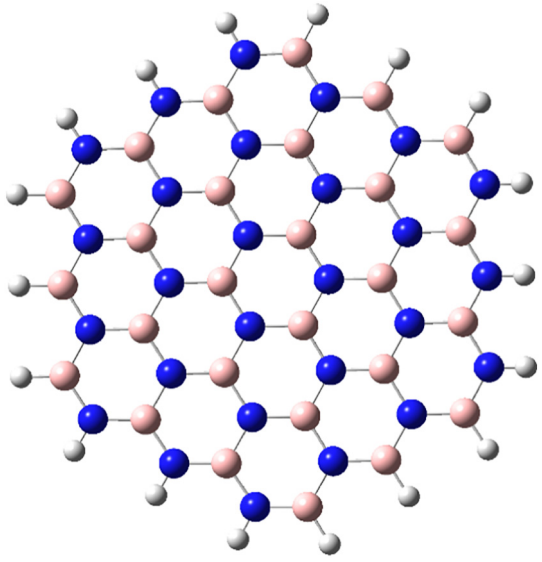

Fig. 12. Hexagonal BNNS optimized using DFT theory with B3LYP hybrid exchange correlational functional and 6-31G basis set.

[305] leads them to the biomedical applications like drug sensors and drug delivery which will be reviewed in this section of our study.

It was previously observed that many anticancer drugs have a structure like nucleobases as the operation of these drugs includes interactions with DNA and RNAs. Several of these anticancer drugs 6-mercaptopurine (MP), 6-thioguanine (TG) and 5-fluorouracil (FU) which have structures akin to nucleobases adenine, guanine and uracil were subjected to be studied by M. Vatanparast et al. for an efficient drug delivery system as they have a significant amount of side effects and they came up with BNNS on this purpose [99]. All three anticancer drugs made spontaneous adsorption to the BN, which was confirmed from the negative values for the adsorption energy and change in Gibbs free energies. Hexagonal BNNS showed decent drug delivery properties for the FU and MP drugs, where the most promising result was observed for the TG drug. While BN adsorbed FU and MP drug with an adsorption energy of −19.59 and −23.19 kcal/mol, it was −26.53 kcal/mol for the TG drug. Another important property for the drug delivery application, dipole moment, indicating the solubility of the system in a polar medium, was also as high as 10.675 Debye for TG-BN complex while it was only 5.292 and 5.797 Debye for FU-BN and MP-BN complex. This increased reactivity of the structures was also observed from the quantum reactivity descriptors where global hardness was decreased with an increase to the chemical potential and electrophilicity. Though the HOMO-LUMO energy gap (H-L gap) decreased in case of all three drug adsorption on the BN, the least was observed as 4.30 eV for the TG adsorption with a maximum of 5.16 eV for FU adsorption while it was 5.07 eV for MP adsorption. The interaction of the drugs with BNNS was closed-shell non-covalent in nature as the total electron energy density was observed positive with $-G_b/V_b > 1$ in the QTAIM analysis where G_b indicates kinetic electron energy density and V_b represents potential electron energy density. Finally, a decrease in the adsorption energy of those drugs with BN in the acidic medium confirmed their drug release in the low pH cancerous cell area. In another study, instead of any drug with the structure like a nucleobase, J. Castro-Medina et al. investigated the interaction of thymine, a pyrimidine nucleobase, with BN [306]. It was observed that the among 4 × 4, 5 × 5, and 6 × 6 BN, thymine was adsorbed more strongly towards 6 × 6 BN with an adsorption energy of −38.37 kcal/mol which was further increased to −60.63 kcal/mol in case of an Al atom doping. Hence the size of the nanosheet along with doping it with impurity atoms plays a significant role in the drug adsorption.

Furthermore, using Van Der Waals corrected DFT theory (DFT-D2), S. D Dabhi et al. proposed a sensor to sense all DNA and RNA nucleobases using one-dimensional armchair and zigzag boron nanoribbons (BNNR) which can also be further applied for DNA sequencing purpose [307]. The adsorption profile of the nucleobases adsorbed in parallel with the armchair BNNR (A-BNNR) was observed as G > T > A > U > C with adsorption energies ranging from −8.95 to −14.39 kcal/mol with an adsorbent-adsorbate distance ranging as 2.73 Å to 2.95 Å. The A-BNNR responded towards all the nucleobases significantly by decreasing the H-L energy gaps ranging as 3.25 eV to 3.73 eV while it was 4.89 eV for the A-BNNR alone. The least H-L energy gap was observed for C + A-BNNR complex as 3.25 eV indicated that A-BNNR was most sensitive towards cytosine (C) and least towards adenine (A). On the contrary to the H-L energy gap, the work function of the A-BNNR increased noticeably with adsorption of the nucleobases. The zigzag BNNR (Z-BNNR) also followed the same trend upon the adsorption of nucleobases. But the adsorption energies were this time observed as G > C > A > T > U with a range of −13.07 to −18.33 kcal/mol. Z-BNNR was also most sensitive towards the C with a least H-L energy gap 3.37 eV following by G, U, T, and A. Here, the work function again increased upon the adsorption of the nucleobases towards the Z-BNNR. Hence the BNNR may not function as a work function based sensor but holds the potential of an electronic sensor to detect nucleobases.

In several other theoretical studies, the performance of BNNS was compared with other BN nanostructures for several other drug sensing.

K. Nejati et al. made a first-principles investigation using DFT theory with B3LYP hybrid functional on the interaction of cathinone drug with BNNS, zigzag (6, 0) BNNT, and $B_{12}N_{12}$ nanocage (BNNC) [308]. Though the BNNS showed a moderate sensitivity towards cathinone, it failed to adsorb the drug sufficiently. For different orientations of cathinone, BNNS adsorbed with adsorption energies of −0.5 and −5.0 kcal/mol with a decrease in the H-L energy gap 23.0% and 12.9% respectively. The same trend was observed with BNNT while it failed to adsorb cathinone if shows sensitivity towards the drug. Though BNNT still showed more enhanced performance than BNNS by adsorbing the drug with adsorption energies as −2.6 and −14.0 kcal/mol for different orientations, with a decrease in the H-L energy gap by 27.6% and 15.5%. The NBO charge transfer was also greater in the BNNT from cathinone as 0.15e and 0.24e while it was only 0.03e and 0.09e respectively for BNNS. The most alluring sensing properties towards cathinone was observed from BNNC while it adsorbed the drug with adsorption energies as −5.8 and −16.1 kcal/mol with a significant decrease in the H-L energy gap as 57.0% and 46.0% respectively. The NBO charge transfer from cathinone to BNNC was observed as 0.25e and 0.33e made it a potential candidate for the development of an electronic sensor to detect cathinone drug. Besides, all three nanostructures benefit from a short recovery time of 0.54 s for BNNC following by 0.02 s for BNNT, and 4.4 ns for BNNS at the room temperature of 298 K.

The BNNS, BNNT, and BNNC also showed the same sensing properties towards another anticancer chemotherapeutic drug, mercaptopurine (MP), which was revealed by S. A. Aslanzadeh from DFT calculations using B3LYP/6-31g (d) level of theory [309]. Alike from cathinone, BNNS also showed inferior adsorption properties towards MP with an adsorption energy of −3.2 kcal/mol with a decrease in the H-L energy gap only by 0.5%. This time also the most sensitivity and the most stable adsorption of MP was observed with BNNC. BNNC adsorbed the MP drug with maximum adsorption energy −28.6 kcal/mol while the range of decrease in H-L energy gap was observed as 47.8% to 51.9%. But due to this strong adsorption, this time the BNNC suffered from an unrealistic high recovery time of 8.8×10^8 seconds. Besides this time, the most promising adsorption behaviour of MP drug was observed from BNNT. BNNT adsorbed the drug with a decent maximum adsorption energy of −18.7 kcal/mol while the decrease in H-L energy gap was observed from 43.3% to 46.3% for different orientations of the drug. Besides, the BNNT also benefits from a shorter recovery time of 49.5 s at the room temperature of 298 K. Hence, BNNT holds the most potentiality in the development of an electrochemical sensor to detect MP drug.

4.2. Boron nitride nanotube

After the discovery of CNT in 1991 [150], the novel properties of BNNS lead to the successful discovery of another polymorph of graphitic BN, BNNT in 1995 by N. G. Chopra et al. [310] shortly after its theoretical prediction in 1994 [311]. By that time, the availability of many different methods to grow CNT and BNs lead BNNTs to be synthesized using many popular methods like arc discharge [312], ball mailing method [313], laser ablation method [314], and chemical vapour deposition (CVD) [315]. Being made of BNs the BNNT also shares the similar properties as BNNS like high thermal and chemical stability [316,317], high thermal conductivity [318], high oxidation resistance [319] and a wide insulating bandgap of ~5.5 eV [320]. Besides, having a tubular structure provided it excellent mechanical strength with the elastic modulus in TPa level as CNT [321]. These properties made its applications as nanocomposites [322], nano light source [323], oil-polluted water treatment [324], radiation shielding [325], sensor [97,326,327] etc. Finally, BNNTs were found to be non-toxic to the human body and biocompatible, which lead it to many biomedical applications [328–331].

An efficient sensor for the broadly used sulfonamide (SA) antibacterial drugs is crucial to the medical community as it causes an adverse reaction to the 3% of its general consumers which rises 60% to the patients with human immunodeficiency virus (HIV) [332]. Hence Z. Rahmani et al. made a first-principles investigation on the BNNT and several other doped (Al, Si) BNNT using DFT theory along with M06-2X functional and 6-311G (d) basis set to study their SA drugs sensing ability [333]. Unlike the majority of the drug sensors, in this case, pristine BNNT performed as a better SA drugs sensor than Si and Al-doped BNNT. In the most stable position, BNNT adsorbed SA drugs with an adsorption energy of −25.41 kcal/mol with an 18% reduction to the H-L energy gap. Though the value for adsorption energy increased dramatically for Al-doped BNNT to −59.73 kcal/mol, it failed to decrease the energy gap significantly, which was only 6.2%. Hence with this poor sensing ability but strong adsorption of SA drug made Al-BNNT a decomposition agent for SA drugs. For, Si-BNNT the SA drug was adsorbed with an adsorption energy of −51.69 kcal/mol at the most stable orientation but increased the H-L energy gap by 19.8% which was enhanced in another orientation where SA decreased H-L energy gap by 28.7% but was adsorbed with an adsorption energy of −4.5 kcal/mol only. So, Si-BNNT is not ideal to be used either as a sensor or to decompose SA drug.

The popular anticancer drug 5-fluorouracil (FU) which was reported to be carried out by several carbon and boron-based nanoclusters, is also reported to make strong chemisorption with zigzag and armchair BNNT. From a first-principles investigation lead by A. Soltani et al., it was observed that the (8, 0) zigzag BNNT adsorbed FU more strongly with a reduction in the H-L energy gap significantly with an increase in the dipole moment (DM) compared to the (5, 0) zigzag BNNT [132]. The (5, 0) zigzag BNNT adsorbed FU with an adsorption energy of −2.54 kcal/mol with a DM of only 5.08 debye and an increase in the H-L energy gap by 0.8% whereas the (8, 0) zigzag BNNT adsorbed FU with an adsorption energy of −3.00 kcal/mol with an increased DM of 12.73 debye and decrease in the H-L energy gap by 10.89%. So they further doped (8, 0) zigzag BNNT with Al, Ga and Ge to enhance the adsorption of FU to BNNT. The most promising result was observed for Al-doped (8, 0) zigzag BNNT (Al-BNNT) where it adsorbed FU strongly with chemisorption of −42.89 kcal/mol with a significant decrease in the energy gap by 38.01% where the DM was observed as high as 19.13 debye. After that, a promising result was also observed from the Ga-BNNT where it adsorbed FU with an adsorption energy of −34.59 kcal/mol and decreased the H-L energy gap by 39.02% with a DM of 16.37 debye. Among doped BNNT the least promising performance was observed from Ge-BNNT but better than the pristine (8, 0) zigzag BNNT. Ge-BNNT adsorbed FU with an adsorption energy of −12.22 kcal/mol with a cut to the H-L energy gap by 28.91% and an increase in the DM to 13.42 debye. This increase in the reactivity was further verified from a decrease in the global hardness and changes in the global reactivity parameters accordingly. Though the adsorption process of FU drug to the (8, 0) zigzag BNNT wasn't spontaneous as it was seen from the change in Gibbs free energy (ΔG), for Al and Ga doped BNNT it was spontaneous with a negative value for ΔG. And the adsorption process of FU to all adsorbent was exothermic with a decrease in the entropy. So analyzing the results, they came to a conclusion that Ga-BNNT can be used as a potential drug delivery system for FU for its enhanced NBO charge transfer properties where Al-BNNT can be a potentially stable sensor FU with high adsorption energy and reduction in the H-L energy gap. Besides zigzag BNNT, K. Shayan et al. investigated the interaction of FU with a wide number of armchair BNNT [334]. Though the armchair BNNTs adsorbed FU with less adsorption energies compared to the zigzag BNNTs, from a detailed analysis of thermodynamical parameters, charge transfer, and global reactivity descriptors it was revealed that armchair BNNTs also could be a potential drug delivery systems to deliver FU drug.

The DFT theory with M06-2X and B3LYP exchange correlational functional with 6-31G* basis set was also employed to investigate the –OH functionalized (6, 0) zigzag BNNT (f-BNNT) as a drug delivery system for another anticancer drug carmustine (BCNU) [91]. BCMU is a potential anticancer drug that is used to treat many kinds of brain cancers

for over few decades, but sometimes it induces unwanted side effects like acute interstitial pneumonitis, myocardial ischemia etc. [335–337]. Using the B3LYP hybrid exchange correlational functional, it was observed that the BNCU interacted with f-BNNT with a maximum adsorption energy of −8.04 kcal/mol in the gas phase which decreased to −4.69 kcal/mol in the water phase. This interaction energy was increased as high as −18.77 (−10.89) kcal/mol in the gas (water) phase, while the dispersion corrected M06-2X functional was used. This significant difference in the adsorption energies using two different functional indicated that the weak Van Der Waals (vdw) interactions played an important role in the BNCU adsorption on f-BNNT. This was then confirmed from the MD simulations where vdw energy increased to −3.42 kcal/mol from −0.54 kcal/mol for a single drug molecule with an increase in the temperature to 310 K from 270 K. The adsorption process was spontaneous and thermodynamically possible with an exothermic one in both gaseous and water phase. But the adsorption of BNCU barely affected the charge transfer and electronic properties with an increase in the H-L energy gap. Besides the reactivity of the structures was also decreased with an increase in the global hardness of the BNCU adsorbed f-BNNT.

The biocompatibility and non-toxicity of BNNTs encouraged S. Ghahremani et al. to encapsulate an anticancer drug floxuridine (FUDR) into a (9, 9-7) armchair BNNT [338]. FUDR is an anticancer drug to treat colorectal cancer and often causes side effects like toxicity, diarrhoea etc. which requires immediate medical attention and hospitalization [339–341]. FUDR was encapsulated inside the (9, 9-7) BNNT with interaction energy of −0.28 kcal/mol only. But the encapsulation of FUDR decreased the energy gap to 0.191 eV from 0.231 eV, which was occurred due to a significant increase in the LUMO energy to −0.044 eV from −0.004 eV. More importantly, the DM of the FUDR encapsulated (9, 9-7) BNNT increased significantly to the 9.02 debye while it was 0.00 for the (9, 9-7) BNNT. This increase in the DM indicated an enhanced reactivity of the structure in a polar medium. This enhancement in the reactivity was also reflected in the quantum reactivity descriptors where the global hardness of the structure was increased to 0.095 eV where it was 0.115 eV for the (9, 9-7) BNNT alone and the global softness increased to 10.46 eV^{-1} from 8.63 eV^{-1} along with an increase in the electrophilicity to 0.102 eV from 0.062 eV. From NBO analysis, it was observed that the electron is most like to flow towards BNNT from FUDR which made FUDR an electron donor and BNNT an electron acceptor. The weak physisorption was further confirmed from the QTAIM analysis where it was observed that the interaction between the FUDR and BNNT was weak Van der Waals interactions with a small value for the electron density and a negative value for $\nabla^2\rho$ where five hydrogen bonds were also observed. These promising results lead them to propose a drug carrier for the FUDR based on (9, 9-7) BNNT to reduce the unwanted effects of the FUDR drug in our body.

Besides the anticancer drug delivery, the sensing properties of BNNT on anti-fever and pain-reducing drugs like paracetamol (PA) and phenacetin (PH) was also observed from several studies as the overdose of these drugs may induce some liver and kidney damage [342]. The interaction of both PA and PH with several armchair BNNTs with different chirality was investigated by H. Ghasempour et al. using dispersion corrected DFT-D theory with GGA functional [343]. Interestingly, instead of adsorbing PA, it was desorbed in the inside of (5, 5) BNNT with a positive adsorption energy of 47.25 kcal/mol while it was adsorbed strongly with an adsorption energy of −21.34 kcal/mol in the outside of the (5, 5) BNNT. But the reverse effect was observed in case of the (6, 6) and (7, 7) BNNT where PA was adsorbed more stably inside the BNNT with an adsorption energy of −49.20 and −35.42 kcal/mol respectively while it was −23.30 and −23.07 kcal/mol respectively for the adsorption of PA on the outside of (6, 6) and (7, 7) BNNTs. Again more enhanced properties on sensing PA like a high drop in the H-L energy gap and an increase in the DM was observed while the drug was in the outside of (6, 6) and (7, 7) BNNTs. The exact same adsorption properties like desorption inside (5, 5) BNNT but more stable adsorption inside (6, 6) and (7, 7) BNNTs, more decrease in the energy gap and more increase in the DM while the drug was adsorbed on the outer surface of (6, 6) and (7, 7) BNNTs was also observed for the PH adsorption on the BNNTs. The more effect on the PA adsorption towards BNNT was further investigated by Z. Iranmanesh-Zarandy et al. using MD simulations in terms of change in nanotube's size, length, chirality and temperature [344]. The binding free energy of PA was increased with an increase in the diameter of the BNNT. The binding free energy of PA towards the (4, 4) BNNT with diameter 5.63 Å was observed as −16.03 kcal/mol while it was gradually increased to −35.13 kcal/mol for the (10, 10) BNNT with a diameter of 13.96 Å. But a significant decrease in the stability was observed in cases like an increase in the length of BNNT and chirality along with a minor decrease in the stability for increasing temperature.

Recently several computational works also had been done on investigating BNNT as a sensor for several harmful chemical compounds, a long exposure of which may induce harmful effect to the human body. B. Makiabadi et al. investigated the sensing properties of (4, 0) zigzag BNNT and three Al-doped $B_{3Al}NNT$ with a diameter ranging 3.289–3.638 Å using B3LYP/6-311++G(d) level of theory, to sense carcinogenic compounds nitrosamine (NA) and thionitrosamine (TNA) which can make an entry to the human body through cigarette smoke, water, foods etc. and induce gastric and oesophageal cancer [345–348]. Both BNNT and $B_{3Al}NNT$ adsorbed NA and TNA with stable negative adsorption energies along with a decrease in the H-L energy gap hence increase in the conductivity, and increase in the reactivity by a decreasing chemical hardness with increasing chemical softness and electrophilicity. $B_{3Al}NNT$ showed more stable adsorption of NA and TNA with adsorption energy (BSSE corrected) ranging −25.91 to −33.22 kcal/mol while it was −2.07 to −9.59 kcal/mol for the BNNT. Besides more charge transfer from NA and TNA to BNNT was observed than $B_{3Al}NNT$ and all the bonds between the adsorbent and adsorbate were covalent in nature. G. Fan et al. proposed another sensor for acetone based on zigzag BNNTs from a dispersion corrected DFT-D study which can have a potential application on the detection of diabetes as a patient with diabetes produces more acetone in their body than a normal person [349]. It was observed that the pristine BNNTs adsorbed acetone with decent stability but hardly able to sense it which was further improved by doping impurity atoms to the BNNT hence an acetone sensor can be developed with flexible sensing properties based on the necessity. Besides, the interaction of the oxazole and isoxazole with BNNT was investigated by J. Kaur et al. as many drugs have a structure similar to these heterocyclic aromatic organic compounds hence plays an essential role in the development of many drugs [102]. Though the (6, 0) zigzag BNNT adsorbed oxazole in both gaseous and solvent phase with an adsorption energy of −2.54 and −18.68 kcal/mol respectively, it adsorbed isoxazole only in the solvent phase with an adsorption energy of −15.22 kcal/mol. But the (5, 5) armchair BNNT desorbed both oxazole and isoxazole in both gaseous and solvent phase with a positive value for the adsorption energy. A higher reactivity with a significantly increased DM was also observed for the (6, 0) BNNT than (5, 5) BNNT. Hence the solvent and the chirality of the BNNT affects the adsorption properties of oxazole and isoxazole significantly.

4.3. Boron nitride nanocage

Prior to the advancement of the CNT and C fullerenes, the investigation on the BNNT and boron nitride nanocages (BNNC) also started with almost the same timeline. Research on the BNNCs got immense attention after a report from F. Jensen and H. Toftlund stating that $B_{12}N_{12}$ nanocage offers higher stability compared to the C_{24} fullerenes [350]. Shortly after that, in 1994 the first accidental observation of the nested BNNC was reported by 0. Stephan et al. during doping the CNT with B and N atoms using the electric arc-discharge method [351]. Furthermore, many groups reported the growth of the BNNC using various

methods including the formation of octahedral $B_{12}N_{12}$ BNNC (Fig. 13) using electron beam irradiation by D. Golberg et al. [352], the formation of $B_{24}N_{24}$ using an arc-melting method by T. Oku et al. [353] etc. Being made of boron nitrides, BNNCs also benefit from the unique properties shown by other BN polymorphs like wide bandgap, high resistance to the oxidation, high thermal and chemical stability etc. which lead its application as good lubrication [354], wastewater treatment [355], hydrogen storage [356], gas sensors [357] etc.

BNNCs are also reported to have a potential application in the anticancer drug sensing and delivery system. Thioguanine or 6-thioguanine (TG), a drug that has clinical applications to treat several types of acute leukaemia, have many unwanted side effects like bone marrow suppression, liver toxicity etc. [358–360]. To reduce these adverse effects on the human body, M. Noormohammadbeigi et al. investigated pristine $B_{12}N_{12}$ nanocage to work as a potential nano-drug delivery vehicle for TG delivery [361]. Considering non-covalent calculations, they chose M06-2X functional along with widely used 6-31G (d,p) basis set and DFT theory as the M06-2X functional have a higher percentage of Hartree-Fock exchange (54%). The fascinating property upon TG adsorption on $B_{12}N_{12}$ was the decrease in the H-L energy gap by a noticeable change ranging 27.12–35.70% which was confirmed from the DOS spectrum of structures hence made a significant rise to the electrical conductivity of TG adsorbed structures. Besides this sensitivity towards TG, $B_{12}N_{12}$ was also spontaneously adsorbed TG by strong chemisorption with an exothermic process. The adsorption energy of the TG on $B_{12}N_{12}$ was in a range of −29.48 to −36.03 kcal/mol for different orientations and isomers of the drug in the gaseous phase. However, this range increased into −36.16 to −38.85 kcal/mol in the water solvent phase with a significant increase in the DM to as high as 13.58 debye. Higher charge polarization transfer from TG to $B_{12}N_{12}$ was also observed in the water phase. These properties made them conclude $B_{12}N_{12}$ nanocage as a nano drug delivery system for TG drug.

Ifosfamide (IFO) is another anticancer drug which has a potential application to treat several kinds of cancer and tumours including testicular cancer, small cell lung cancer, ovarian cancer etc. and have relatively fewer side effects [362]. But sometimes, it is capable of inducing life-threatening toxicities like cardiac toxicity, hemorrhagic cystitis, nephrotoxicity, encephalopathy and neuropathy [363]. A. Soltani et al. investigated the interaction of IFO with pristine $B_{12}N_{12}$ and carbon atom doped $B_{12}N_6C_6$ and $B_6N_6C_{12}$ fullerenes which revealed that those unwanted side effects of IFO might be reduced by using BN fullerenes as a nano-drug delivery system for the IFO [364]. Besides the DFT theory, they chose one GGA and another hybrid functional with a high percentage of HF (Hartree-Fock) exchange as GGA PBE-1 was observed to have results closer to the experimental outcomes for $B_{12}N_{12}$, and the hybrid M06-2X was used widely for $B_6N_6C_{12}$, graphene and other nanosystems.

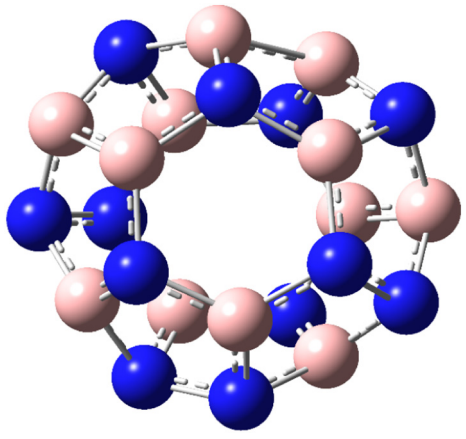

Fig. 13. $B_{12}N_{12}$ nanocage relaxed using DFT theory with B3LYP hybrid exchange correlational functional and 6-31G (d,p) basis set.

Unlike many other nanostructures, pristine $B_{12}N_{12}$ fullerene adsorbed IFO drug with strong chemisorption of −27.90 kcal/mol in its most stable orientations which was further enhanced in the water solution where it became −29.28 kcal/mol. This interaction between the IFO and BNNC became stronger due to the substitution of carbon atoms, and the interaction energies were observed as −42.89 and −45.89 kcal/mol while the adsorbents were $B_{12}N_6C_6$ and $B_6N_6C_{12}$ fullerenes, respectively. The DM for the IFO adsorbed structures increased in the solvent medium and was observed as high as 23.67 debye for $B_{12}N_6C_6$ and 16.58 debye for $B_6N_6C_{12}$ fullerene. These properties ensured the IFO drug loading ability of $B_{12}N_6C_6$ and $B_6N_6C_{12}$ and the biocompatibility of the structures were increased with a decrease in the toxicity which was confirmed from an increasing reactivity observed from the increasing chemical potential and electrophilicity with a decrease in the global hardness.

Besides delivering the TG and IFO anticancer drugs, BNNC was also reported to be worked as a potential sensor candidate for another anticancer drug cisplatin (CP) which was revealed from a first-principles investigation made by S. Onsori et al. [365]. It was observed that at the most stable interaction, the $B_{12}N_{12}$ nanocage adsorbed CP drug with an adsorption energy of −14.9 kcal/mol. But one of the key features for sensor development, decrease in the H-L energy gap, was observed with the highest decrease of 44.2%, which was analyzed from the DOS spectrum. For the different orientation of CP drug the reduction in the H-L energy gap ranges from 30.30% to 44.2% which ensured that $B_{12}N_{12}$ nanocage could detect CP drug in various orientations efficiently with an increase in the conductivity to produce a detectable signal. Besides the recovery time of the sensor was also found as low as ~81 ms ensured that pristine $B_{12}N_{12}$ nanocage could be a potential candidate for CP drug sensor without any modification, doping or decoration. Furthermore, BNNC was considered to be a potential sensor to detect another anticancer drug α-cyano-4-hydroxycinnamic acid (CHC) [366]. Frontier molecular orbital analysis with DOS revealed that due to the adsorption of CHC the H-L energy gap of $B_{12}N_{12}$ nanocage decreased by a minimum of 39.3% to a maximum of 55.2% for different orientations which ensured its sensitivity towards CHC drug. Almost the same sensitivity was also observed in the water solvent where the decrease in the H-L energy gap was observed as 30.5% to 46.1% for different orientations of CHC on $B_{12}N_{12}$ nanocage. Besides, it adsorbed CHC with a maximum adsorption energy of −23.7 kcal/mol, which leads the sensor to be suffered by a moderately large recovery time of 22.7 s at the room temperature. Hence the $B_{12}N_{12}$ nanocage can be considered as a potential sensor candidate to detect CP and CHC drug.

In addition, BNNC was studied to design a nano-vehicle for an anti-inflammatory drug like Celecoxib (CXB) and a sensor for Metformin (MF) that is used to treat type 2 diabetes. First, N. Abdolahi et al. investigated the adsorption properties of CXB drug adsorption on $B_{12}N_{12}$ fullerene (BNNC) and found that BNNC can be a potential candidate for the nano-vehicle of CXB to transfer it into the targeted cell [367]. The rising importance on the drug delivery system is associated with adverse effects of CXB like hypertension, diarrhoea, gastrointestinal effects besides its use as a COX-2 selective nonsteroidal anti-inflammatory drug (NSAID) [368–370]. The BNNC firmly bound the CXB drug by strong chemisorption with an adsorption energy of −30.21 kcal/mol in a vacuum and with −26.75 kcal/mol in water medium at its most stable state. Besides the BNNC was also sensitive towards the CXB drug as a decrease of 45.83% in the H-L energy gap was observed from the DOS spectrum analysis. Due to the adsorption of CXB, the reactivity of the structure also increased with a decreasing global hardness, chemical potential, and electrophilicity along with an increase in the global softness while the DM of the structure was also increased to as high as 10.89 debye from zero for the pristine symmetric $B_{12}N_{12}$ fullerene which raised the potentiality of BNNC as a nano-vehicle for CXB in drug delivery application. In another study, A.S. Ghasemi et al. initiated an investigation lead by dispersion corrected DFT-D theory to find the drug delivery capability of pristine and doped $B_{12}N_{12}$ and $B_{16}N_{16}$ fullerenes

to deliver MF but ended up with finding sensor application of BNNC to sense MF [371]. Without any doping or functionalization of $B_{12}N_{12}$ and $B_{16}N_{16}$ fullerenes, both interacted with MF strongly with an adsorption energy of −37.35 and −36.44 kcal/mol respectively with a decrease in the H-L energy gap by 28.46% and 28.17%. Besides the reactivity of the structures increase with an increase in the DM up to 15.34 debye along with an increase in global softness and decrease in the global hardness, chemical potential, and electrophilicity. Hence the pristine $B_{12}N_{12}$ and $B_{16}N_{16}$ fullerenes can be potential candidate in the sensor development of MF drug. Due to doping $B_{12}N_{12}$ fullerenes with Al, Si, Ge and Ga, while the most stable interaction of MF was observed with $AlB_{11}N_{12}$ with a large adsorption energy of −74.95 kcal/mol, $GeB_{11}N_{12}$ was most sensitive towards MF drug with a decrease in the H-L energy gap by 66.67% with an acceptable adsorption energy of −37.13 kcal/mol. Hence the study concludes $GeB_{11}N_{12}$ fullerene as the most potential nanostructure to work as a biosensor for MF drug.

4.4. Quasi-planar boron nanoclusters

The popular pyridine nucleobase uracil like anticancer drug fluorouracil (FU) was further adsorbed with the quasi-planar B_{36} boron nanosheet (Fig. 14) in order to investigate if the B_{36} can be used as a novel drug carrier system for the FU drug [372]. All the quantum mechanical calculations were carried out by time-dependent DFT (TD-DFT) theory, and for the exchange correlational functional they depended on the hybrid TPSSH functional with 6-31+G (d) basis set. First, the FU drug failed to generate any detectable signal where no noticeable change in the H-L energy gap was observed while the drug interacted with the concave and convex surface of B_{36} nanosheet with weak interaction energy of −2.2 to −4.8 kcal/mol. But these interactions were greatly enhanced while the drug interacted with its O atom on the edge of the B_{36} nanosheet. While a single molecule was adsorbed on the edge of B_{36} nanosheet, in the gaseous medium the adsorption energy was observed as high as −24.5 kcal/mol with maximum deformation energy of 18.1 kcal/mol. The B_{36} also detected FU with a noticeable decrease in the H-L energy gap of 47% with an NBO charge transfer of 0.302 a.u. The DM of these structures was also observed as high as 16.6 debye, which indicated an increase in the reactivity in the polar medium. While instead of one FU, two FU molecule was adsorbed on the B_{36} nanosheet, the adsorption energy per molecule was slightly decreased with a maximum value of −22.2 kcal/mol but increased the deformation energy as high as 36.3 kcal/mol. Despite a less interaction the sensitivity and reactivity increased significantly where the decrease in the H-L energy gap was as high as 64% with NBO charge transfer ranging 0.425 to 0.588 a.u. while the DM was observed as high as 22.5 debye. Besides, a more strong interaction of FU with B_{36} was observed in the aqueous solution where the adsorption energy was as high as −27.3 kcal/mol with an increased reactivity where the highest DM was observed as 36.4 debye, but no significant change in the H-L energy gap was observed. Hence these enhanced adsorption properties in the polar medium made B_{36} nanosheet a potential candidate for the nanodrug carrier of FU.

Besides, drug delivery application, B_{36} nanosheet was further investigated by C. Xiao et al. in a search for an electrochemical sensor development to sense metronidazole (ML) drug [373]. This antibiotic drug is used to treat a number of diseases including bacterial vaginosis, perineal Crohn's disease, trichomoniasis etc. but an extensive usage of it can lead to unwanted carcinogenic effects on the human body [374–376]. The DFT theory based B3LYP-gCP-D3/6-31G* level of theory was applied to optimize the structures which further found that like FU, ML also interacted more strongly with the B_{36} nanosheet by its edge with adsorption energy as high as −22.1 kcal/mol while the adsorption process was spontaneous with a negative value for the change in Gibbs free energy as −19.3 kcal/mol. But the maximum adsorption energy of the complexes was slightly decreased to −20.9 kcal/mol with an increase in the solvation energy to −12.5 kcal/mol. Despite a very slight change in the work function of the B_{36} nanosheet due to the adsorption of ML, the change in the H-L energy gap was dramatic with the highest drop by 64.4% to 0.66 eV from 1.84 eV ensuring a significant increase in the conductivity of the structure. This significant decrease in the H-L energy gap also caused an NBO charge transfer of 0.23e between the ML and B_{36} nanosheet which will be able to induce a detectable electrochemical signal and can be used to develop a potential sensor to sense ML drug. The recovery time of the sensor was further found to be as low as 1.53 s for the most stable adsorption in the room temperature.

Using the different sensing properties towards the four DNA nucleobases Adenine, Guanine, Cytosine, Thymine, the quasi-planar B_{36} nanosheet was further proposed for an application as a DNA sequencing device by a DFT investigation from A. Rastgou et al. [377]. It was observed that the B_{36} nanosheet was most sensitive towards the cytosine with its edge than other nucleobases with a massive decrease in the H-L energy gap by 95.5%. For the thymine, this decrease in the H-L energy gap was observed within the range 28.9% to 35.5% and was the second most sensitive structure towards B_{36} nanosheet. The sensitivity of adenine and guanine was almost similar towards the B_{36} nanosheet, but the sensitivity was slightly higher for adenine with a decrease in the energy gap by 17.5% to 20.2% following by 14.8% to 15.6% for guanine although two orientations can decrease the energy gap by 26.6% and 47.9%. Hence the highest peak in the conductivity will be observed for cytosine following by the thymine, adenine and guanine from which these DNA nucleobases can be identified. Though the electronic sensitivity was observed as cytosine>thymine> adenine ~ guanine, the energetic sensitivity of B_{36} nanosheet was observed as adenine>guanine> cytosine>thymine.

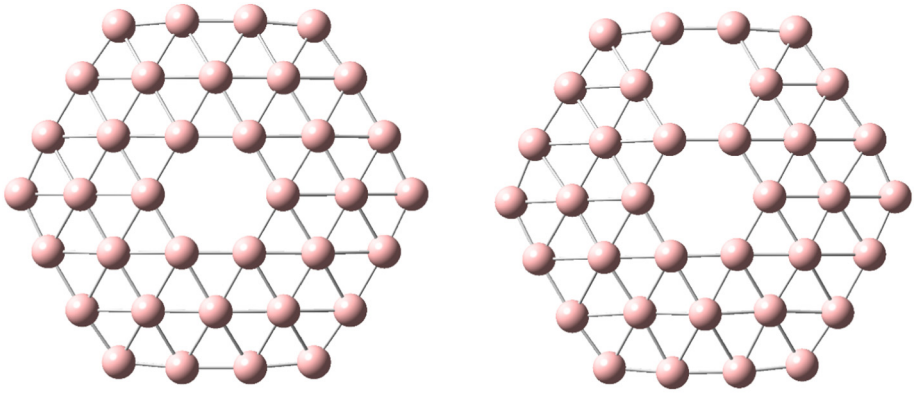

Fig. 14. Quasi-planner (a) B_{36} and (b) B_{35} nanostructures optimized using DFT theory with B3LYP hybrid exchange correlational functional and 6-31G, LanL2DZ basis sets respectively.

Table 1
Summary of the applications of carbon based LDNs on biomolecule sensing, drug sensing, and drug delivery field.

Adsorbate	Adsorbent	Adsorption energy, E_{ads} in kcal/mol	Remarks	References
β-Lapachone	Graphene	−21.22	Potential candidate for β-lapachone drug delivery	[123]
	Pt-doped graphene	−40.82		
	Au-doped graphene	−38.28		
Ampyra	Graphene (G)	−5.17	Potential candidate for Ampyra drug delivery	[130]
	G-O	−7.16		
	G-OH	−4.12		
	G-CO	−6.59		
	G-COOH	−7.64		
5-Fluorouracil	GQD	−15.54	Potential candidate for 5-fluorouracil drug delivery	[133]
	AlN doped GQD	−47.29		
	BN doped GQD	−17.36		
	BP doped GQD	−21.65		
	AlP doped GQD	−30.61		
Tegafur	Graphene (G)-CO	−24.85	Potential candidate for β-lapachone drug delivery	[136]
	G-COOH	−16.01		
	G-O	−20.37		
	G-OH	−23.31		
Adrucil	Si-doped Pha-graphene	−14.0	Potential candidate for Tegafur drug delivery	[149]
Fluorouracil	C_{54} nanosheet	−15.5	Potential candidate for Fluorouracil, Mercaptopurine, and Thioguanine drugs delivery	[138]
Mercaptopurine		−16.0		
Thioguanine		−20.0		
Glycine	Graphene	−7.61	Potential candidate for biosensor applications	[147]
Histidine		−11.76		
Phenylalanine		−14.01		
Guanine	Al doped graphene	−45.10	Potential candidate for Guanine sensor	[141]
Adenine	Ni doped graphene	−44.50	Potential candidate for Adenine sensor	[140]
Penicillamine	SWCNT	−3.18	Potential candidate for Penicillamine drug delivery	[180]
	SWCNT- COOH	−11.22		
Isoniazid	SWCNT	−15.59	Potential candidate for Isoniazid drug delivery	[182]
	Si doped SWCNT	−68.30		
Gemcitabine	SWCNT-pyrrolidine	−11.15	Potential candidate for Gemcitabine drug delivery	[190]
Carmustine	SWCNT-COOH	−4.65	Potential candidate for Carmustine drug delivery	[195]
Flutamide	SWCNT-COOH	−5.38	Potential candidate for Flutamide drug delivery	[194]
Metformin	SWCNT	−1.85	Potential candidate for Metformin drug delivery	[199]
	Al doped SWCNT	−48.66		
	Si doped SWCNT	−38.74		
D-atropine	Ca doped SWCNT	−36.07	Potential candidate for Atropine drug delivery	[200]
L-atropine		−41.87		
Acetaminophen	MWCNT	−195	Potential candidate for Acetaminophen sensor	[210]
Fluoxetine	MWCNT	−51.56	Potential candidate for Fluoxetine sensor	[209]
Lactic acid	SWCNT	−13.39	Potential candidate for lactic acid adsorption	[213]
Histidine	Pd doped SWCNT	−419.93	Potential candidate for Histidine adsorption	[212]
5-Fluorouracil	C_{24} fullerene	−3.2	Potential candidate for 5-Fluorouracil drug delivery	[239]
	B doped C_{24} fullerene	−27.2		
Penicillamine	Al doped C_{60} fullerene	41.83	Potential candidate for Penicillamine drug delivery	[245]
4-Phenylpyridine	B doped C_{60} fullerene	−41.65	Potential candidate for 4-phenylpyridine drug delivery	[240]
	Si doped C_{60} fullerene	−50.31		
Adenine	Cr doped C_{20} fullerene	−48.99	Potential candidate for Adenine sensor	[238]
	Ni doped C_{20} fullerene	−47.94		
Ibuprofen	NiN_4C_{55}	−23.11	Potential candidate for Ibuprofen drug delivery	[254]
	CoN_4C_{55}	−17.81		
	FeN_4C_{55}	−18.07		
Isoniazid	$C_{30}B_{15}N_{15}$	−21.95	Potential candidate for Isoniazid drug delivery	[255]
Phenylalanine	Al doped C_{60} fullerene	−60.09	Potential candidate for Phenylalanine sensor	[256]
	Si doped C_{60} fullerene	−48.70		
Amphetamine	Si-doped BC_3 nano tube	−21.3	Potential candidate for Amphetamine detection	[257]
β-Keto-amphetamine	BC_2N nano tube	−15.7	Potential candidate for β-keto-amphetamine detection	[258]
Glycine	BC_2N nano tube	−41.74	Potential candidate for Glycine detection	[259]
Sumatriptan	GO	−10.59	Potential candidate for Sumatriptan drug delivery	[260]
Doxorubicin	Fluorinated GO	−11.6	Potential candidate for Doxorubicin and Camptothecin drugs delivery	[261]
Camptothecin		−16.2		
Ellipticin	GO	−28.04	Potential candidate for Ellipticin drug delivery	[262]
Sorafenib	Graphdiyne nanosheet	−15.22	Potential candidate for Sorafenib and Regorafenib drugs delivery	[263]
Regorafenib		−14.78		
Flutamide	Graphdiyne nanotube	−18.31	Potential candidate for Flutamide drug delivery	[264]
Cytosine	Graphyne nanosheet	−14.69	Potential candidate for Cytosine and Guanine detection	[265]
Guanine		−14.27		
5-Fluorouracil	Graphyne nanosheet	−14.87	Potential candidate for 5-fluorouracil and Quercetin drugs delivery	[90]
Quercetin		−17.59		

Another quasi-planar boron nanocluster, bowl-shaped B_{30} nanostructure was proposed to function as a drug delivery system for amantadine drug as it often comes with unwanted adverse effects like insomnia, depression, hallucinations etc. besides its application to treat Parkinson's disease and influenza A [378–381]. Like B_{36} nanosheet the strongest interaction of amantadine was observed on the edge of B_{30} nanostructure with an adsorption energy of - 46.44 kcal/mol while for other orientations it ranged between −16.73 to −26.83 kcal/mol

ensuring strong chemisorption for every orientation. The amantadine adsorption by B_{30} nanostructure further got stronger on the water solvent while the range of the adsorption energy became −30.75 to as high as −53.34 kcal/mol. Besides B_{30} nanostructure was more sensitive to amantadine by its edge but still not sufficient to develop a sensor as the maximum drop in the H-L energy gap was observed as only 8.50% while for the other orientations this was observed with a range 7.19% to 7.79%. Finally, the polarity and reactivity of the B_{30} nanostructure increased significantly with a major increase in the DM as high as 14.14 debye from 3.85 debye for the pristine B_{30} nanostructure. For other orientations, the dipole moment was also almost similar within the range of 13.06 to 14.07 debye. This increase in the polarity and reactivity with decent adsorption energy which also increased significantly in the aqueous solution made B_{30} nanostructure a potential candidate as a nano-drug delivery system for amantadine drug.

5. Miscellaneous LDNs for drug delivery and sensing applications

5.1. Metal oxide nanostructures

As usual, metal oxide (MO) nanostructures were also studied as a drug delivery system for several therapeutic anticancer drugs. R. Khorram et al. investigated the drug delivery properties maghemite (γ-Fe_2O_3) nanostructure to deliver carmustine (BCNU) anticancer therapeutic drug which was previously discussed in this study to be delivered using –OH functionalized (6, 0) zigzag BNNT (f-BNNT) [382]. Like f-BNNT, BCNU was also made a weak interaction with maghemite with a maximum adsorption energy −12.34 kcal/mol while other orientation of the drug it was also observed as low as −0.26 kcal/mol. From thermodynamical parameter analysis, it was observed that the drug adsorption process was spontaneous and exothermic in nature as the change in the Gibbs free energy and enthalpy was negative. The DM of the structures increased significantly to as high as 8.8 debye due to the adsorption of BCNU from 2.94 debye for the maghemite which increased the polarity and reactivity of the structures noticeably, and this played a crucial role into the delivery of BCNU using maghemite. The AIM analysis was also done to investigate the type of interaction between the drug and maghemite which revealed the presence of partial covalent interaction between them. Besides, NBO analysis identified the BCNU as electron donor where maghemite was a receiver, and this was further verified from a more negative value of chemical potential for maghemite as −5.02 eV compared to −4.69 eV for BCNU. This work with maghemite besides f-BNNT will surely advance the study to find a nano-drug carrier for BCNU drug. Besides drug delivery, another study from S. Onsori and E. Alipour proposed another MO, $Zn_{12}O_{12}$ nanocluster, to develop an electrochemical sensor for another anticancer drug cisplatin (CP) with brand name Platinol for which another sensor was discussed previously on this study using $B_{12}N_{12}$ nanocage [383]. The $Zn_{12}O_{12}$ nanocluster made a stronger interaction with CP compared to the $B_{12}N_{12}$ nanocage but with a less sensitivity where the maximum adsorption energy and decrease in the H-L energy gap were observed as −31.7 kcal/mol and 31.76% respectively. The adsorption process was spontaneous with a negative value for the change in Gibbs free energy as high as a −20.8 kcal/mol with a maximum change transfer of 0.25e between the CP and $Zn_{12}O_{12}$ nanocluster. The sensitivity of the $Zn_{12}O_{12}$ nanostructure towards CP was enhanced in the aqueous solution with a maximum drop in the H-L energy gap by 37.2% with a slight reduction in the maximum adsorption energy to −17.6 kcal/mol. The sensor also had a short recovery time of 1.7 s in the combination of which made $Zn_{12}O_{12}$ nanostructure a promising sensor candidate for CP drug.

The isonicotinic acid hydrazide (INH) with brand name Isoniazid, a prodrug to treat the deadly infectious disease tuberculosis (TB), which was previously discussed to be delivered using SWCNT by N. Saikia et al., was also proposed to be delivered using another MO framework $Mg_{12}O_{12}$ nanocage by I. Ravaei et al. [384]. The pristine $Mg_{12}O_{12}$ nanocage made a strong interaction with INH drug with a maximum adsorption energy of −35.51 kcal/mol but failed to alter the reactivity and electronic properties with no noticeable change in the global reactivity parameters and H-L energy gap of the structures. This problem was overcome by replacing an Mg atom by Al atom to the $Mg_{12}O_{12}$ nanocage, which decreased the H-L energy gap to 3.15 eV from 7.56 eV. The H-L energy gap was further reduced to 1.98 eV by 37.18% due to the adsorption of INH drug on Al-$Mg_{11}O_{12}$ nanocage with an increase in the reactivity by lowering the global hardness and chemical potential. Due to the doping of Al atom, the interaction of the INH drug also got stronger with an increase in the adsorption energy to as high as −59.49 kcal/mol. Besides from AIM and NBO analysis, it was revealed that the interaction between the drug and carrier was partially covalent in nature and the electrons were transferred from INH drug to the Al-$Mg_{11}O_{12}$ nanocage.

In another first-principles investigation, M. Rezaei-Sameti et al. investigated the interaction of another MO, $Be_{12}O_{12}$ nanocluster with mercaptopyridine (MCP) drug [385]. Interestingly, pristine $Be_{12}O_{12}$ nanocluster showed more encouraging adsorption properties towards MCP than Sc and Ti-doped $Be_{12}O_{12}$ nanocluster in order to develop a nano-drug carrier system for MCP drug with maximum adsorption energy and DM of −38.91 kcal/mol and 7.87 debye respectively. Doping the nanocluster with Sc and Ti increased the adsorption energy to as high as −59.68 kcal/mol but decreased the maximum DM to 5.44 debye. But the doping of Sc and Ti increased the sensitivity of the $Be_{12}O_{12}$ nanocluster towards the MCP drug by reducing the H-L energy gap significantly, which was not observed noticeably for pristine $Be_{12}O_{12}$ nanocluster. Hence, those nanoclusters can hold future potential for the sensor development of MCP drug. Furthermore, the adsorption process was spontaneous, exothermic, ordered for all investigated structures except the MCP adsorption with S atom towards the pristine $Be_{12}O_{12}$ nanocluster with a positive value for the change in Gibbs free energy. Besides MCP, another MO nanocluster, ZnO single-walled nanotube (SWNT) was also proposed to be a potential sensor candidate for Protein tyrosine nitration (PTN), 3-nitrotyrosine, which can be produced during the post-translational modifications in proteins and cause several human disorders like rheumatoid arthritis, Parkinson's disease, Alzheimer etc. [386]. The interaction of the PTN increased significantly with the increasing chirality of the ZnO SWNTs. The maximum binding energy of the (3,0) ZnO SWNT was observed as 37.59 kcal/mol while it was increased to 41.74 kcal/mol for ZnO SWNT. Finally, a noticeable alteration in the electronic band structure of the ZnO SWNT indicated its sensitivity towards PTN.

5.2. Al and Ga nitride nanostructures

The interaction of isoniazid (INH) was also studied with the pristine and Ni-doped (4, 4) armchair GaNNTs by M. Rezaei-Sameti et al. using the DFT cam-B3LYP/6–31G(d) level of theory [387]. It was observed that the pristine and Ni-doped GaNNTs adsorbed the INH drug with an adsorbate-adsorbent distance of 1.68–2.16 Å. The pristine GaNNT adsorbed the INH strongly with adsorption energies ranging −92.23 to −107.14 kcal/mol for different orientations for the drug which hadn't increased due to the doping with Ni. The adsorption processes were exothermic in nature and thermodynamically favourable. All interactions were spontaneous and ordered with negative values for the change in Gibbs free energy and entropy. The H-L energy for all of the investigated structures were ranging between 3.61 eV and 6.49 eV and a decrease in the energy gap was observed in the Ni-doped structures with an increase in the conductivity. Besides, the work function of the investigated structures was observed as −1.81 to −3.25 eV. From the NBO analysis, it was also revealed that the INH worked as the electron donor in the INH-GaNNT complexes with a positive value for $\Delta\rho_{(NBO)}$ which agreed with the positive values for maximum electronic charge transfer (ΔN). These alluring adsorption properties may

lead (4, 4) armchair GaNNTs to a potential sensor candidate for the INH drug.

The sensor for another drug, benzoylethanamine (BEA) or β-keto-amphetamine, was reported by A. Hosseinian et al. using AlN nanoclusters [389]. Another sensor for BEA was previously discussed in this review using Si-doped BC_2N nanotube, which had a good sensitivity towards BEA with a short recovery time of 0.27 s [258]. However, the AlN nanoclusters were also able to adsorb the BEA with strong chemisorption where AlN nanocage adsorbed the drug with a maximum adsorption energy of −35.16 kcal/mol following by −30.16 kcal/mol for AlN nanotube and −15.77 kcal/mol for AlN nanosheet. Despite the highest stability of AlN nanocage, the least sensitivity towards the BEA was observed for AlN nanocage by decreasing the H-L energy gap by 29.1% to 2.80 eV whereas the AlN nanotube decreased it by 31.7% and AlN nanosheet decreased it by 41.9% making AlN nanosheet most sensitive towards BEA drug. Besides, the AlN nanosheet also has a very short recovery time of 0.33 s in the room temperature. Though the AlN nanoclusters hadn't shown better properties than the Si-doped BC_2N nanotube, as pristine structures they showed better sensing properties than pristine BC_3 nanotube, and these nanoclusters can be considered as potential candidates to develop a sensor for BEA drug (Table 2).

Besides the sensor for BEA, AlN nanocage was also reported to have a potential application in the development of a work function based sensor for antiparkinsonian drug amantadine (AM) drug whose delivery was previously discussed by Z. Noroozi et al. [92,378]. At its most stable state, the AlN nanocage adsorbed the AM drug with an adsorption energy of −38.4 kcal/mol with an adsorbent-adsorbate distance of 2.03 Å. Though a charge transfer of 0.12e from AM to the nanocage which was confirmed by NBO analysis, AM hardly able to decrease the H-L energy gap of the nanocage upon its adsorption. The decrease in the energy gap was observed by only 2.0% leading no significant change in the conductivity of the nanocage. But the adsorption of AM significantly decreased the work function by 18.7% to 3.66 eV from 4.50 eV for pristine AlN nanocage. Hence the AlN was considered to have potential on the development of a work function based biosensor for AM drug. On the other hand, the BNNC was observed to decrease its H-L energy gap by 26.7% to 5.01 eV on the adsorption of AM drug. Besides, BNNC also adsorbed the AM drug with a decent adsorption energy of −31.3 kcal/mol. Hence the BNNC was considered as a potential electrochemical sensor to detect AM drug. Both AlN and BN sensors were benefited from a shorter recovery time of 137 s and 0.11 s at a high temperature of 350 K, and their interactions with the AM drug was electrostatic and covalent in nature, respectively. The similar kind of response was also observed on the adsorption of acetylsalicylic acid (ASA) drug on the AlN and BNNC [390]. Here, the ASA was also adsorbed by AlN nanocage strongly with an adsorption energy of −62.8 kcal/mol but failed to alter the electronic properties of AlN nanocage. Besides, this time AlN nanocage also suffered from an unrealistic large recovery time of 9.8×10^{38} s. On the other side, ASA was adsorbed on the BNNC with a relatively weak adsorption energy of −21.9 kcal/mol but decreased the H-L energy gap by 35.1%. Besides the BNNC also benefitted from a short recovery time of ~109 s. Again, the BNNC could not work as a work function based sensor as it increased the work function by 10% to 4.75 eV from 4.28 eV. Hence BNNC can only be considered as a potential electrochemical sensor to detect ASA. The result from adsorption of ASA and AM on AlN and BN was also extended by R. Padash et al. for 4-aminopyridine (4-AP) drug and exactly the same trends were followed [391]. The $Al_{12}N_{12}$ nanocage was again adsorbed the 4-AP drug with the highest adsorption energy of −31.36 kcal/mol followed by −31.13 kcal/mol for $B_{12}N_{12}$ nanocage, and −25.13 kcal/mol for both $Al_{12}P_{12}$ and $B_{12}P_{12}$ nanocages. Following the same trend, while adsorption of 4-AP on BNNC decreased the H-L energy gap only to 6.25 eV from 6.31 eV, it hadn't decreased at all from 4.79 eV for AlP nanocage. On the other side, the H-L energy gap was reduced to 8.05 eV from 9.43 eV on the adsorption of 4-AP towards BNNC following by 5.17 eV from 5.55 eV for BP nanocage. Hence it was concluded that the sensitivity of the BN and BP was higher than AlN and AlP towards 4-AP made BN and BP structures a potential sensor candidate to detect 4-AP.

Finally, the AlN nanoclusters were also proposed to be applied as a sensor for anticancer drug Purinethol (PE) or mercaptopurine, by S. A. Javarsineh et al. using DFT theory with B3LYP hybrid functional and the 6-31G (d) basis set [388]. In early 1950s PE drug was first evaluated to treat leukaemia, but this hepatotoxic drug comes with several serious adverse effects like bone-marrow depression, abnormal liver function etc. which sometimes requires withdrawal of the drug from the human body which indicates rising importance for the PE sensor [393]. The AlN nanocage made spontaneous chemisorption with the PE drug with a maximum adsorption energy of −38.2 kcal/mol. Also, it showed relatively good sensitivity towards the PE drug with a maximum decrease in the H-L energy gap by 37.2% to 2.48 eV with a maximum charge transfer of 0.23e from drug to the nanocage. These made AlN nanocage a promising candidate for the PE drug, but unfortunately, it suffers from a considerable recovery time of 3.1×10^{11} s. On the other hand, the AlN nanocone made a relatively weak interaction with PE with a maximum adsorption energy of −23.4 kcal/mol but showed relatively higher sensitivity towards the PE drug with a maximum decrease in the H-L energy gap by 59.5% to 1.22 eV. Besides, the AlN nanocone also benefits from a comparatively shorter recovery time of 20.8 s on the adsorption of PE in room temperature. Hence, the AlN nanocone holds a potential in the development of an electrochemical sensor to detect PE drug.

5.3. Gold and silver nanoparticles

B. Khodashenas et al. used the gelatin-coated gold nanoparticles (GNPs) to investigate the nanostructure's size effects on the curcumin drug encapsulations with the drug release mechanism using DFT theory with B3LYP hybrid functional and LanL2DZ basis set along with an experimental mechanism [392]. In order to do that, they have first synthesized GNPs with three different sizes (20, 50, and 100 nm) and then coated them with gelatin. The characterization of the structures was further ensured by the FT-IR spectroscopy, UV–Vis spectroscopy, dynamic light scattering, and scanning electron microscopy. From the DFT investigation, a further strong interaction between the GNP and gelatin was revealed with a binding energy of −22.73 kcal/mol and the gelatin works as an electron donor in the complex. Finally, it was observed that the efficiency of the curcumin drug encapsulations was increased slightly with an increase in the nanocluster size. For Au–gelatin (101 nm) structure the efficiency was 98.51% while the least was observed for the Au–gelatin (31.9 nm) as 97.8% following by 98.4% for the Au–gelatin (58.9 nm). Besides the drug release rate was observed higher at a low pH (5.4) environment compared to the relatively neutral environment with 7.4 pH.

Another experimental work along with DFT theory was carried out using by K. Geetha et al. to investigate the drug delivery properties of silver nanoparticles for the aromatic organic compounds, anthraquinone derivatives, which induced a potential interest in the biological applications in recent years [394]. They have prepared the anthraquinone derivative 1, 4-Dimethoxy 2-nitro-3-methylanthracene-9, 10-dione (DMNMAD) using an available method in the literature [395] and the silver nanoparticles were synthesized solution combustion method. For the quantum mechanical calculations, they have used the B3PW91 functional and LANL2DZ basis set with DFT theory. From the surface-enhanced Raman spectroscopy spectrum it was observed that the theoretical values from the DFT calculations for different vibrational modes of the structures were very close to the experimental values which ensured the validity of first-principles calculations for this system. Further from the DFT calculations the H-L energy gap of the DMNMAD was found as 2.81 eV which decreased to the 1.17 eV in the Ag- DMNMAD complex. This alteration in the electronic properties of DMNMAD holds a promise in the future drug delivery of anthraquinone derivatives

Table 2
Summary of the applications of various LDNs e.g., BN, AlN, GaN, MO, silicene, phosphorene etc. on biomolecule sensing, drug sensing, and drug delivery.

Adsorbate	Adsorbent	Adsorption energy, E_{ads} in kcal/mol	Remarks	References
Thioguanine	$B_{12}N_{12}$ nanocage	−38.85	Potential candidate for Thioguanine drug delivery	[361]
Ifosfamide	$B_{12}N_6C_6$	−42.89	Potential candidate for Ifosfamide drug delivery	[364]
	$B_6N_6C_{12}$	−45.89		
Cisplatin	$B_{12}N_{12}$ nanocage	−14.9	Potential candidate for Cisplatin detection	[365]
α-Cyano-4-hydroxycinnamic acid	$B_{12}N_{12}$ nanocage	−23.7	Potential candidate for α-cyano-4-hydroxycinnamic acid detection	[366]
Celecoxib	$B_{12}N_{12}$ nanocage	−30.21	Potential candidate for Celecoxib detection	[367]
Metformin	$B_{12}N_{12}$ nanocage	−37.35	Potential candidate for Metformin detection	[371]
	$GeB_{11}N_{12}$ nanocage	−37.13		
	$B_{16}N_{16}$ nanocage	−36.44		
Thymine	Al doped BN	−60.63	Potential candidate for Thymine adsorption	[306]
5-Fluorouracil	BNNS	−19.59	Potential candidate for 5-fluorouracil and 6-mercapto purine drugs delivery and 6-thioguanine detection	[99]
6-Mercaptopurine		−23.19		
6-Thioguanine		−26.53		
G > T > A > U > C	Armchair BN nano ribbon	−8.95 to −14.39	Potential candidate for nucleobases sensing	[307]
G > C > A > T > U	Zigzag BN nano ribbon	−13.07 to −18.33	Potential candidate for nucleobases sensing	
Cathinone	$B_{12}N_{12}$ nanocage	−16.1	Potential candidate for Cathinone detection	[308]
Mercaptopurine	BNNT	−18.7	Potential candidate for Mercaptopurine detection	[309]
Sulfonamide	BNNT	−25.41	Potential candidate for Sulfonamide detection	[333]
	Al doped BNNT	−59.73	Potential candidate of decomposition agent for Sulfonamide	
5-Fluorouracil	Ga doped BNNT	−34.59	Potential candidate for 5-fluorouracil drug delivery	[132]
	Al doped BNNT	−42.89	Potential candidate for 5-fluorouracil detection	
	Armchair BNNT	−9.01	Potential candidate for 5-fluorouracil drug delivery	[334]
Carmustine	-OH functionalized BNNT	−18.77	Potential candidate for Carmustine drug delivery	[91]
Floxuridine	(9, 9-7) armchair BNNT	−0.28	Potential candidate for Floxuridine drug delivery	[338]
Paracetamol	Armchair BNNT	−49.20	Potential candidate for Paracetamol adsorption	[343]
Nitrosamine	$B_{3Al}NNT$	−33.22	Potential candidate for Nitrosamine sensor	[345]
Oxazole	(6, 0) zigzag BNNT	−18.68	Potential candidate for Oxazole and Isoxazole detection	[102]
Isoxazole		−15.22		
Fluorouracil	B_{36} nanosheet	−24.5	Potential candidate for Fluorouracil drug delivery	[372]
Metronidazole	B_{36} nanosheet	−22.1	Potential candidate for Metronidazole detection	[373]
A > G > C > T	B_{36} nanosheet	−4.4 to - 57.3	Potential candidate for DNA sequencing	[377]
Amantadine	B_{30} nanosheet	−53.34	Potential candidate for Amantadine drug delivery	[378]
Cisplatin	$Zn_{12}O_{12}$ nanocage	−31.7	Potential candidate for Cisplatin sensor	[383]
Carmustine	Maghemite (γ-Fe2O3) nanoparticle	−12.34	Potential candidate for Carmustine drug delivery	[382]
Isoniazid	Al doped $Mg_{12}O_{12}$ nanocage	−59.49	Potential candidate for Isoniazid drug delivery	[384]
Mercaptopyridine	$Be_{12}O_{12}$ nanocluster	−38.91	Potential candidate for Mercaptopyridine sensor	[385]
	Sc and Ti doped $Be_{12}O_{12}$ nanocluster	−59.68		
Isoniazid	Ni-doped (4, 4) armchair GaNNT	−107.14	Potential candidate for Isoniazid sensor	[387]
Mercaptopurine	AlN nanocone	−23.4	Potential candidate for Mercaptopurine sensor	[388]
β-Keto-amphetamine	AlN nanosheet	−15.77	Potential candidate for β-keto-amphetamine sensor	[389]
Amantadine	AlN nanocage	−38.4	Potential candidate for Amantadine sensor	[92]
	BNNC	−31.3		
Acetylsalicylic acid	BNNC	−21.9	Potential candidate for Acetylsalicylic acid sensor	[390]
4-Aminopyridine	BNNC	−31.13	Potential candidate for 4-aminopyridine drug delivery	[391]
Curcumin	Gold nanoparticles	−22.73	Potential candidate for Curcumin drug delivery	[392]
Acetaminophen	Silicene	−25.83	Potential candidate for Acetaminophen drug delivery	[89]
	Phosphorene	−20.99	Potential candidate for Acetaminophen detection	
	BNNS	−25.37		

which was further investigated using UV–Vis spectroscopy, molecular electrostatic potential etc. Another micromolecule, poly (amido-amine) (PAMAM) dendrimers, recently had attention for working as a drug delivery system, electrochemical sensor etc. and the interaction of PAMAM with GNPs was investigated by M. B. Camarada using DFT theory with B3LYP hybrid exchange correlational [396]. It was observed that the PAMAM interacted with the GNPs with maximum interaction energy of 35.196 kcal/mol (BSSE corrected) with an adsorbent-adsorbate distance ranging as 2.177 to 2.435 Å. This interaction increased the DM of the complex significantly to a maximum of 13.74 debye from 7.54 debye with a maximum decrease in the H-L energy gap to 1.83 eV from 5.57 eV. These alterations in the electronic properties indicate a promising application of Au- PAMAM in the field of drug delivery and sensor.

5.4. Phosphorene nanosheet

D. Cortés-Arriagada et al. used another graphene-like nanosheet, phosphorene, to investigate the interaction of nucleobases which plays an important role in designing drug molecules [397]. For the DFT calculations, they have used DFT-D methods with PBE functional and def2-SVP basis sets. The nucleobases were observed to be adsorbed on the surface of phosphorene nanosheet more strongly than the GNS where the most stable interaction was observed with guanine (G) nucleobase. The range of adsorption energies for the nucleobases on GNS was observed on a range 12.45 to 18.68 kcal/mol which increased as 14.76 to 21.68 kcal/mol on the phosphorene nanosheet with weak long-range electrostatic closed-shell interactions. The stability was further increased while the nucleobases worked as a base pair

and the most stable pair was C-G pair on the adsorption towards phosphorene with an adsorption energy of 33.20 kcal/mol following by 32.05 and 29.52 kcal/mol for A-T and A-U bases. During the interactions of nucleobases with phosphorene, a significant contribution to the Van Der Waals dispersion energy was observed, and it was in the range of 15.91 to 22.37 kcal/mol for single nucleobases while was 35.05 to 38.51 kcal/mol for base pairs adsorption on phosphorene. But the adsorption of nucleobases almost failed to alter the electronic properties of phosphorene but increased the DM to as high as 3.57 debye in the base pairs and 3.30 debye for the single nucleobases while it was zero for the phosphorene nanosheet alone. These properties hold potential for the phosphorene nanosheet in the development of biosensors, nano-drug carrier vehicles or to be applied in DNA/RNA sequencing.

The phosphorene nanosheet was further investigated by U. Saikia et al. to find an efficient electrochemical sensor or nano-drug delivery vehicle for acetaminophen drug or more commonly known as paracetamol [89]. It was observed that phosphorene adsorbed acetaminophen drug slightly more strongly compared to graphene with an adsorption energy of −20.99 kcal/mol and an adsorbent-adsorbate distance of 3.28 Å following by −20.06 kcal/mol and 3.13 Å for graphene. But the phosphorene clearly outnumbered the graphene and BNNS in terms of charge transfer and DM which was 0.27e and 6.1 debye respectively for phosphorene following by 0.01e and 2.5 debye for graphene, and 0.06e and 3.2 debye for BNNS though BNNS adsorbed acetaminophen more strongly than phosphorene with an adsorption energy of −25.37 kcal/mol with a lower adsorbent-adsorbate distance of 3.07 Å. However, the most alluring interaction properties were observed for acetaminophen adsorption on the silicene, a two-dimensional nanosheet made of silicon atoms. When the drug was adsorbed in parallel with silicene, it was adsorbed with an adsorption energy of −21.68 kcal/mol but with a small adsorbent-adsorbate distance of 1.83 Å. This lead to a higher amount charge transfer between the drug and nanosheet of 0.57e along with a significantly increased DM of 16.2 debye. For the perpendicular orientation of the drug with silicene, a more stable interaction was observed with an adsorption energy of −25.83 kcal/mol but with a slightly less charge transfer and DM of 0.48e and 15.7 debye respectively. Hence, the silicene surely holds a potential to be applied as a nano-drug carrier for acetaminophen drug, whereas other structures may work as a sensor to detect acetaminophen drug which can be explored through experimental research.

6. Conclusion

After analyzing this vast number of research works, LDNs can be concluded as promising candidate for the bio-sensing and drug delivery related applications. The biocompatibility and a great variety of the LDNs with significant noble properties made these materials to work as sensors and delivery systems for many different types of drugs and biomolecules. Besides, the quantum mechanical calculations have shown a considerable accuracy on predicting the different properties of the nanomaterials in the nanoscale range with a close resemblance to the experimental outcomes. Furthermore, these first-principles calculation methods hold a promising future with the increasing computational abilities, which will significantly assist experimental researchers in developing any biomedical devices in a considerably short period of time during an emergency-response-situation. We have observed that the first-principles calculations allow researchers to calculate a wide range of essential properties from an atomic perspective to firmly understand the interaction of drug molecules with the nanomaterials. For the drug delivery systems, it also allows investigating the drug release mechanism in the targeted cell region. The excellent mechanical and electronic properties along with the biocompatibility of carbon-based LDNs, e.g. graphene, CNT, fullerenes etc. made themselves even-handed to be investigated more extensively than other nanomaterials to be applied in the stable drug sensor and drug delivery systems for various kind of drugs which show significant adverse effects in the human and animal bodies. Among other nanomaterials, BNNS and its allotropes, e.g. BNNT, BNNC showed a comparable mechanical strength, enhanced thermal stability, and other properties similar to the carbon-based nanomaterials which are being applied in the development of highly durable biosensors and drug delivery systems. Other nanostructures like quasi-planar B_{36}, phosphorene, gold nanoparticles, metal nitrides etc. were investigated less extensively but showed promising sensing behaviour towards many drugs and biomolecules. Especially, phosphorene, semimetal and post-transition metal nanostructures were studied to detect many toxic nerve agent, kidney biomarkers etc. Hence, these nanomaterials can further be investigated to develop biosensors to detect many other drugs and biomolecules. In conclusion, the wide variety of LDNs with many alluring novel properties holds a great potential in biomedical applications where first-principles investigations with rapidly increasing computational abilities will assist researchers in understanding these systems from the atomic perspective at a low cost with considerable accuracy.

CRediT authorship contribution statement

Hamidur Rahman: Writing - original draft, Formal analysis, Investigation. **Md. Rakib Hossain:** Conceptualization, Supervision, Writing - review & editing, Validation. **Tahmina Ferdous:** Project administration, Funding acquisition, Supervision.

Declaration of competing interest

The authors declare that they have no known competing financial interests or personal relationships that could have appeared to influence the work reported in this paper.

Acknowledgements

We thankfully acknowledge the Higher Education Quality Enhancement Program (HEQEP) subproject CP-3415, University Grant Commission (UGC) of Bangladesh, and the World Bank for the financial assistance to set up the Computational Physics (CP) Research Lab in the Department of Physics at Jahangirnagar University. Also, we would like to give our special gratitude to Ahmad Azuad Yaseer and Shawon Mahmud for their valuable assistance with the graphical content creation.

References

[1] R. Feynman, There's plenty of room at the bottom, Feynman Comput. (2018) 63–76, https://doi.org/10.1201/9780429500459.
[2] H.W. Kroto, J.R. Heath, S.C. O'Brien, R.F. Curl, R.E. Smalley, C60: buckminsterfullerene, Nature 318 (1985) 162–163, https://doi.org/10.1038/318162a0.
[3] H.E. Jeong, J.-K. Lee, H.N. Kim, S.H. Moon, K.Y. Suh, A nontransferring dry adhesive with hierarchical polymer nanohairs, Proc. Natl. Acad. Sci. 106 (2009) 5639 LP–5644, https://doi.org/10.1073/pnas.0900323106.
[4] M.M.G. Alemany, L. Tortajada, X. Huang, M.L. Tiago, L.J. Gallego, J.R. Chelikowsky, Role of dimensionality and quantum confinement in p-type semiconductor indium phosphide quantum dots, Phys. Rev. B 78 (2008), 233101, https://doi.org/10.1103/PhysRevB.78.233101.
[5] J.A. Rogers, M.G. Lagally, R.G. Nuzzo, Synthesis, assembly and applications of semiconductor nanomembranes, Nature 477 (2011) 45–53, https://doi.org/10.1038/nature10381.
[6] M. Engel, D.B. Farmer, J.T. Azpiroz, J.-W.T. Seo, J. Kang, P. Avouris, M.C. Hersam, R. Krupke, M. Steiner, Graphene-enabled and directed nanomaterial placement from solution for large-scale device integration, Nat. Commun. 9 (2018) 4095, https://doi.org/10.1038/s41467-018-06604-4.
[7] H. Kwon, X. Li, J. Hong, C.E. Park, Y.J. Jeong, H.C. Moon, S.H. Kim, Non-lithographic direct patterning of carbon nanomaterial electrodes via electrohydrodynamic-printed wettability patterns by polymer brush for fabrication of organic field-effect transistor, Appl. Surf. Sci. 515 (2020), 145989, https://doi.org/10.1016/j.apsusc.2020.145989.
[8] J. Liu, S. Wang, Y. Qie, C. Zhang, Q. Sun, High-pressure-assisted design of porous topological semimetal carbon for Li-ion battery anode with high-rate performance, Phys. Rev. Mater. 2 (2018) 25403, https://doi.org/10.1103/PhysRevMaterials.2.025403.

[9] E.C. Ahn, H.-S.P. Wong, E. Pop, Carbon nanomaterials for non-volatile memories, Nat. Rev. Mater. 3 (2018), 18009, https://doi.org/10.1038/natrevmats.2018.9.
[10] H. Lee, W.I. Choi, J. Ihm, Combinatorial search for optimal hydrogen-storage nanomaterials based on polymers, Phys. Rev. Lett. 97 (2006) 56104, https://doi.org/10.1103/PhysRevLett.97.056104.
[11] R. Yu, Q. Lin, S.-F. Leung, Z. Fan, Nanomaterials and nanostructures for efficient light absorption and photovoltaics, Nano Energy 1 (2012) 57–72, https://doi.org/10.1016/j.nanoen.2011.10.002.
[12] X. Ma, W. Luo, M. Yan, L. He, L. Mai, In situ characterization of electrochemical processes in one dimensional nanomaterials for energy storages devices, Nano Energy 24 (2016) 165–188, https://doi.org/10.1016/j.nanoen.2016.03.023.
[13] Y. Xia, Nanomaterials at work in biomedical research, Nat. Mater. 7 (2008) 758–760, https://doi.org/10.1038/nmat2277.
[14] Y. Zhao, G. Xing, Z. Chai, Are carbon nanotubes safe? Nat. Nanotechnol. 3 (2008) 191–192, https://doi.org/10.1038/nnano.2008.77.
[15] W. Park, H. Shin, B. Choi, W.-K. Rhim, K. Na, D. Keun Han, Advanced hybrid nanomaterials for biomedical applications, Prog. Mater. Sci. 114 (2020), 100686, https://doi.org/10.1016/j.pmatsci.2020.100686.
[16] U.R. Dahal, E.E. Dormidontova, Spontaneous insertion, helix formation, and hydration of polyethylene oxide in carbon nanotubes, Phys. Rev. Lett. 117 (2016) 27801, https://doi.org/10.1103/PhysRevLett.117.027801.
[17] A. Kenry, Y. Geldert, K.P. Liu, C. Loh, Teck Lim, Nano-bio interactions between carbon nanomaterials and blood plasma proteins: why oxygen functionality matters, NPG Asia Mater. 9 (2017) e422, https://doi.org/10.1038/am.2017.129.
[18] J.P.A. Ioannidis, B.Y.S. Kim, A. Trounson, How to design preclinical studies in nanomedicine and cell therapy to maximize the prospects of clinical translation, Nat. Biomed. Eng. 2 (2018) 797–809, https://doi.org/10.1038/s41551-018-0314-y.
[19] N.C. Seeman, H.F. Sleiman, DNA nanotechnology, Nat. Rev. Mater. 3 (2017), 17068, https://doi.org/10.1038/natrevmats.2017.68.
[20] E.J. Siochi, Graphene in the sky and beyond, Nat. Nanotechnol. 9 (2014) 745–747, https://doi.org/10.1038/nnano.2014.231.
[21] S. Singh, K. Rathi, K. Pal, Synthesis, characterization of graphene oxide wrapped silicon carbide for excellent mechanical and damping performance for aerospace application, J. Alloys Compd. 740 (2018) 436–445, https://doi.org/10.1016/j.jallcom.2017.12.069.
[22] M.S. Islam, Y. Deng, L. Tong, S.N. Faisal, A.K. Roy, A.I. Minett, V.G. Gomes, Grafting carbon nanotubes directly onto carbon fibers for superior mechanical stability: towards next generation aerospace composites and energy storage applications, Carbon N. Y. 96 (2016) 701–710, https://doi.org/10.1016/j.carbon.2015.10.002.
[23] M. Daniyal, A. Azam, S. Akhtar, in: Z.H. Khan (Ed.), Application of Nanomaterials in Civil Engineering BT-nanomaterials and Their Applications, Springer Singapore, Singapore 2018, pp. 169–189, https://doi.org/10.1007/978-981-10-6214-8_6.
[24] F. Pacheco-Torgal, S. Jalali, Nanotechnology: advantages and drawbacks in the field of construction and building materials, Constr. Build. Mater. 25 (2011) 582–590, https://doi.org/10.1016/j.conbuildmat.2010.07.009.
[25] R. Olawoyin, Nanotechnology: the future of fire safety, Saf. Sci. 110 (2018) 214–221, https://doi.org/10.1016/j.ssci.2018.08.016.
[26] M.J. Hanus, A.T. Harris, Nanotechnology innovations for the construction industry, Prog. Mater. Sci. 58 (2013) 1056–1102, https://doi.org/10.1016/j.pmatsci.2013.04.001.
[27] Nanofood for thought, Nat. Nanotechnol. 5 (2010) 89, https://doi.org/10.1038/nnano.2010.22.
[28] T.V. Duncan, Applications of nanotechnology in food packaging and food safety: barrier materials, antimicrobials and sensors, J. Colloid Interface Sci. 363 (2011) 1–24, https://doi.org/10.1016/j.jcis.2011.07.017.
[29] X. He, H. Deng, H. Hwang, The current application of nanotechnology in food and agriculture, J. Food Drug Anal. 27 (2019) 1–21, https://doi.org/10.1016/j.jfda.2018.12.002.
[30] A.I.S. Neves, D.P. Rodrigues, A. De Sanctis, E.T. Alonso, M.S. Pereira, V.S. Amaral, L.V. Melo, S. Russo, I. de Schrijver, H. Alves, M.F. Craciun, Towards conductive textiles: coating polymeric fibres with graphene, Sci. Rep. 7 (2017) 4250, https://doi.org/10.1038/s41598-017-04453-7.
[31] A. Zubair, X. Wang, F. Mirri, D.E. Tsentalovich, N. Fujimura, D. Suzuki, K.P. Soundarapandian, Y. Kawano, M. Pasquali, J. Kono, Carbon nanotube woven textile photodetector, Phys. Rev. Mater. 2 (2018) 15201, https://doi.org/10.1103/PhysRevMaterials.2.015201.
[32] W. He, P. Song, B. Yu, Z. Fang, H. Wang, Flame retardant polymeric nanocomposites through the combination of nanomaterials and conventional flame retardants, Prog. Mater. Sci. 114 (2020), 100687, https://doi.org/10.1016/j.pmatsci.2020.100687.
[33] K. Khezri, M. Saeedi, S. Maleki Dizaj, Application of nanoparticles in percutaneous delivery of active ingredients in cosmetic preparations, Biomed. Pharmacother. 106 (2018) 1499–1505, https://doi.org/10.1016/j.biopha.2018.07.084.
[34] L.M. Katz, K. Dewan, R.L. Bronaugh, Nanotechnology in cosmetics, Food Chem. Toxicol. 85 (2015) 127–137, https://doi.org/10.1016/j.fct.2015.06.020.
[35] D.M. Bowman, G. van Calster, S. Friedrichs, Nanomaterials and regulation of cosmetics, Nat. Nanotechnol. 5 (2010) 92, https://doi.org/10.1038/nnano.2010.12.
[36] C. Lee, X. Wei, J.W. Kysar, J. Hone, Measurement of the elastic properties and intrinsic strength of monolayer graphene, Science (80-.) 321 (2008) 385–388, https://doi.org/10.1126/science.1157996.
[37] Qian Dong, J. Wagner Gregory, W.K. Liu, M.-F. Yu, R.S. Ruoff, Mechanics of carbon nanotubes, Appl. Mech. Rev. 55 (2002) 495–533, https://doi.org/10.1115/1.1490129.
[38] A. Zunger, A. Katzir, A. Halperin, Optical properties of hexagonal boron nitride, Phys. Rev. B 13 (1976) 5560–5573, https://doi.org/10.1103/PhysRevB.13.5560.
[39] B. Lalmi, H. Oughaddou, H. Enriquez, A. Kara, S. Vizzini, B. Ealet, B. Aufray, Epitaxial growth of a silicene sheet, Appl. Phys. Lett. 97 (2010), 223109, https://doi.org/10.1063/1.3524215.
[40] H. Liu, A.T. Neal, Z. Zhu, Z. Luo, X. Xu, D. Tománek, P.D. Ye, Phosphorene: an unexplored 2D semiconductor with a high hole mobility, ACS Nano 8 (2014) 4033–4041, https://doi.org/10.1021/nn501226z.
[41] M.E. Dávila, L. Xian, S. Cahangirov, A. Rubio, G. Le Lay, Germanene: a novel two-dimensional germanium allotrope akin to graphene and silicene, New J. Phys. 16 (2014), 095002, https://doi.org/10.1088/1367-2630/16/9/095002.
[42] Y. Xu, B. Yan, H.-J. Zhang, J. Wang, G. Xu, P. Tang, W. Duan, S.-C. Zhang, Large-gap quantum spin hall insulators in tin films, Phys. Rev. Lett. 111 (2013), 136804, https://doi.org/10.1103/PhysRevLett.111.136804.
[43] V.L. Colvin, The potential environmental impact of engineered nanomaterials, Nat. Biotechnol. 21 (2003) 1166–1170, https://doi.org/10.1038/nbt875.
[44] The Royal Society, T.R.A. of Engineering, A. Dowling, R. Clift, N. Grobert, D. Hutton, R. Oliver, O. O'neill, J. Pethica, N. Pidgeon, J. Porritt, J. Ryan, et al., Nanoscience and nanotechnologies: opportunities and uncertainties, London R. Soc. R. Acad. Eng. Rep. 46 (2004) 618, https://doi.org/10.1007/s00234-004-1255-6.
[45] A.D. Maynard, R.J. Aitken, T. Butz, V. Colvin, K. Donaldson, G. Oberdörster, M.A. Philbert, J. Ryan, A. Seaton, V. Stone, S.S. Tinkle, L. Tran, N.J. Walker, D.B. Warheit, Safe handling of nanotechnology, Nature 444 (2006) 267–269, https://doi.org/10.1038/444267a.
[46] J. Morris, J. Willis, D. De Martinis, B. Hansen, H. Laursen, J.R. Sintes, P. Kearns, M. Gonzalez, Science policy considerations for responsible nanotechnology decisions, Nat. Nanotechnol. 6 (2011) 73–77, https://doi.org/10.1038/nnano.2010.191.
[47] H. Fan, L. Wang, K. Zhao, N. Li, Z. Shi, Z. Ge, Z. Jin, Fabrication, mechanical properties, and biocompatibility of graphene-reinforced chitosan composites, Biomacromolecules 11 (2010) 2345–2351, https://doi.org/10.1021/bm100470q.
[48] Z. Liu, S.M. Tabakman, Z. Chen, H. Dai, Preparation of carbon nanotube bioconjugates for biomedical applications, Nat. Protoc. 4 (2009) 1372–1381, https://doi.org/10.1038/nprot.2009.146.
[49] S.K. Smart, A.I. Cassady, G.Q. Lu, D.J. Martin, The biocompatibility of carbon nanotubes, Carbon N. Y. 44 (2006) 1034–1047, https://doi.org/10.1016/j.carbon.2005.10.011.
[50] S.T. Zuckerman, W.J. Kao, in: M.M. de Villiers, P. Aramwit, G.S. Kwon (Eds.), Nanomaterials and Biocompatibility: Carbon Nanotubes and Fullerenes BT-nanotechnology in Drug Delivery, Springer New York, New York, NY 2009, pp. 229–266, https://doi.org/10.1007/978-0-387-77668-2_8.
[51] M. Tatullo, B. Zavan, F. Genovese, B. Codispoti, I. Makeeva, S. Rengo, L. Fortunato, G. Spagnuolo, Borophene is a promising 2D allotropic material for biomedical devices, Appl. Sci. 9 (2019)https://doi.org/10.3390/app9173446.
[52] G. Ciofani, S. Danti, S. Nitti, B. Mazzolai, V. Mattoli, M. Giorgi, Biocompatibility of boron nitride nanotubes: an up-date of in vivo toxicological investigation, Int. J. Pharm. 444 (2013) 85–88, https://doi.org/10.1016/j.ijpharm.2013.01.037.
[53] A. Hulanicki, S. Glab, F. Ingman, Chemical sensors: definitions and classification, Pure Appl. Chem. 63 (1991) 1247–1250, https://doi.org/10.1351/pac199163091247.
[54] R. Boroujerdi, A. Abdelkader, R. Paul, State of the art in alcohol sensing with 2D materials, Nano-Micro Lett 12 (2020) 33, https://doi.org/10.1007/s40820-019-0363-0.
[55] M.T. Hwang, M. Heiranian, Y. Kim, S. You, J. Leem, A. Taqieddin, V. Faramarzi, Y. Jing, I. Park, A.M. van der Zande, S. Nam, N.R. Aluru, R. Bashir, Ultrasensitive detection of nucleic acids using deformed graphene channel field effect biosensors, Nat. Commun. 11 (2020) 1543, https://doi.org/10.1038/s41467-020-15330-9.
[56] A. Özkan, N. Atar, M.L. Yola, Enhanced surface plasmon resonance (SPR) signals based on immobilization of core-shell nanoparticles incorporated boron nitride nanosheets: development of molecularly imprinted SPR nanosensor for anticancer drug, etoposide, Biosens. Bioelectron. 130 (2019) 293–298, https://doi.org/10.1016/j.bios.2019.01.053.
[57] W. Zhang, B. Jia, H. Furumai, Fabrication of graphene film composite electrochemical biosensor as a pre-screening algal toxin detection tool in the event of water contamination, Sci. Rep. 8 (2018), 10686, https://doi.org/10.1038/s41598-018-28959-w.
[58] X. Pei, Z. Zhu, Z. Gan, J. Chen, X. Zhang, X. Cheng, Q. Wan, J. Wang, PEGylated nanographene oxide as a nanocarrier for delivering mixed anticancer drugs to improve anticancer activity, Sci. Rep. 10 (2020) 2717, https://doi.org/10.1038/s41598-020-59624-w.
[59] X.T. Zheng, P. Chen, C.M. Li, Anticancer efficacy and subcellular site of action investigated by real-time monitoring of cellular responses to localized drug delivery in single cells, Small 8 (2012) 2670–2674, https://doi.org/10.1002/smll.201102636.
[60] V.K. Rana, M.-C. Choi, J.-Y. Kong, G.Y. Kim, M.J. Kim, S.-H. Kim, S. Mishra, R.P. Singh, C.-S. Ha, Synthesis and drug-delivery behavior of chitosan-functionalized graphene oxide hybrid nanosheets, Macromol. Mater. Eng. 296 (2011) 131–140, https://doi.org/10.1002/mame.201000307.
[61] Y. Pan, H. Bao, N.G. Sahoo, T. Wu, L. Li, Water-soluble poly(N-isopropylacrylamide)–graphene sheets synthesized via click chemistry for drug delivery, Adv. Funct. Mater. 21 (2011) 2754–2763, https://doi.org/10.1002/adfm.201100078.
[62] L. Feng, S. Zhang, Z. Liu, Graphene based gene transfection, Nanoscale 3 (2011) 1252–1257, https://doi.org/10.1039/C0NR00680G.
[63] H. Kim, R. Namgung, K. Singha, I.-K. Oh, W.J. Kim, Graphene oxide–polyethylenimine nanoconstruct as a gene delivery vector and bioimaging tool, Bioconjug. Chem. 22 (2011) 2558–2567, https://doi.org/10.1021/bc200397j.
[64] T. Ren, L. Li, X. Cai, H. Dong, S. Liu, Y. Li, Engineered polyethylenimine/graphene oxide nanocomposite for nuclear localized gene delivery, Polym. Chem. 3 (2012) 2561–2569, https://doi.org/10.1039/C2PY20343J.

[65] L. Zhang, Z. Lu, Q. Zhao, J. Huang, H. Shen, Z. Zhang, Enhanced chemotherapy efficacy by sequential delivery of siRNA and anticancer drugs using PEI-grafted graphene oxide, Small 7 (2011) 460–464, https://doi.org/10.1002/smll.201001522.
[66] F. Zhi, H. Dong, X. Jia, W. Guo, H. Lu, Y. Yang, H. Ju, X. Zhang, Y. Hu, Functionalized graphene oxide mediated Adriamycin delivery and miR-21 gene silencing to overcome tumor multidrug resistance in vitro, PLoS One 8 (2013), e60034, https://doi.org/10.1371/journal.pone.0060034.
[67] Y. Sun, J. Zhou, Q. Cheng, D. Lin, Q. Jiang, A. Dong, Z. Liang, L. Deng, Fabrication of mPEGylated graphene oxide/poly(2-dimethyl aminoethyl methacrylate) nanohybrids and their primary application for small interfering RNA delivery, J. Appl. Polym. Sci. 133 (2016)https://doi.org/10.1002/app.43303.
[68] P. Huang, C. Xu, J. Lin, C. Wang, X. Wang, C. Zhang, X. Zhou, S. Guo, D. Cui, Folic acid-conjugated graphene oxide loaded with photosensitizers for targeting photodynamic therapy, Theranostics 1 (2011) 240–250, https://doi.org/10.7150/thno/v01p0240.
[69] J. Hong, N.J. Shah, A.C. Drake, P.C. DeMuth, J.B. Lee, J. Chen, P.T. Hammond, Graphene multilayers as gates for multi-week sequential release of proteins from surfaces, ACS Nano 6 (2012) 81–88, https://doi.org/10.1021/nn202607r.
[70] M. Choi, K.-G. Kim, J. Heo, H. Jeong, S.Y. Kim, J. Hong, Multilayered graphene nanofilm for controlled protein delivery by desired electro-stimuli, Sci. Rep. 5 (2015), 17631, https://doi.org/10.1038/srep17631.
[71] E. Czarniewska, L. Mrówczyńska, M. Jędrzejczak-Silicka, P. Nowicki, M. Trukawka, E. Mijowska, Non-cytotoxic hydroxyl-functionalized exfoliated boron nitride nanoflakes impair the immunological function of insect haemocytes in vivo, Sci. Rep. 9 (2019) 14027, https://doi.org/10.1038/s41598-019-50097-0.
[72] X. Li, X. Wang, J. Zhang, N. Hanagata, X. Wang, Q. Weng, A. Ito, Y. Bando, D. Golberg, Hollow boron nitride nanospheres as boron reservoir for prostate cancer treatment, Nat. Commun. 8 (2017), 13936, https://doi.org/10.1038/ncomms13936.
[73] X. Li, C. Zhi, N. Hanagata, M. Yamaguchi, Y. Bando, D. Golberg, Boron nitride nanotubes functionalized with mesoporous silica for intracellular delivery of chemotherapy drugs, Chem. Commun. 49 (2013) 7337–7339, https://doi.org/10.1039/C3CC42743A.
[74] C.-Y. Sun, C. Qin, C.-G. Wang, Z.-M. Su, S. Wang, X.-L. Wang, G.-S. Yang, K.-Z. Shao, Y.-Q. Lan, E.-B. Wang, Chiral nanoporous metal-organic frameworks with high porosity as materials for drug delivery, Adv. Mater. 23 (2011) 5629–5632, https://doi.org/10.1002/adma.201102538.
[75] W. Chen, J. Ouyang, H. Liu, M. Chen, K. Zeng, J. Sheng, Z. Liu, Y. Han, L. Wang, J. Li, L. Deng, Y.-N. Liu, S. Guo, Black phosphorus nanosheet-based drug delivery system for synergistic photodynamic/photothermal/chemotherapy of cancer, Adv. Mater. 29 (2017), 1603864, https://doi.org/10.1002/adma.201603864.
[76] G.F. Paciotti, L. Myer, D. Weinreich, D. Goia, N. Pavel, R.E. McLaughlin, L. Tamarkin, Colloidal gold: a novel nanoparticle vector for tumor directed drug delivery, Drug Deliv 11 (2004) 169–183, https://doi.org/10.1080/10717540490433895.
[77] A.D. Bani-Yaseen, A.S. Al-Jaber, H.M. Ali, Probing the solute-solvent interaction of an azo-bonded prodrug in neat and binary media: combined experimental and computational study, Sci. Rep. 9 (2019) 3023, https://doi.org/10.1038/s41598-019-39028-1.
[78] N. Singh, M. Arish, P. Kumar, A. Rub, U. Riaz, Experimental and theoretical studies of novel azo benzene functionalized conjugated polymers: in-vitro antileishmanial activity and bioimaging, Sci. Rep. 10 (2020) 57, https://doi.org/10.1038/s41598-019-56975-x.
[79] R.A. Khan, M. Usman, R. Dhivya, P. Balaji, A. Alsalme, H. AlLohedan, F. Arjmand, K. AlFarhan, M.A. Akbarsha, F. Marchetti, C. Pettinari, S. Tabassum, Heteroleptic copper(I) complexes of "Scorpionate" bis-pyrazolyl carboxylate ligand with auxiliary phosphine as potential anticancer agents: an insight into cytotoxic mode, Sci. Rep. 7 (2017), 45229, https://doi.org/10.1038/srep45229.
[80] G.K. Pierens, T.K. Venkatachalam, D.C. Reutens, NMR and DFT investigations of structure of colchicine in various solvents including density functional theory calculations, Sci. Rep. 7 (2017) 5605, https://doi.org/10.1038/s41598-017-06005-5.
[81] G. Li, Y. Nieves-Quinones, H. Zhang, Q. Liang, S. Su, Q. Liu, M.C. Kozlowski, T. Jia, Transition-metal-free formal cross-coupling of aryl methyl sulfoxides and alcohols via nucleophilic activation of C-S bond, Nat. Commun. 11 (2020) 2890, https://doi.org/10.1038/s41467-020-16713-8.
[82] M.D. Ganji, S. Mirzaei, Z. Dalirandeh, Molecular origin of drug release by water boiling inside carbon nanotubes from reactive molecular dynamics simulation and DFT perspectives, Sci. Rep. 7 (2017) 4669, https://doi.org/10.1038/s41598-017-04981-2.
[83] V.M. Larkin, Introduction, Assist. Technol. 16 (2004) 73–84, https://doi.org/10.1080/10400435.2004.10132076.
[84] N. Saikia, R.C. Deka, First principles study on the boron-nitrogen domains segregated within (5,5) and (8,0) single-wall carbon nanotubes: formation energy, electronic structure and reactivity, Comput. Theor. Chem. 996 (2012) 11–20, https://doi.org/10.1016/j.comptc.2012.07.004.
[85] H. Sajid, S. Khan, K. Ayub, T. Mahmood, High selectivity of cyclic tetrapyrrole over tetrafuran and tetrathiophene toward toxic chemicals; a first-principles study, Microporous Mesoporous Mater. 299 (2020) 110126, https://doi.org/10.1016/j.micromeso.2020.110126.
[86] H. Ullah, K. Ayub, Z. Ullah, M. Hanif, R. Nawaz, A.-H.A. Shah, S. Bilal, Theoretical insight of polypyrrole ammonia gas sensor, Synth. Met. 172 (2013) 14–20, https://doi.org/10.1016/j.synthmet.2013.03.021.
[87] M.A. Hossain, M.R. Hossain, M.K. Hossain, J.I. Khandaker, F. Ahmed, T. Ferdous, M.A. Hossain, An ab initio study of the B35 boron nanocluster for application as atmospheric gas (NO,NO2,N2O,NH3) sensor, Chem. Phys. Lett. 754 (2020) 137701, https://doi.org/10.1016/j.cplett.2020.137701.
[88] J. Princy Maria, V. Nagarajan, R. Chandiramouli, Boron trifluoride interaction studies on graphdiyne nanotubes – a first-principles insight, Chem. Phys. Lett. 738 (2020), 136841, https://doi.org/10.1016/j.cplett.2019.136841.
[89] U. Saikia, N. Saikia, K. Waters, R. Pandey, M.B. Sahariah, Electronic properties of acetaminophen adsorbed on 2D clusters: a first principles density functional study, Chemistry Select 2 (2017) 3613–3621, https://doi.org/10.1002/slct.201601593.
[90] V. Nagarajan, R. Chandiramouli, A study on quercetin and 5-fluorouracil drug interaction on graphyne nanosheets and solvent effects—a first-principles study, J. Mol. Liq. 275 (2019) 713–722, https://doi.org/10.1016/j.molliq.2018.11.083.
[91] A. Mortazavifar, H. Raissi, A. Akbari, DFT and MD investigations on the functionalized boron nitride nanotube as an effective drug delivery carrier for Carmustine anticancer drug, J. Mol. Liq. 276 (2019) 577–587, https://doi.org/10.1016/j.molliq.2018.12.028.
[92] X. Sun, X. Wan, G. Li, J. Yu, V. Vahabi, Amantadine antiparkinsonian drug adsorption on the AlN and BN nanoclusters: a computational study, Phys. Lett. A 384 (2020), 126128, https://doi.org/10.1016/j.physleta.2019.126128.
[93] S.U.D. Shamim, T. Hussain, M.R. Hossian, M.K. Hossain, F. Ahmed, T. Ferdous, M.A. Hossain, A DFT study on the geometrical structures, electronic, and spectroscopic properties of inverse sandwich monocyclic boron nanoclusters ConBm (n = 1.2; m = 6–8), J. Mol. Model. 26 (2020) 153, https://doi.org/10.1007/s00894-020-04419-z.
[94] G. Makov, Chemical hardness in density functional theory, J. Phys. Chem. 99 (1995) 9337–9339, https://doi.org/10.1021/j100023a006.
[95] T.A. Koopmans, Ordering of wave functions and eigenenergies to the individual electrons of an atom, Physica. 1 (1934) 104–113.
[96] R.G. Parr, L.V. Szentpály, S. Liu, Electrophilicity index, J. Am. Chem. Soc. 121 (1999) 1922–1924, https://doi.org/10.1021/ja983494x.
[97] M. Solimannejad, M. Noormohammadbeigi, Boron nitride nanotube (BNNT) as a sensor of hydroperoxyl radical (HO2): a DFT study, J. Iran. Chem. Soc. 14 (2017) 471–476, https://doi.org/10.1007/s13738-016-0994-8.
[98] M. Kamel, H. Raissi, A. Morsali, Theoretical study of solvent and co-solvent effects on the interaction of flutamide anticancer drug with carbon nanotube as a drug delivery system, J. Mol. Liq. 248 (2017) 490–500, https://doi.org/10.1016/j.molliq.2017.10.078.
[99] M. Vatanparast, Z. Shariatinia, Hexagonal boron nitride nanosheet as novel drug delivery system for anticancer drugs: insights from DFT calculations and molecular dynamics simulations, J. Mol. Graph. Model. 89 (2019) 50–59, https://doi.org/10.1016/j.jmgm.2019.02.012.
[100] I. Rozas, I. Alkorta, J. Elguero, Behavior of ylides containing N, O, and C atoms as hydrogen bond acceptors, J. Am. Chem. Soc. 122 (2000) 11154–11161, https://doi.org/10.1021/ja0017864.
[101] R.G. Parr, R.G. Pearson, Absolute hardness: companion parameter to absolute electronegativity, J. Am. Chem. Soc. 105 (1983) 7512–7516, https://doi.org/10.1021/ja00364a005.
[102] J. Kaur, P. Singla, N. Goel, Adsorption of oxazole and isoxazole on BNNT surface: a DFT study, Appl. Surf. Sci. 328 (2015) 632–640, https://doi.org/10.1016/j.apsusc.2014.12.099.
[103] V. Koncar, 4-Structural health monitoring of processes related to composite manufacturing, in: V.B.T.-S.T. for I.S.M. of C. Koncar (Ed.), Text. Inst. B. Ser, Woodhead Publishing 2019, pp. 295–381, https://doi.org/10.1016/B978-0-08-102308-2.00004-8.
[104] H. Chang, X. Lv, H. Zhang, J. Li, Quantum dots sensitized graphene: in situ growth and application in photoelectrochemical cells, Electrochem. Commun. 12 (2010) 483–487, https://doi.org/10.1016/j.elecom.2010.01.025.
[105] J. Liu, L. Cui, D. Losic, Graphene and graphene oxide as new nanocarriers for drug delivery applications, Acta Biomater. 9 (2013) 9243–9257, https://doi.org/10.1016/j.actbio.2013.08.016.
[106] M. Shahabi, H. Raissi, Investigation of the solvent effect, molecular structure, electronic properties and adsorption mechanism of Tegafur anticancer drug on graphene nanosheet surface as drug delivery system by molecular dynamics simulation and density functional approach, J. Incl. Phenom. Macrocycl. Chem. 88 (2017) 159–169, https://doi.org/10.1007/s10847-017-0713-9.
[107] S.S. Varghese, S. Lonkar, K.K. Singh, S. Swaminathan, A. Abdala, Recent advances in graphene based gas sensors, Sensors Actuators B Chem. 218 (2015) 160–183, https://doi.org/10.1016/j.snb.2015.04.062.
[108] T. Kuila, S. Bose, P. Khanra, A.K. Mishra, N.H. Kim, J.H. Lee, Recent advances in graphene-based biosensors, Biosens. Bioelectron. 26 (2011) 4637–4648, https://doi.org/10.1016/j.bios.2011.05.039.
[109] K.S. Novoselov, A.K. Geim, S.V. Morozov, D. Jiang, Y. Zhang, S.V. Dubonos, I.V. Grigorieva, A.A. Firsov, Electric field in atomically thin carbon films, Science (80-.) 306 (2004) 666–669, https://doi.org/10.1126/science.1102896.
[110] X. Li, G. Zhang, X. Bai, X. Sun, X. Wang, E. Wang, H. Dai, Highly conducting graphene sheets and Langmuir-Blodgett films, Nat. Nanotechnol. 3 (2008) 538–542, https://doi.org/10.1038/nnano.2008.210.
[111] A. Reina, X. Jia, J. Ho, D. Nezich, H. Son, V. Bulovic, M.S. Dresselhaus, K. Jing, Large area, few-layer graphene films on arbitrary substrates by chemical vapor deposition, Nano Lett. 9 (2009) 30–35, https://doi.org/10.1021/nl801827v.
[112] S. Stankovich, D.A. Dikin, R.D. Piner, K.A. Kohlhaas, A. Kleinhammes, Y. Jia, Y. Wu, S.B.T. Nguyen, R.S. Ruoff, Synthesis of graphene-based nanosheets via chemical reduction of exfoliated graphite oxide, Carbon N. Y. 45 (2007) 1558–1565, https://doi.org/10.1016/j.carbon.2007.02.034.
[113] P. Lazar, R. Zbořil, M. Pumera, M. Otyepka, Chemical nature of boron and nitrogen dopant atoms in graphene strongly influences its electronic properties, Phys. Chem. Chem. Phys. 16 (2014) 14231–14235, https://doi.org/10.1039/c4cp01638f.
[114] A.A. Balandin, S. Ghosh, W. Bao, I. Calizo, D. Teweldebrhan, F. Miao, C.N. Lau, Superior thermal conductivity of single-layer graphene, Nano Lett. 8 (2008) 902–907, https://doi.org/10.1021/nl0731872.

[115] A.A. Balandin, Thermal properties of graphene and nanostructured carbon materials, Nat. Mater. 10 (2011) 579–581, https://doi.org/10.1038/nmat3064.
[116] X. Du, I. Skachko, A. Barker, E.Y. Andrei, Approaching ballistic transport in suspended graphene, Nat. Nanotechnol. 3 (2008) 491–495, https://doi.org/10.1038/nnano.2008.199.
[117] K.H. Liao, Y.S. Lin, C.W. MacOsko, C.L. Haynes, Cytotoxicity of graphene oxide and graphene in human erythrocytes and skin fibroblasts, ACS Appl. Mater. Interfaces 3 (2011) 2607–2615, https://doi.org/10.1021/am200428v.
[118] P. Wu, Q. Shao, Y. Hu, J. Jin, Y. Yin, H. Zhang, C. Cai, Direct electrochemistry of glucose oxidase assembled on graphene and application to glucose detection, Electrochim. Acta 25 (2010) 8606–8614, https://doi.org/10.1016/j.electacta.2010.07.079.
[119] Z. Wang, X.F. Zhou, X. Zhang, Q. Zhu, H. Dong, M. Zhao, A.R. Oganov, Phagraphene: a low-energy graphene allotrope composed of 5-6-7 carbon rings with distorted Dirac cones, Nano Lett. 15 (2015) 6182–6186, https://doi.org/10.1021/acs.nanolett.5b02512.
[120] C.J. Li, C. Wang, A.B. Pardee, Induction of apoptosis by β-lapachone in human prostate cancer cells, Cancer Res. 55 (1995) 3712 LP–3715http://cancerres.aacrjournals.org/content/55/17/3712.abstract.
[121] M. Ough, A. Lewis, E.A. Bey, J. Gao, J.M. Ritchie, W. Bornmann, D.A. Boothman, L.W. Oberley, J.J. Cullen, Efficacy of beta-lapachone in pancreatic cancer treatment: exploiting the novel, therapeutic target NQO1, Cancer Biol. Ther. 4 (2005) 102–109, https://doi.org/10.4161/cbt.4.1.1382.
[122] Y. Li, X. Sun, J.T. LaMont, A.B. Pardee, C.J. Li, Selective killing of cancer cells by β-lapachone: direct checkpoint activation as a strategy against cancer, Proc. Natl. Acad. Sci. 100 (2003) 2674 LP–2678, https://doi.org/10.1073/pnas.0538044100.
[123] Z. Khodadadi, L. Torkian, Studying metal-doped graphene nanosheet as a drug carrier for anticancer drug β-lapachone using density functional theory (DFT), Mater. Res. Express. 6 (2019), 065058, https://doi.org/10.1088/2053-1591/ab102c.
[124] E.L. De Beer, A.E. Bottone, E.E. Voest, Doxorubicin and mechanical performance of cardiac trabeculae after acute and chronic treatment: a review, Eur. J. Pharmacol. 415 (2001) 1–11, https://doi.org/10.1016/S0014-2999(01)00765-8.
[125] D.D. von Hoff, M.W. Layard, P. Basa, H.L. Davis, A.N.N.L. von Hoff, M. Rozencweig, F.M. Muggia, Risk factors for doxorubicin-induced congestive heart failure, Ann. Intern. Med. 91 (1979) 710–717, https://doi.org/10.7326/0003-4819-91-5-710.
[126] C.F. Thorn, C. Oshiro, S. Marsh, T. Hernandez-Boussard, H. McLeod, T.E. Klein, R.B. Altman, Doxorubicin pathways: pharmacodynamics and adverse effects, Pharmacogenet. Genomics 21 (2011), https://journals.lww.com/jpharmacogenetics/Fulltext/2011/07000/Doxorubicin_pathways___pharmacodynamics_and.11.aspx.
[127] M.Z. Tonel, M.O. Martins, I. Zanella, R.B. Pontes, S.B. Fagan, A first-principles study of the interaction of doxorubicin with graphene, Comput. Theor. Chem. 1115 (2017) 270–275, https://doi.org/10.1016/j.comptc.2017.07.004.
[128] Z. Wang, C. Zhou, J. Xia, B. Via, Y. Xia, F. Zhang, Y. Li, L. Xia, Fabrication and characterization of a triple functionalization of graphene oxide with Fe3O4, folic acid and doxorubicin as dual-targeted drug nanocarrier, Colloids Surfaces B Biointerfaces 106 (2013) 60–65, https://doi.org/10.1016/j.colsurfb.2013.01.032.
[129] T. Zhou, X. Zhou, D. Xing, Controlled release of doxorubicin from graphene oxide based charge-reversal nanocarrier, Biomaterials 35 (2014) 4185–4194, https://doi.org/10.1016/j.biomaterials.2014.01.044.
[130] N. Dastani, A. Arab, H. Raissi, Adsorption of Ampyra anticancer drug on the graphene and functionalized graphene as template materials with high efficient carrier, Adsorption 11 (2019) 1650038, https://doi.org/10.1007/s10450-019-00142-1.
[131] M.K. Hazrati, Z. Javanshir, Z. Bagheri, B24N24 fullerene as a carrier for 5-fluorouracil anti-cancer drug delivery: DFT studies, J. Mol. Graph. Model. 77 (2017) 17–24, https://doi.org/10.1016/j.jmgm.2017.08.003.
[132] A. Soltani, M.T. Baei, E. Tazikeh Lemeski, S. Kaveh, H. Balakheyli, A DFT study of 5-fluorouracil adsorption on the pure and doped BN nanotubes, J. Phys. Chem. Solids 86 (2015) 57–64, https://doi.org/10.1016/j.jpcs.2015.06.008.
[133] M. Vatanparast, Z. Shariatinia, AlN and AlP doped graphene quantum dots as novel drug delivery systems for 5-fluorouracil drug: theoretical studies, J. Fluor. Chem. 211 (2018) 81–93, https://doi.org/10.1016/j.jfluchem.2018.04.003.
[134] J.W.B. Cooke, R. Bright, M.J. Coleman, K.P. Jenkins, Process research and development of a dihydropyrimidine dehydrogenase inactivator: large-scale preparation of eniluracil using a Sonogashira coupling, Org. Process. Res. Dev. 5 (2001) 383–386, https://doi.org/10.1021/op0100100.
[135] N. Zhang, Y. Yin, S.J. Xu, W.S. Chen, 5-Fluorouracil: mechanisms of resistance and reversal strategies, Molecules 13 (2008) 1551–1569, https://doi.org/10.3390/molecules13081551.
[136] M. Shahabi, H. Raissi, Screening of the structural, topological, and electronic properties of the functionalized graphene nanosheets as potential Tegafur anticancer drug carriers using DFT method, J. Biomol. Struct. Dyn. 36 (2018) 2517–2529, https://doi.org/10.1080/07391102.2017.1360209.
[137] H. Ovaa, C. Kuijl, J. Neefjes, Recent and new targets for small molecule anti-cancer agents, Drug Discov. Today Technol. 6 (2009) e3–e11, https://doi.org/10.1016/j.ddtec.2010.01.001.
[138] C. Rungnim, R. Chanajaree, T. Rungrotmongkol, S. Hannongbua, N. Kungwan, P. Wolschann, A. Karpfen, V. Parasuk, How strong is the edge effect in the adsorption of anticancer drugs on a graphene cluster? J. Mol. Model. 22 (2016)https://doi.org/10.1007/s00894-016-2937-9.
[139] E. Miliordos, E. Aprà, S.S. Xantheas, Benchmark theoretical study of the π-π binding energy in the benzene dimer, J. Phys. Chem. A 118 (2014) 7568–7578, https://doi.org/10.1021/jp5024235.
[140] S. Gholami, A. Shokuhi Rad, A. Heydarinasab, M. Ardjmand, Adsorption of adenine on the surface of nickel-decorated graphene; a DFT study, J. Alloys Compd. 686 (2016) 662–668, https://doi.org/10.1016/j.jallcom.2016.06.097.
[141] A. Shokuhi Rad, Y.M. Jouibary, V.P. Foukolaei, E. Binaeian, Study on the structure and electronic property of adsorbed guanine on aluminum doped graphene: first principles calculations, Curr. Appl. Phys. 16 (2016) 527–533, https://doi.org/10.1016/j.cap.2016.02.004.
[142] A.R. Korenke, M.P. Rivey, D.R. Allington, Sustained-release fampridine for symptomatic treatment of multiple sclerosis, Ann. Pharmacother. 42 (2008) 1458–1465, https://doi.org/10.1345/aph.1L028.
[143] F. Shojaie, M. Dehghan, Theoretical study of functionalized single-walled carbon nanotube (5, 5) with mitoxantrone drug, Nanomedicine J. 3 (2016) 115–126, https://doi.org/10.7508/nmj.2016.02.005.
[144] M. Malhotra, P. Ghai, B. Narasimhan, A. Deep, Dalfampridine: review on its recent development for symptomatic improvement in patients with multiple sclerosis, Arab. J. Chem. 9 (2016) S1443–S1449, https://doi.org/10.1016/j.arabjc.2012.03.017.
[145] H. Yanagisawa, T. Tanaka, Y. Ishida, M. Matsue, E. Rokuta, S. Otani, C. Oshima, Phonon dispersion curves of a BC3 honeycomb epitaxial sheet, Phys. Rev. Lett. 93 (2004), 177003, https://doi.org/10.1103/PhysRevLett.93.177003.
[146] B. Saha, P.K. Bhattacharyya, Adsorption of amino acids on boron and/or nitrogen doped functionalized graphene: a Density Functional Study, Comput. Theor. Chem. 1086 (2016) 45–51, https://doi.org/10.1016/j.comptc.2016.04.017.
[147] H. Tavassoli Larijani, M. Darvish Ganji, M. Jahanshahi, Trends of amino acid adsorption onto graphene and graphene oxide surfaces: a dispersion corrected DFT study, RSC Adv. 5 (2015) 92843–92857, https://doi.org/10.1039/C5RA16683G.
[148] J.H. Chen, H.T. Chen, Computational explanation for interaction between amino acid and nitrogen-containing graphene, Theor. Chem. Accounts 137 (2018) 176, https://doi.org/10.1007/s00214-018-2392-z.
[149] R. Bagheri, M. Babazadeh, E. Vessally, M. Es'haghi, A. Bekhradnia, Si-doped phagraphene as a drug carrier for adrucil anti-cancer drug: DFT studies, Inorg. Chem. Commun. 90 (2018) 8–14, https://doi.org/10.1016/j.inoche.2018.01.020.
[150] S. Iijima, Helical microtubules of graphitic carbon, Nature 354 (1991) 56–58, https://doi.org/10.1038/354056a0.
[151] M.-F. Yu, O. Lourie, M.J. Dyer, K. Moloni, T.F. Kelly, R.S. Ruoff, Strength and breaking mechanism of multiwalled carbon nanotubes under tensile load, Science (80-.) 287 (2000) 637 LP–640, https://doi.org/10.1126/science.287.5453.637.
[152] E.A. Laird, F. Kuemmeth, G.A. Steele, K. Grove-Rasmussen, J. Nygård, K. Flensberg, L.P. Kouwenhoven, Quantum transport in carbon nanotubes, Rev. Mod. Phys. 87 (2015) 703–764, https://doi.org/10.1103/RevModPhys.87.703.
[153] A. Star, Y. Lu, K. Bradley, G. Grüner, Nanotube optoelectronic memory devices, Nano Lett. 4 (2004) 1587–1591, https://doi.org/10.1021/nl049337f.
[154] E. Pop, D. Mann, Q. Wang, K. Goodson, H. Dai, Thermal conductance of an individual single-wall carbon nanotube above room temperature, Nano Lett. 6 (2006) 96–100, https://doi.org/10.1021/nl052145f.
[155] G. Liu, Y. Zhao, K. Deng, Z. Liu, W. Chu, J. Chen, Y. Yang, K. Zheng, H. Huang, W. Ma, L. Song, H. Yang, C. Gu, G. Rao, C. Wang, S. Xie, L. Sun, Highly dense and perfectly aligned single-walled carbon nanotubes fabricated by diamond wire drawing dies, Nano Lett. 8 (2008) 1071–1075, https://doi.org/10.1021/nl073007o.
[156] S. Berber, Y.-K. Kwon, D. Tománek, Unusually high thermal conductivity of carbon nanotubes, Phys. Rev. Lett. 84 (2000) 4613–4616, https://doi.org/10.1103/PhysRevLett.84.4613.
[157] X.-M. Liu, Z. dong Huang, S. woon Oh, B. Zhang, P.-C. Ma, M.M.F. Yuen, J.-K. Kim, Carbon nanotube (CNT)-based composites as electrode material for rechargeable Li-ion batteries: a review, Compos. Sci. Technol. 72 (2012) 121–144, https://doi.org/10.1016/j.compscitech.2011.11.019.
[158] N. Saifuddin, A.Z. Raziah, A.R. Junizah, Carbon nanotubes: a review on structure and their interaction with proteins, J. Chem. 2013 (2013) 676815, https://doi.org/10.1155/2013/676815.
[159] E.T. Thostenson, Z. Ren, T.-W. Chou, Advances in the science and technology of carbon nanotubes and their composites: a review, Compos. Sci. Technol. 61 (2001) 1899–1912, https://doi.org/10.1016/S0266-3538(01)00094-X.
[160] M. José-Yacamán, M. Miki-Yoshida, L. Rendón, J.G. Santiesteban, Catalytic growth of carbon microtubules with fullerene structure, Appl. Phys. Lett. 62 (1993) 657–659, https://doi.org/10.1063/1.108857.
[161] A.G. Rinzler, J. Liu, H. Dai, P. Nikolaev, C.B. Huffman, F.J. Rodríguez-Macías, P.J. Boul, A.H. Lu, D. Heymann, D.T. Colbert, R.S. Lee, J.E. Fischer, A.M. Rao, P.C. Eklund, R.E. Smalley, Large-scale purification of single-wall carbon nanotubes: process, product, and characterization, Appl. Phys. A Mater. Sci. Process. 67 (1998) 29–37, https://doi.org/10.1007/s003390050734.
[162] O. Smiljanic, B.L. Stansfield, J.-P. Dodelet, A. Serventi, S. Désilets, Gas-phase synthesis of SWNT by an atmospheric pressure plasma jet, Chem. Phys. Lett. 356 (2002) 189–193, https://doi.org/10.1016/S0009-2614(02)00132-X.
[163] J. Ren, F.-F. Li, J. Lau, L. González-Urbina, S. Licht, One-pot synthesis of carbon nanofibers from CO2, Nano Lett. 15 (2015) 6142–6148, https://doi.org/10.1021/acs.nanolett.5b02427.
[164] Z.F. Ren, Z.P. Huang, J.W. Xu, J.H. Wang, P. Bush, M.P. Siegal, P.N. Provencio, Synthesis of large arrays of well-aligned carbon nanotubes on glass, Science (80-.) 282 (1998) 1105 LP–1107, https://doi.org/10.1126/science.282.5391.1105.
[165] C. Journet, W.K. Maser, P. Bernier, A. Loiseau, M.L. de la Chapelle, S. Lefrant, P. Deniard, R. Lee, J.E. Fischer, Large-scale production of single-walled carbon nanotubes by the electric-arc technique, Nature 388 (1997) 756–758, https://doi.org/10.1038/41972.
[166] P. Nikolaev, M.J. Bronikowski, R.K. Bradley, F. Rohmund, D.T. Colbert, K.A. Smith, R.E. Smalley, Gas-phase catalytic growth of single-walled carbon nanotubes from carbon monoxide, Chem. Phys. Lett. 313 (1999) 91–97, https://doi.org/10.1016/S0009-2614(99)01029-5.
[167] M. Meyyappan, L. Delzeit, A. Cassell, D. Hash, Carbon nanotube growth by PECVD: a review, Plasma Sources Sci. Technol. 12 (2003) 205–216, https://doi.org/10.1088/0963-0252/12/2/312.

[168] A. Iqbal, A. Saeed, A. Ul-Hamid, A review featuring the fundamentals and advancements of polymer/CNT nanocomposite application in aerospace industry, Polym. Bull. (2020)https://doi.org/10.1007/s00289-019-03096-0.
[169] P. Prakash, K. Mohana Sundaram, M. Anto Bennet, A review on carbon nanotube field effect transistors (CNTFETs) for ultra-low power applications, Renew. Sust. Energ. Rev. 89 (2018) 194–203, https://doi.org/10.1016/j.rser.2018.03.021.
[170] N.A.C. Sidik, M.N.A.W.M. Yazid, S. Samion, A review on the use of carbon nanotubes nanofluid for energy harvesting system, Int. J. Heat Mass Transf. 111 (2017) 782–794, https://doi.org/10.1016/j.ijheatmasstransfer.2017.04.047.
[171] Z. Xiao, L.B. Kong, S. Ruan, X. Li, S. Yu, X. Li, Y. Jiang, Z. Yao, S. Ye, C. Wang, T. Zhang, K. Zhou, S. Li, Recent development in nanocarbon materials for gas sensor applications, Sensors Actuators B Chem. 274 (2018) 235–267, https://doi.org/10.1016/j.snb.2018.07.040.
[172] S. Alim, J. Vejayan, M.M. Yusoff, A.K.M. Kafi, Recent uses of carbon nanotubes & gold nanoparticles in electrochemistry with application in biosensing: a review, Biosens. Bioelectron. 121 (2018) 125–136, https://doi.org/10.1016/j.bios.2018.08.051.
[173] J. Kaur, G.S. Gill, K. Jeet, Chapter 5 - applications of carbon nanotubes in drug delivery: a comprehensive review, in: S.S. Mohapatra, S. Ranjan, N. Dasgupta, R.K. Mishra, S.B.T.-C. and B. of N. for D.D. Thomas (Eds.), Micro Nano Technol., Elsevier, 2019: pp. 113–135. doi:https://doi.org/10.1016/B978-0-12-814031-4.00005-2.
[174] U. Arsawang, O. Saengsawang, T. Rungrotmongkol, P. Sornmee, K. Wittayanarakul, T. Remsungnen, S. Hannongbua, How do carbon nanotubes serve as carriers for gemcitabine transport in a drug delivery system? J. Mol. Graph. Model. 29 (2011) 591–596, https://doi.org/10.1016/j.jmgm.2010.11.002.
[175] S. Soylemez, B. Yoon, L. Toppare, T.M. Swager, Quaternized polymer–single-walled carbon nanotube scaffolds for a chemiresistive glucose sensor, ACS Sensors 2 (2017) 1123–1127, https://doi.org/10.1021/acssensors.7b00323.
[176] A. Bianco, Carbon nanotubes for the delivery of therapeutic molecules, Expert Opin. Drug Deliv. 1 (2004) 57–65, https://doi.org/10.1517/17425247.1.1.57.
[177] E. Katz, I. Willner, Biomolecule-functionalized carbon nanotubes: applications in nanobioelectronics, ChemPhysChem 5 (2004) 1084–1104, https://doi.org/10.1002/cphc.200400193.
[178] J. Li, S.Q. Yap, C.F. Chin, Q. Tian, S.L. Yoong, G. Pastorin, W.H. Ang, Platinum(iv) prodrugs entrapped within multiwalled carbon nanotubes: selective release by chemical reduction and hydrophobicity reversal, Chem. Sci. 3 (2012) 2083–2087, https://doi.org/10.1039/C2SC01086K.
[179] W. Zhang, Z. Zhang, Y. Zhang, The application of carbon nanotubes in target drug delivery systems for cancer therapies, Nanoscale Res. Lett. 6 (2011) 555, https://doi.org/10.1186/1556-276X-6-555.
[180] H. Shaki, H. Raissi, F. Mollania, H. Hashemzadeh, Modeling the interaction between anti-cancer drug penicillamine and pristine and functionalized carbon nanotubes for medical applications: density functional theory investigation and a molecular dynamics simulation, J. Biomol. Struct. Dyn. 38 (2020) 1322–1334, https://doi.org/10.1080/07391102.2019.1602080.
[181] J. Liu, Tuberculosis and the tubercle bacillus, Emerg. Infect. Dis. 11 (2005) 1331, https://doi.org/10.3201/eid1108.050611.
[182] N. Saikia, S. Rajkhowa, R.C. Deka, Si-doped single-walled carbon nanotubes interacting with isoniazid—a density functional and molecular docking study, RSC Adv. 6 (2016) 94651–94660, https://doi.org/10.1039/c6ra16020d.
[183] Y.-T. Li, T.-C. Chen, Effect of B/N co-doping on the stability and electronic structure of single-walled carbon nanotubes by first-principles theory, Nanotechnology 20 (2009), 375705, https://doi.org/10.1088/0957-4484/20/37/375705.
[184] U. Pelzer, K. Kubica, J. Stieler, I. Schwaner, G. Heil, M. Görner, M. Mölle, A. Hilbig, B. Dörken, H. Riess, H. Oettle, A randomized trial in patients with gemcitabine refractory pancreatic cancer. Final results of the CONKO 003 study, J. Clin. Oncol. 26 (2008) 4508, https://doi.org/10.1200/jco.2008.26.15_suppl.4508.
[185] R.P. Abratt, W.R. Bezwoda, G. Falkson, L. Goedhals, D. Hacking, T.A. Rugg, Efficacy and safety profile of gemcitabine in non-small-cell lung cancer: a phase II study, J. Clin. Oncol. 12 (1994) 1535–1540, https://doi.org/10.1200/JCO.1994.12.8.1535.
[186] U. Gatzemeier, F.A. Shepherd, T. Le Chevalier, P. Weynants, B. Cottier, H.J.M. Groen, R. Rosso, K. Mattson, H. Cortes-Funes, M. Tonato, R.L. Burkes, M. Gottfried, M. Voi, Activity of gemcitabine in patients with non-small cell lung cancer: a multicentre, extended phase II study, Eur. J. Cancer 32 (1996) 243–248, https://doi.org/10.1016/0959-8049(95)00444-0.
[187] K.S. Albain, S.M. Nag, G. Calderillo-Ruiz, J.P. Jordaan, A.C. Llombart, A. Pluzanska, J. Rolski, A.S. Melemed, J.M. Reyes-Vidal, J.S. Sekhon, L. Simms, J. O'Shaughnessy, Gemcitabine plus paclitaxel versus paclitaxel monotherapy in patients with metastatic breast cancer and prior anthracycline treatment, J. Clin. Oncol. 26 (2008) 3950–3957, https://doi.org/10.1200/JCO.2007.11.9362.
[188] N. Pavlakis, D.R. Bell, M.J. Millward, J.A. Levi, Fatal pulmonary toxicity resulting from treatment with gemcitabine, Cancer. 80 (1997) 286–291, https://doi.org/10.1002/(SICI)1097-0142(19970715)80:2<286::AID-CNCR17>3.0.CO;2-Q.
[189] R. Linskens, R. Golding, C. Groeningen, G. Giaccone, Severe acute lung injury induced by gemcitabine, Neth. J. Med. 56 (2000) 232–235, https://doi.org/10.1016/S0300-2977(00)00029-2.
[190] H. Moradnia, H. Raissi, A. Bakhtiari, A density functional theory-based analysis of the structural, topological and electronic properties of gemcitabine drug adsorption on the pyrrolidine functionalized single-walled carbon nanotube, J. Biomol. Struct. Dyn. 37 (2019) 2477–2486, https://doi.org/10.1080/07391102.2018.1491892.
[191] M. García Cortés, R.J. Andrade, M.I. Lucena, H. Sánchez Martínez, M.C. Fernández, T. Ferrer, R. Martín-Vivaldi, G. Peláez, F. Suárez, M. Romero-Gómez, J.L. Montero, E. Fraga, R. Camargo, R. Alcántara, M.A. Pizarro, E. García-Ruiz, M. Rosemary-Gómez, Flutamide-induced hepatotoxicity: report of a case series, Rev. Esp. Enfermedades Dig. Organo Of. La Soc. Esp. Patol. Dig. 93 (2001) 423–432.
[192] F. Chentli, F. Belhimer, Severe gynecomastia due to anti androgens intake: a case report and literature review, Indian J. Endocrinol. Metab. 17 (2013) 730–732, https://doi.org/10.4103/2230-8210.113770.
[193] F. Labrie, Mechanism of action and pure antiandrogenic properties of flutamide, Cancer. 72 (1993) 3816–3827, https://doi.org/10.1002/1097-0142(19931215)72:12+<3816::AID-CNCR2820721711>3.0.CO;2-3.
[194] M. Kamel, H. Raissi, A. Morsali, M. Shahabi, Assessment of the adsorption mechanism of Flutamide anticancer drug on the functionalized single-walled carbon nanotube surface as a drug delivery vehicle: An alternative theoretical approach based on DFT and MD, Appl. Surf. Sci. 434 (2018) 492–503, https://doi.org/10.1016/j.apsusc.2017.10.165.
[195] R. Khorram, H. Raissi, A. Morsali, Assessment of solvent effects on the interaction of Carmustine drug with the pristine and COOH-functionalized single-walled carbon nanotubes: a DFT perspective, J. Mol. Liq. 240 (2017) 87–97, https://doi.org/10.1016/j.molliq.2017.05.035.
[196] J.L. Wright, J.L. Stanford, Metformin use and prostate cancer in Caucasian men: results from a population-based case-control study, Cancer Causes Control 20 (2009) 1617–1622, https://doi.org/10.1007/s10552-009-9407-y.
[197] S. Jiralerspong, S.L. Palla, S.H. Giordano, F. Meric-Bernstam, C. Liedtke, C.M. Barnett, L. Hsu, M.C. Hung, G.N. Hortobagyi, A.M. Gonzalez-Angulo, Metformin and pathologic complete responses to neoadjuvant chemotherapy in diabetic patients with breast cancer, J. Clin. Oncol. 27 (2009) 3297–3302, https://doi.org/10.1200/JCO.2009.19.6410.
[198] D. Li, S.C.J. Yeung, M.M. Hassan, M. Konopleva, J.L. Abbruzzese, Antidiabetic therapies affect risk of pancreatic cancer, Gastroenterology 137 (2009) 482–488, https://doi.org/10.1053/j.gastro.2009.04.013.
[199] M.S. Hoseininezhad-Namin, P. Pargolghasemi, S. Alimohammadi, A.S. Rad, L. Taqavi, Quantum Chemical Study on the adsorption of metformin drug on the surface of pristine, Si- and Al-doped (5, 5) SWCNTs, Phys. E Low-Dimensional Syst. Nanostructures. 90 (2017) 204–213, https://doi.org/10.1016/j.physe.2017.04.002.
[200] M. Mirmotahari, E. Sani, A. Shokuhi Rad, M.A. Khalilzadeh, Calcium-doped single-wall nanotubes (Ca/SWCNTs) as a superior carrier for atropine drug delivery: a quantum-chemical study in gas and solvent phases, J. Biomol. Struct. Dyn. 37 (2019) 4267–4273, https://doi.org/10.1080/07391102.2018.1546233.
[201] A.-S. Lemaire-Hurtel, J.-C. Alvarez, in: P.B.T.-T.A. of D.-F.C. Kintz (Ed.), Chapter 3 - Drugs Involved in Drug-facilitated Crime—Pharmacological Aspects, Academic Press, Oxford 2014, pp. 47–91, https://doi.org/10.1016/B978-0-12-416748-3.00003-7.
[202] P. Zanos, R. Moaddel, P.J. Morris, L.M. Riggs, J.N. Highland, P. Georgiou, E.F.R. Pereira, E.X. Albuquerque, C.J. Thomas, C.A. Zarate, T.D. Gould, Ketamine and ketamine metabolite pharmacology: insights into therapeutic mechanisms, Pharmacol. Rev. 70 (2018) 621–660, https://doi.org/10.1124/pr.117.015198.
[203] R. Zhiani, I. Razavipanah, S. Emrani, Functionalized single-walled carbon nanotube for ketamine sensing: DFT and MD studies, Struct. Chem. 29 (2018) 1807–1815, https://doi.org/10.1007/s11224-018-1160-y.
[204] R. Bushra, N. Aslam, An overview of clinical pharmacology of ibuprofen, Oman Med. J. 25 (2010) 155–161, https://doi.org/10.5001/omj.2010.49.
[205] J.J. Lazarević, S. Uskoković-Marković, M. Jelikić-Stankov, M. Radonjić, D. Tanasković, N. Lazarević, Z.V. Popović, Intermolecular and low-frequency intramolecular Raman scattering study of racemic ibuprofen, Spectrochim. Acta-Part A Mol. Biomol. Spectrosc. 126 (2014) 301–305, https://doi.org/10.1016/j.saa.2014.01.135.
[206] C. Parlak, Ö. Alver, Adsorption of ibuprofen on silicon decorated fullerenes and single walled carbon nanotubes: a comparative DFT study, J. Mol. Struct. 1184 (2019) 110–113, https://doi.org/10.1016/j.molstruc.2019.02.023.
[207] A.M. El Mahdy, Density functional investigation of CO and NO adsorption on TM-decorated C 60 fullerene, Appl. Surf. Sci. 383 (2016) 353–366, https://doi.org/10.1016/j.apsusc.2016.04.037.
[208] M. Khodam Hazrati, N. L. Hadipour, A DFT study on the functionalization of C60 fullerene with 1,2-benzoquinone, Comput. Theor. Chem. 1098 (2016) 63–69, https://doi.org/10.1016/j.comptc.2016.11.007.
[209] D. Shahabi, H. Tavakol, DFT, NBO and molecular docking studies of the adsorption of fluoxetine into and on the surface of simple and sulfur-doped carbon nanotubes, Appl. Surf. Sci. 420 (2017) 267–275, https://doi.org/10.1016/j.apsusc.2017.05.068.
[210] C.P. Sousa, M.A. Salvador, P. Homem-de-Mello, F.W.P. Ribeiro, P. de Lima-Neto, A.N. Correia, Computational modeling of functionalized multi-walled carbon nanotubes dispersed in polyethylenimine for electrochemical sensing of acetaminophen, Sensors Actuators B Chem. 246 (2017) 969–978, https://doi.org/10.1016/j.snb.2017.02.124.
[211] Y. Xu, D. Li, J. Xing, Absorption behavior of small biomolecules on carbon nanotube by density functional theory, Integr. Ferroelectr. 169 (2016) 58–63, https://doi.org/10.1080/10584587.2016.1163171.
[212] M. Yoosefian, N. Etminan, Pd-doped single-walled carbon nanotube as a nanobiosensor for histidine amino acid, a DFT study, RSC Adv. 5 (2015) 31172–31178, https://doi.org/10.1039/C5RA00834D.
[213] A. Najafi Chermahini, A. Teimouri, H. Farrokhpour, A DFT-D study on the interaction between lactic acid and single-wall carbon nanotubes, RSC Adv. 5 (2015) 97724–97733, https://doi.org/10.1039/C5RA19949B.
[214] H.P. Schultz, Topological organic chemistry. polyhedranes and prismanes, J. Org. Chem. 30 (1965) 1361–1364, https://doi.org/10.1021/jo01016a005.
[215] E. Osawa, Superaromaticity, Kagaku (Chemistry) 25 (1970) 854–863.
[216] Y.-P. An, C.-L. Yang, M.-S. Wang, X.-G. Ma, D.-H. Wang, Geometrical and electronic properties of the clusters of C20 cage doped with alkali metal atoms, J. Clust. Sci. 22 (2011) 31–39, https://doi.org/10.1007/s10876-011-0354-x.
[217] M.T. Baei, First-principles study of NO2 adsorption on C20 fullerene, Heteroat. Chem. 24 (2013) 516–523, https://doi.org/10.1002/hc.21128.

[218] R.P.S.A. Kumar, S. Dev, B.K. Mishra, N. Sathyamurthy, Stabilization of the C_{20} cage by encapsulation of H^+ and He^{2+} ions, Curr. Sci. 106 (2014) 1255–1259http://www.jstor.org/stable/24102342.
[219] W. Krätschmer, L.D. Lamb, K. Fostiropoulos, D.R. Huffman, Solid C60: a new form of carbon, Nature 347 (1990) 354–358, https://doi.org/10.1038/347354a0.
[220] H. Ajie, M.M. Alvarez, S.J. Anz, R.D. Beck, F. Diederich, K. Fostiropoulos, D.R. Huffman, W. Kraetschmer, Y. Rubin, et al., Characterization of the soluble all-carbon molecules C60 and C70, J. Phys. Chem. 94 (1990) 8630–8633, https://doi.org/10.1021/j100387a004.
[221] R.F. Bunshah, S. Jou, S. Prakash, H.J. Doerr, L. Isaacs, A. Wehrsig, C. Yeretzian, H. Cynn, F. Diederich, Fullerene formation in sputtering and electron beam evaporation processes, J. Phys. Chem. 96 (1992) 6866–6869, https://doi.org/10.1021/j100196a005.
[222] S. Chuanchen, G. Haibin, F. Dufei, Extraction of C60 cluster ion beam, Rev. Sci. Instrum. 65 (1994) 1405–1407, https://doi.org/10.1063/1.1144976.
[223] P. Hebgen, A. Goel, J.B. Howard, L.C. Rainey, J.B. Vander Sande, Synthesis of fullerenes and fullerenic nanostructures in a low-pressure benzene/oxygen diffusion flame, Proc. Combust. Inst. 28 (2000) 1397–1404, https://doi.org/10.1016/S0082-0784(00)80355-0.
[224] M. Caraman, G. Lazar, M. Stamate, I. Lazar, Arc discharge instalation for fullerene production, Rom. Reports Phys. 53 (2008) 273–278.
[225] F. Diederich, C. Thilgen, Covalent fullerene chemistry, Science (80-.) 271 (1996) 317 LP–324, https://doi.org/10.1126/science.271.5247.317.
[226] R.A. Jishi, M.S. Dresselhaus, G. Dresselhaus, Electron-phonon coupling and the electrical conductivity of fullerene nanotubules, Phys. Rev. B 48 (1993) 11385–11389, https://doi.org/10.1103/PhysRevB.48.11385.
[227] C.E. Bunker, G.E. Lawson, Y.-P. Sun, Fullerene-styrene random copolymers. Novel optical properties, Macromolecules 28 (1995) 3744–3746, https://doi.org/10.1021/ma00114a034.
[228] M. Prato, [60]Fullerene chemistry for materials science applications, J. Mater. Chem. 7 (1997) 1097–1109, https://doi.org/10.1039/A700080D.
[229] R.O. Loutfy, S. Katagiri, in: E. Ōsawa (Ed.), Fullerene Materials for Lithium-ion Battery Applications BT-perspectives of Fullerene Nanotechnology, Springer Netherlands, Dordrecht 2002, pp. 357–367, https://doi.org/10.1007/0-306-47621-5_32.
[230] R.B. Ross, C.M. Cardona, D.M. Guldi, S.G. Sankaranarayanan, M.O. Reese, N. Kopidakis, J. Peet, B. Walker, G.C. Bazan, E. Van Keuren, B.C. Holloway, M. Drees, Endohedral fullerenes for organic photovoltaic devices, Nat. Mater. 8 (2009) 208–212, https://doi.org/10.1038/nmat2379.
[231] B.S. Sherigara, W. Kutner, F. D'Souza, Electrocatalytic properties and sensor applications of fullerenes and carbon nanotubes, Electroanalysis 15 (2003) 753–772, https://doi.org/10.1002/elan.200390094.
[232] J. Ma, Q. Guo, H.-L. Gao, X. Qin, Synthesis of C60/graphene composite as electrode in supercapacitors, Fullerenes, Nanotub. Carbon Nanostructures. 23 (2015) 477–482, https://doi.org/10.1080/1536383X.2013.865604.
[233] R.S. Ruoff, D.S. Tse, R. Malhotra, D.C. Lorents, Solubility of fullerene (C60) in a variety of solvents, J. Phys. Chem. 97 (1993) 3379–3383, https://doi.org/10.1021/j100115a049.
[234] D.Y. Lyon, L.K. Adams, J.C. Falkner, P.J.J. Alvarez, Antibacterial activity of fullerene water suspensions: effects of preparation method and particle size, Environ. Sci. Technol. 40 (2006) 4360–4366, https://doi.org/10.1021/es0603655.
[235] R. Sijbesma, G. Srdanov, F. Wudl, J.A. Castoro, C. Wilkins, S.H. Friedman, D.L. DeCamp, G.L. Kenyon, Synthesis of a fullerene derivative for the inhibition of HIV enzymes, J. Am. Chem. Soc. 115 (1993) 6510–6512, https://doi.org/10.1021/ja00068a006.
[236] J. Shi, Y. Liu, L. Wang, J. Gao, J. Zhang, X. Yu, R. Ma, R. Liu, Z. Zhang, A tumoral acidic pH-responsive drug delivery system based on a novel photosensitizer (fullerene) for in vitro and in vivo chemo-photodynamic therapy, Acta Biomater. 10 (2014) 1280–1291, https://doi.org/10.1016/j.actbio.2013.10.037.
[237] N.P. Shetti, S.J. Malode, S.T. Nandibewoor, Electrochemical behavior of an antiviral drug acyclovir at fullerene-C60-modified glassy carbon electrode, Bioelectrochemistry 88 (2012) 76–83, https://doi.org/10.1016/j.bioelechem.2012.06.004.
[238] A.S. Rad, S.M. Aghaei, E. Aali, M. Peyravi, Study on the electronic structure of Cr- and Ni-doped fullerenes upon adsorption of adenine: a comprehensive DFT calculation, Diam. Relat. Mater. 77 (2017) 116–121, https://doi.org/10.1016/j.diamond.2017.06.013.
[239] A. Hosseinian, E. Vessally, S. Yahyaei, L. Edjlali, A. Bekhradnia, A density functional theory study on the interaction between 5-fluorouracil drug and C24 fullerene, J. Clust. Sci. 28 (2017) 2681–2692, https://doi.org/10.1007/s10876-017-1253-6.
[240] Y. Gökpek, M. Bilge, D. Bilge, Ö. Alver, C. Parlak, Adsorption mechanism, structural and electronic properties: 4-Phenylpyridine & undoped or doped (B or Si) C60, J. Mol. Liq. 238 (2017) 225–228, https://doi.org/10.1016/j.molliq.2017.04.128.
[241] M. Moradi, M. Nouraliei, R. Moradi, Theoretical study on the phenylpropanolamine drug interaction with the pristine, Si and Al doped [60] fullerenes, Phys. E Low-Dimensional Syst. Nanostructures. 87 (2017) 186–191, https://doi.org/10.1016/j.physe.2016.11.027.
[242] E. Bernstein, B.M. Diskant, Phenylpropanolamine: a potentially hazardous drug, Ann. Emerg. Med. 11 (1982) 311–315, https://doi.org/10.1016/S0196-0644(82)80130-3.
[243] C.R. Lake, S. Gallant, E. Masson, P. Miller, Adverse drug effects attributed to phenylpropanolamine: a review of 142 case reports, Am. J. Med. 89 (1990) 195–208, https://doi.org/10.1016/0002-9343(90)90299-S.
[244] D.L. Howrie, J.H. Wolfson, Phenylpropanolamine-induced hypertensive seizures, J. Pediatr. 102 (1983) 143–145, https://doi.org/10.1016/S0022-3476(83)80314-X.
[245] A.S. Ghasemi, F. Mashhadban, F. Ravari, A DFT study of penicillamine adsorption over pure and Al-doped C60 fullerene, Adsorption 24 (2018) 471–480, https://doi.org/10.1007/s10450-018-9960-3.
[246] J.M. Walshe, Penicillamine, a new oral therapy for Wilson's disease, Am. J. Med. 21 (1956) 487–495, https://doi.org/10.1016/0002-9343(56)90066-3.
[247] Multicentre Trial Group, Controlled trial of D(−)penicillamine in severe rheumatoid arthritis, Lancet 301 (1973) 275–280, https://doi.org/10.1016/S0140-6736(73)91536-5.
[248] S. Bashiri, E. Vessally, A. Bekhradnia, A. Hosseinian, L. Edjlali, Utility of extrinsic [60] fullerenes as work function type sensors for amphetamine drug detection: DFT studies, Vacuum 136 (2017) 156–162, https://doi.org/10.1016/j.vacuum.2016.12.003.
[249] J.T. Cody, R. Schwarzhoff, Fluorescence polarization immunoassay detection of amphetamine, methamphetamine, and illicit amphetamine analogues, J. Anal. Toxicol. 17 (1993) 23–33, https://doi.org/10.1093/jat/17.1.26.
[250] C. Parlak, Ö. Alver, A density functional theory investigation on amantadine drug interaction with pristine and B, Al, Si, Ga, Ge doped C60 fullerenes, Chem. Phys. Lett. 678 (2017) 85–90, https://doi.org/10.1016/j.cplett.2017.04.025.
[251] G. Hubsher, M. Haider, M.S. Okun, Amantadine: the journey from fighting flu to treating Parkinson disease, Neurology 78 (2012) 1096 LP–1099, https://doi.org/10.1212/WNL.0b013e31824e8f0d.
[252] D.L. Blanchard, Amantadine caused corneal edema, Cornea 9 (1990) 181–182https://journals.lww.com/corneajrnl/Fulltext/1990/04000/Amantadine_Caused_Corneal_Edema.17.aspx.
[253] O. Ergürhan, C. Parlak, Ö. Alver, M. Şenyel, Conformational and electronic properties of hydroquinone adsorption on C60 fullerenes: doping atom, solvent and basis set effects, J. Mol. Struct. 1167 (2018) 227–231, https://doi.org/10.1016/j.molstruc.2018.04.092.
[254] E. Alipour, F. Alimohammady, A. Yumashev, A. Maseleno, Fullerene C60 containing porphyrin-like metal center as drug delivery system for ibuprofen drug, J. Mol. Model. 26 (2019) 7, https://doi.org/10.1007/s00894-019-4267-1.
[255] M.K. Hazrati, Z. Bagheri, A. Bodaghi, Application of C30B15N15 heterofullerene in the isoniazid drug delivery: DFT studies, Phys. E Low-Dimensional Syst. Nanostructures. 89 (2017) 72–76, https://doi.org/10.1016/j.physe.2017.02.009.
[256] M.F. Kaya, Ö. Alver, C. Parlak, P. Ramasami, Theoretical insight of alpha amino acid phenylalanine adsorption on pristine and decorated fullerenes, Main Gr. Met. Chem. 42 (2019) 135–142, https://doi.org/10.1515/mgmc-2019-0015.
[257] A.R. Moosavi-zare, M. Abdolmaleki, H. Goudarziafshar, H. Soleymanabadi, Adsorption behavior of amphetamine on the inorganic BC3 nanotube and nanosheet: DFT studies, Inorg. Chem. Commun. 91 (2018) 95–101, https://doi.org/10.1016/j.inoche.2018.03.017.
[258] K. Nejati, E. Vessally, P. Delir Kheirollahi Nezhad, H. Mofid, A. Bekhradnia, The electronic response of pristine, Al and Si doped BC2N nanotubes to a cathinone molecule: computational study, J. Phys. Chem. Solids 111 (2017) 238–244, https://doi.org/10.1016/j.jpcs.2017.08.005.
[259] A. Soltani, Z. Azmoodeh, M.B. Javan, E.T. Lemeski, L. Karami, A DFT study of adsorption of glycine onto the surface of BC2N nanotube, Appl. Surf. Sci. 384 (2016) 230–236, https://doi.org/10.1016/j.apsusc.2016.04.162.
[260] Z. Jafari, R. Baharfar, A.S. Rad, S. Asghari, Potential of graphene oxide as a drug delivery system for Sumatriptan: a detailed density functional theory study, J. Biomol. Struct. Dyn. (2020) 1–10, https://doi.org/10.1080/07391102.2020.1736161.
[261] P. Gong, L. Zhang, X. Yuan, X. Liu, X. Diao, Q. Zhao, Z. Tian, J. Sun, Z. Liu, J. You, Multifunctional fluorescent PEGylated fluorinated graphene for targeted drug delivery: an experiment and DFT study, Dyes Pigments 162 (2019) 573–582, https://doi.org/10.1016/j.dyepig.2018.10.031.
[262] Z. Hasanzade, H. Raissi, Density functional theory calculations and molecular dynamics simulations of the adsorption of ellipticine anticancer drug on graphene oxide surface in aqueous medium as well as under controlled pH conditions, J. Mol. Liq. 255 (2018) 269–278, https://doi.org/10.1016/j.molliq.2018.01.159.
[263] U. Srimathi, V. Nagarajan, R. Chandiramouli, Investigation on graphdiyne nanosheet in adsorption of sorafenib and regorafenib drugs: a DFT approach, J. Mol. Liq. 277 (2019) 776–785, https://doi.org/10.1016/j.molliq.2019.01.003.
[264] V. Nagarajan, R. Chandiramouli, Flutamide drug interaction studies on graphdiyne nanotube – a first-principles study, Comput. Theor. Chem. 1167 (2019) 112590, https://doi.org/10.1016/j.comptc.2019.112590.
[265] S. Madhumitha, V. Nagarajan, R. Chandiramouli, Adsorption behavior of cytosine and guanine nucleobases on graphyne nanosheets: a DFT study, Comput. Theor. Chem. 1163 (2019) 112514, https://doi.org/10.1016/j.comptc.2019.112514.
[266] M. Li, Y. Wei, G. Zhang, F. Wang, M. Li, H. Soleymanabadi, A DFT study on the detection of isoniazid drug by pristine, Si and Al doped C70 fullerenes, Phys. E Low-Dimensional Syst. Nanostructures. 118 (2020) 113878, https://doi.org/10.1016/j.physe.2019.113878.
[267] F.J. van Spronsen, M. Hoeksma, D.-J. Reijngoud, Brain dysfunction in phenylketonuria: is phenylalanine toxicity the only possible cause? J. Inherit. Metab. Dis. 32 (2009) 46, https://doi.org/10.1007/s10545-008-0946-2.
[268] M.J. de Groot, M. Hoeksma, N. Blau, D.J. Reijngoud, F.J. van Spronsen, Pathogenesis of cognitive dysfunction in phenylketonuria: review of hypotheses, Mol. Genet. Metab. 99 (2010) S86–S89, https://doi.org/10.1016/j.ymgme.2009.10.016.
[269] B.C. Brodie XIII. On the atomic weight of graphite, Philos. Trans. R. Soc. London. 149 (1859) 249–259. doi:https://doi.org/10.1098/rstl.1859.0013.
[270] L. Staudenmaier, Verfahren zur Darstellung der Graphitsäure, Berichte Der Dtsch. Chem. Gesellschaft. 31 (1898) 1481–1487, https://doi.org/10.1002/cber.18980310237.
[271] W.S. Hummers, R.E. Offeman, Preparation of graphitic oxide, J. Am. Chem. Soc. 80 (1958) 1339, https://doi.org/10.1021/ja01539a017.

[272] C. Chung, Y.-K. Kim, D. Shin, S.-R. Ryoo, B.H. Hong, D.-H. Min, Biomedical applications of graphene and graphene oxide, Acc. Chem. Res. 46 (2013) 2211–2224, https://doi.org/10.1021/ar300159f.
[273] L. Feng, L. Wu, X. Qu, New horizons for diagnostics and therapeutic applications of graphene and graphene oxide, Adv. Mater. 25 (2013) 168–186, https://doi.org/10.1002/adma.201203229.
[274] W.H. Visser, N. Jaspers, R.H.M. de Vriend MD Ferrari, Chest symptoms after Sumatriptan: a two-year clinical practice review in 735 consecutive migraine patients, Cephalalgia 16 (1996) 554–559, https://doi.org/10.1046/j.1468-2982.1996.1608554.x.
[275] P. Gong, J. Du, D. Wang, B. Cao, M. Tian, Y. Wang, L. Sun, S. Ji, Z. Liu, Fluorinated graphene as an anticancer nanocarrier: an experimental and DFT study, J. Mater. Chem. B 6 (2018) 2769–2777, https://doi.org/10.1039/C8TB00102B.
[276] G. Li, Y. Li, H. Liu, Y. Guo, Y. Li, D. Zhu, Architecture of graphdiyne nanoscale films, Chem. Commun. 46 (2010) 3256–3258, https://doi.org/10.1039/B922733D.
[277] V. Gupta-Abramson, A.B. Troxel, A. Nellore, K. Puttaswamy, M. Redlinger, K. Ransone, S.J. Mandel, K.T. Flaherty, L.A. Loevner, P.J. O'Dwyer, M.S. Brose, Phase II trial of sorafenib in advanced thyroid cancer, J. Clin. Oncol. 26 (2008) 4714–4719, https://doi.org/10.1200/JCO.2008.16.3279.
[278] R.C. Kane, A.T. Farrell, H. Saber, S. Tang, G. Williams, J.M. Jee, C. Liang, B. Booth, N. Chidambaram, D. Morse, R. Sridhara, P. Garvey, R. Justice, R. Pazdur, Sorafenib for the treatment of advanced renal cell carcinoma, Clin. Cancer Res. 12 (2006) 7271 LP–7278, https://doi.org/10.1158/1078-0432.CCR-06-1249.
[279] C. Robert, C. Mateus, A. Spatz, J. Wechsler, B. Escudier, Dermatologic symptoms associated with the multikinase inhibitor sorafenib, J. Am. Acad. Dermatol. 60 (2009) 299–305, https://doi.org/10.1016/j.jaad.2008.06.034.
[280] L. Zhang, Q. Zhou, L. Ma, Z. Wu, Y. Wang, Meta-analysis of dermatological toxicities associated with sorafenib, Clin. Exp. Dermatol. 36 (2011) 344–350, https://doi.org/10.1111/j.1365-2230.2011.04060.x.
[281] D.C. McFarland, K.J. Misiukiewicz, Sorafenib in radioactive iodine-refractory well-differentiated metastatic thyroid cancer, Onco. Targets. Ther. 7 (2014) 1291–1299, https://doi.org/10.2147/OTT.S49430.
[282] D. Strumberg, M.E. Scheulen, B. Schultheis, H. Richly, A. Frost, M. Büchert, O. Christensen, M. Jeffers, R. Heinig, O. Boix, K. Mross, Regorafenib (BAY 73-4506) in advanced colorectal cancer: a phase I study, Br. J. Cancer 106 (2012) 1722–1727, https://doi.org/10.1038/bjc.2012.153.
[283] A.G. Duffy, T.F. Greten, Regorafenib as second-line therapy in hepatocellular carcinoma, Nat. Rev. Gastroenterol. Hepatol. 14 (2017) 141–142, https://doi.org/10.1038/nrgastro.2017.7.
[284] T. Akamine, K. Ando, E. Oki, H. Saeki, Y. Nakashima, Y.U. Imamura, K. Ohgaki, Y. Maehara, Acute liver failure due to regorafenib may be caused by impaired liver blood flow: a case report, Anticancer Res. 35 (2015) 4037–4041.
[285] U. Srimathi, V. Nagarajan, R. Chandiramouli, Interaction of imuran, pentasa and hyoscyamine drugs and solvent effects on graphdiyne nanotube as a drug delivery system - a DFT study, J. Mol. Liq. 265 (2018) 199–207, https://doi.org/10.1016/j.molliq.2018.05.114.
[286] J. Kouvetakis, R.B. Kaner, M.L. Sattler, N. Bartlett, A novel graphite-like material of composition BC3, and nitrogen–carbon graphites, J. Chem. Soc. Chem. Commun. (1986) 1758–1759, https://doi.org/10.1039/C39860001758.
[287] D. Tomanek, R.M. Wentzcovitch, S.G. Louie, M.L. Cohen, Calculation of electronic and structural properties of BC_3, Phys. Rev. B 37 (1988) 3134–3136, https://doi.org/10.1103/PhysRevB.37.3134.
[289] N. Kostoglou, K. Polychronopoulou, C. Rebholz, Thermal and chemical stability of hexagonal boron nitride (h-BN) nanoplatelets, Vacuum 112 (2015) 42–45, https://doi.org/10.1016/j.vacuum.2014.11.009.
[290] T. Ouyang, Y. Chen, Y. Xie, K. Yang, Z. Bao, J. Zhong, Thermal transport in hexagonal boron nitride nanoribbons, Nanotechnology 21 (2010), 245701, https://doi.org/10.1088/0957-4484/21/24/245701.
[291] K.K. Kim, A. Hsu, X. Jia, S.M. Kim, Y. Shi, M. Hofmann, D. Nezich, J.F. Rodriguez-Nieva, M. Dresselhaus, T. Palacios, J. Kong, Synthesis of monolayer hexagonal boron nitride on cu foil using chemical vapor deposition, Nano Lett. 12 (2012) 161–166, https://doi.org/10.1021/nl203249a.
[292] S.M. Kim, A. Hsu, M.H. Park, S.H. Chae, S.J. Yun, J.S. Lee, D.-H. Cho, W. Fang, C. Lee, T. Palacios, M. Dresselhaus, K.K. Kim, Y.H. Lee, J. Kong, Synthesis of large-area multilayer hexagonal boron nitride for high material performance, Nat. Commun. 6 (2015) 8662, https://doi.org/10.1038/ncomms9662.
[293] L. Song, L. Ci, H. Lu, P.B. Sorokin, C. Jin, J. Ni, A.G. Kvashnin, D.G. Kvashnin, J. Lou, B.I. Yakobson, P.M. Ajayan, Large scale growth and characterization of atomic hexagonal boron nitride layers, Nano Lett. 10 (2010) 3209–3215, https://doi.org/10.1021/nl1022139.
[294] P. Marbaniang, I. Patil, M. Lokanathan, H. Parse, D. Catherin Sesu, S. Ingavale, B. Kakade, Nanorice-like structure of carbon-doped hexagonal boron nitride as an efficient metal-free catalyst for oxygen electroreduction, ACS Sustain. Chem. Eng. 6 (2018) 11115–11122, https://doi.org/10.1021/acssuschemeng.8b02609.
[295] S. Sinthika, E.M. Kumar, R. Thapa, Doped h-BN monolayer as efficient noble metal-free catalysts for CO oxidation: the role of dopant and water in activity and catalytic de-poisoning, J. Mater. Chem. A 2 (2014) 12812–12820, https://doi.org/10.1039/C4TA02434F.
[296] S.K. Jang, J. Youn, Y.J. Song, S. Lee, Synthesis and characterization of hexagonal boron nitride as a gate dielectric, Sci. Rep. 6 (2016), 30449, https://doi.org/10.1038/srep30449.
[297] F. Hui, C. Pan, Y. Shi, Y. Ji, E. Grustan-Gutierrez, M. Lanza, On the use of two dimensional hexagonal boron nitride as dielectric, Microelectron. Eng. 163 (2016) 119–133, https://doi.org/10.1016/j.mee.2016.06.015.
[298] J. Eichler, C. Lesniak, Boron nitride (BN) and BN composites for high-temperature applications, J. Eur. Ceram. Soc. 28 (2008) 1105–1109, https://doi.org/10.1016/j.jeurceramsoc.2007.09.005.
[299] M. Rivera, R. Velázquez, A. Aldalbahi, A.F. Zhou, P. Feng, High operating temperature and low power consumption boron nitride nanosheets based broadband UV photodetector, Sci. Rep. 7 (2017), 42973, https://doi.org/10.1038/srep42973.
[300] Y. Zhang, T. Zhang, L. Liu, Q. Chi, C. Zhang, Q. Chen, Y. Cui, X. Wang, Q. Lei, Sandwich-structured PVDF-based composite incorporated with hybrid Fe3O4@BN nanosheets for excellent dielectric properties and energy storage performance, J. Phys. Chem. C 122 (2018) 1500–1512, https://doi.org/10.1021/acs.jpcc.7b10838.
[301] A.F. Khan, D.A.C. Brownson, E.P. Randviir, G.C. Smith, C.E. Banks, 2D hexagonal boron nitride (2D-hBN) explored for the electrochemical sensing of dopamine, Anal. Chem. 88 (2016) 9729–9737, https://doi.org/10.1021/acs.analchem.6b02638.
[302] J. Dauber, A.A. Sagade, M. Oellers, K. Watanabe, T. Taniguchi, D. Neumaier, C. Stampfer, Ultra-sensitive Hall sensors based on graphene encapsulated in hexagonal boron nitride, Appl. Phys. Lett. 106 (2015), 193501, https://doi.org/10.1063/1.4919897.
[303] M. Sajjad, P. Feng, Study the gas sensing properties of boron nitride nanosheets, Mater. Res. Bull. 49 (2014) 35–38, https://doi.org/10.1016/j.materresbull.2013.08.019.
[304] Y. Zhan, J. Yan, M. Wu, L. Guo, Z. Lin, B. Qiu, G. Chen, K. Wong, Boron nitride nanosheets as a platform for fluorescence sensing, Talanta 174 (2017) 365–371, https://doi.org/10.1016/j.talanta.2017.06.032.
[305] S. Mateti, C.S. Wong, Z. Liu, W. Yang, Y. Li, L.H. Li, Y. Chen, Biocompatibility of boron nitride nanosheets, Nano Res. 11 (2018) 334–342, https://doi.org/10.1007/s12274-017-1635-y.
[306] J. Castro-Medina, D. García-Toral, M. López-Fuentes, A. Sánchez-Castillo, S. Torres-Morales, L.M. de la Garza, G.H. Cocoletzi, Thymine adsorption on two-dimensional boron nitride structures: first-principles studies, J. Mol. Model. 23 (2017) 109, https://doi.org/10.1007/s00894-017-3280-5.
[307] S.D. Dabhi, B. Roondhe, P.K. Jha, Nucleobases-decorated boron nitride nanoribbons for electrochemical biosensing: a dispersion-corrected DFT study, Phys. Chem. Chem. Phys. 20 (2018) 8943–8950, https://doi.org/10.1039/C7CP08145F.
[308] K. Nejati, A. Hosseinian, E. Vessally, A. Bekhradnia, L. Edjlali, A comparative DFT study on the interaction of cathinone drug with BN nanotubes, nanocages, and nanosheets, Appl. Surf. Sci. (2017)https://doi.org/10.1016/j.apsusc.2017.06.082.
[309] S.A. Aslanzadeh, Adsorption of mercaptopurine drug on the BN nanotube, nanosheet and nanocluster: a density functional theory study, Mol. Phys. 117 (2019) 531–538, https://doi.org/10.1080/00268976.2018.1525504.
[310] N.G. Chopra, R.J. Luyken, K. Cherrey, V.H. Crespi, M.L. Cohen, S.G. Louie, A. Zettl, Boron nitride nanotubes, Science (80-.) 269 (1995) 966 LP–967, https://doi.org/10.1126/science.269.5226.966.
[311] A. Rubio, J.L. Corkill, M.L. Cohen, Theory of graphitic boron nitride nanotubes, Phys. Rev. B 49 (1994) 5081–5084, https://doi.org/10.1103/PhysRevB.49.5081.
[312] J. Cumings, A. Zettl, Mass-production of boron nitride double-wall nanotubes and nanococoons, Chem. Phys. Lett. 316 (2000) 211–216, https://doi.org/10.1016/S0009-2614(99)01277-4.
[313] Y. Chen, J. Fitz Gerald, J.S. Williams, S. Bulcock, Synthesis of boron nitride nanotubes at low temperatures using reactive ball milling, Chem. Phys. Lett. 299 (1999) 260–264, https://doi.org/10.1016/S0009-2614(98)01252-4.
[314] D. Golberg, Y. Bando, M. Eremets, K. Takemura, K. Kurashima, H. Yusa, Nanotubes in boron nitride laser heated at high pressure, Appl. Phys. Lett. 69 (1996) 2045–2047, https://doi.org/10.1063/1.116874.
[315] O.R. Lourie, C.R. Jones, B.M. Bartlett, P.C. Gibbons, R.S. Ruoff, W.E. Buhro, CVD growth of boron nitride nanotubes, Chem. Mater. 12 (2000) 1808–1810, https://doi.org/10.1021/cm000157q.
[316] T. Dumitrică, B.I. Yakobson, Rate theory of yield in boron nitride nanotubes, Phys. Rev. B 72 (2005) 35418, https://doi.org/10.1103/PhysRevB.72.035418.
[317] D. Golberg, Y. Bando, K. Kurashima, T. Sato, Synthesis and characterization of ropes made of BN multiwalled nanotubes, Scr. Mater. 44 (2001) 1561–1565, https://doi.org/10.1016/S1359-6462(01)00724-2.
[318] C.W. Chang, A.M. Fennimore, A. Afanasiev, D. Okawa, T. Ikuno, H. Garcia, D. Li, A. Majumdar, A. Zettl, Isotope effect on the thermal conductivity of boron nitride nanotubes, Phys. Rev. Lett. 97 (2006) 85901, https://doi.org/10.1103/PhysRevLett.97.085901.
[319] Y. Chen, J. Zou, S.J. Campbell, G. Le Caer, Boron nitride nanotubes: pronounced resistance to oxidation, Appl. Phys. Lett. 84 (2004) 2430–2432, https://doi.org/10.1063/1.1667278.
[320] X. Blase, A. Rubio, S.G. Louie, M.L. Cohen, Stability and band gap constancy of boron nitride nanotubes, Europhys. Lett. 28 (1994) 335–340, https://doi.org/10.1209/0295-5075/28/5/007.
[321] R. Arenal, M.-S. Wang, Z. Xu, A. Loiseau, D. Golberg, Young modulus, mechanical and electrical properties of isolated individual and bundled single-walled boron nitride nanotubes, Nanotechnology 22 (2011), 265704, https://doi.org/10.1088/0957-4484/22/26/265704.
[322] C. Zhi, Y. Bando, T. Terao, C. Tang, H. Kuwahara, D. Golberg, Towards thermoconductive, electrically insulating polymeric composites with boron nitride nanotubes as fillers, Adv. Funct. Mater. 19 (2009) 1857–1862, https://doi.org/10.1002/adfm.200801435.
[323] H. Chen, Y. Chen, C.P. Li, H. Zhang, J.S. Williams, Y. Liu, Z. Liu, S.P. Ringer, Eu-doped boron nitride nanotubes as a nanometer-sized visible-light source, Adv. Mater. 19 (2007) 1845–1848, https://doi.org/10.1002/adma.200700493.
[324] Y. Yu, H. Chen, Y. Liu, V. Craig, L.H. Li, Y. Chen, Superhydrophobic and superoleophilic boron nitride nanotube-coated stainless steel meshes for oil and

water separation, Adv. Mater. Interfaces 1 (2014), 1300002, https://doi.org/10.1002/admi.201300002.
[325] C. Harrison, S. Weaver, C. Bertelsen, E. Burgett, N. Hertel, E. Grulke, Polyethylene/boron nitride composites for space radiation shielding, J. Appl. Polym. Sci. 109 (2008) 2529–2538, https://doi.org/10.1002/app.27949.
[326] M.D. Ganji, M. Rezvani, Boron nitride nanotube based nanosensor for acetone adsorption: a DFT simulation, J. Mol. Model. 19 (2013) 1259–1265, https://doi.org/10.1007/s00894-012-1668-9.
[327] J. Beheshtian, A.A. Peyghan, Z. Bagheri, Detection of phosgene by Sc-doped BN nanotubes: a DFT study, Sensors Actuators B Chem. 171–172 (2012) 846–852, https://doi.org/10.1016/j.snb.2012.05.082.
[328] X. Chen, P. Wu, M. Rousseas, D. Okawa, Z. Gartner, A. Zettl, C.R. Bertozzi, Boron nitride nanotubes are noncytotoxic and can be functionalized for interaction with proteins and cells, J. Am. Chem. Soc. 131 (2009) 890–891, https://doi.org/10.1021/ja807334b.
[329] G. Ciofani, S. Danti, G.G. Genchi, B. Mazzolai, V. Mattoli, Boron nitride nanotubes: biocompatibility and potential spill-over in nanomedicine, Small 9 (2013) 1672–1685, https://doi.org/10.1002/smll.201201315.
[330] S.H. Upadhyay, Boron nitride nanotube-based biosensing of various bacterium/viruses: continuum modelling-based simulation approach, IET Nanobiotechnology. 8 (2014) , 143–148(5) https://digital-library.theiet.org/content/journals/10.1049/iet-nbt.2013.0020.
[331] Z. Khatti, S.M. Hashemianzadeh, Boron nitride nanotube as a delivery system for platinum drugs: drug encapsulation and diffusion coefficient prediction, Eur. J. Pharm. Sci. 88 (2016) 291–297, https://doi.org/10.1016/j.ejps.2016.04.011.
[332] S. Tilles, Practical issues in the management of hypersensitivity reactions, South. Med. J. 94 (2001) 817–824, https://doi.org/10.1097/00007611-200108000-00013.
[333] Z. Rahmani, L. Edjlali, E. Vessally, A. Hosseinian, P.D.K. Nezhad, A density functional theory outlook on the possible sensing ability of boron nitride nanotubes and their Al- and Si-doped derivatives for sulfonamide drugs, J. Sulfur Chem. 41 (2020) 82–95, https://doi.org/10.1080/17415993.2019.1687702.
[334] K. Shayan, A. Nowroozi, Boron nitride nanotubes for delivery of 5-fluorouracil as anticancer drug: a theoretical study, Appl. Surf. Sci. 428 (2018) 500–513, https://doi.org/10.1016/j.apsusc.2017.09.121.
[335] D. Fewer, C.B. Wilson, E.B. Boldrey, K.J. Enot, M.R. Powell, The chemotherapy of brain tumors: clinical experience with carmustine (BCNU) and vincristine, JAMA. 222 (1972) 549–552, https://doi.org/10.1001/jama.1972.03210050021004.
[336] H. Lena, B. Desrues, A. Le Coz, M.L. Quinquenel, P. Delaval, Severe diffuse interstitial pneumonitis induced by carmustine (BCNU), Chest 105 (1994) 1602–1603, https://doi.org/10.1378/chest.105.5.1602.
[337] S.S. Kanj, A.I. Sharara, E.J. Shpall, R.B. Jones, W.P. Peters, Myocardial ischemia associated with high-dose carmustine infusion, Cancer. 68 (1991) 1910–1912, https://doi.org/10.1002/1097-0142(19911101)68:9<1910::AID-CNCR2820680911>3.0.CO;2-E.
[338] S. Ghahremani, M. Samadizadeh, M. Khaleghian, N. Zabarjad Shiraz, Theoretical study of encapsulation of floxuridine anticancer drug into BN (9,9-7) nanotube for medical application, Phosphorus Sulfur Silicon Relat. Elem. 195 (2020) 293–306, https://doi.org/10.1080/10426507.2019.1687479.
[339] T.G. Allen-Mersh, S. Earlam, C. Fordy, K. Abrams, J. Houghton, Quality of life and survival with continuous hepatic-artery floxuridine infusion for colorectal liver metastases, Lancet 344 (1994) 1255–1260, https://doi.org/10.1016/S0140-6736(94)90750-1.
[340] D.C. Hohn, A.A. Rayner, J.S. Economou, R.J. Ignoffo, B.J. Lewis, R.J. Stagg, Toxicities and complications of implanted pump hepatic arterial and intravenous floxuridine infusion, Cancer. 57 (1986) 465–470, https://doi.org/10.1002/1097-0142(19860201)57:3<465::AID-CNCR2820570311>3.0.CO;2-S.
[341] Y.Z. Patt, C.M. McBride, F.C. Ames, L.J. Claghorn, K.R. Cleary, A.W. Boddie, C. Charnsangavej, G.M. Mavligit, Adjuvant perioperative hepatic arterial mitomycin C and floxuridine combined with surgical resection of metastatic colorectal cancer in the liver, Cancer. 59 (1987) 867–873, https://doi.org/10.1002/1097-0142(19870301)59:5<867::AID-CNCR2820590502>3.0.CO;2-J.
[342] M. Li, L. Jing, Electrochemical behavior of acetaminophen and its detection on the PANI–MWCNTs composite modified electrode, Electrochim. Acta 52 (2007) 3250–3257, https://doi.org/10.1016/j.electacta.2006.10.001.
[343] H. Ghasempour, M. Dehestani, S.M.A. Hosseini, Theoretical studies of the paracetamol and phenacetin adsorption on single-wall boron-nitride nanotubes: a DFT and MD investigation, Struct. Chem. (2020)https://doi.org/10.1007/s11224-020-01499-8.
[344] Z. Iranmanesh-Zarandy, M. Dehestani, Molecular dynamics simulation of paracetamol drug adsorption on boron nitride nanotube: effects of temperature, nanotube length, diameter, and chirality, Chemistry Select 4 (2019) 7866–7873, https://doi.org/10.1002/slct.201900644.
[345] B. Makiabadi, M. Zakarianezhad, M.S. Ekrami-Kakhki, S. Zareye, Adsorption of the nitrosamine and thionitrosamine molecules as carcinogen compounds on the BN and B3Al N nanotubes: a DFT study, Phosphorus Sulfur Silicon Relat. Elem. 194 (2019) 57–63, https://doi.org/10.1080/10426507.2018.1487431.
[346] P. Jakszyn, C.-A. Gonzalez, Nitrosamine and related food intake and gastric and oesophageal cancer risk: a systematic review of the epidemiological evidence, World J. Gastroenterol. 12 (2006) 4296–4303, https://doi.org/10.3748/wjg.v12.i27.4296.
[347] Y.-G. Huang, J.-D. Ji, Q.-N. Hou, A study on carcinogenesis of endogenous nitrite and nitrosamine, and prevention of cancer, Mutat. Res. Mol. Mech. Mutagen. 358 (1996) 7–14, https://doi.org/10.1016/0027-5107(96)00087-5.
[348] S.S. Hecht, Biochemistry, biology, and carcinogenicity of tobacco-specific N-nitrosamines, Chem. Res. Toxicol. 11 (1998) 559–603, https://doi.org/10.1021/tx980005y.
[349] G. Fan, S. Zhu, X. Li, K. Ni, H. Xu, Ab initio investigation of pristine and doped single-walled boron nitride nanotubes as acetone sensor, Comput. Theor. Chem. 1115 (2017) 208–216, https://doi.org/10.1016/j.comptc.2017.06.024.
[350] F. Jensen, H. Toftlund, Structure and stability of C24 and B12N12 isomers, Chem. Phys. Lett. 201 (1993) 89–96, https://doi.org/10.1016/0009-2614(93)85039-Q.
[351] O. Stephan, P.M. Ajayan, C. Colliex, P. Redlich, J.M. Lambert, P. Bernier, P. Lefin, Doping graphitic and carbon nanotube structures with boron and nitrogen, Science (80-.) 266 (1994) 1683 LP–1685, https://doi.org/10.1126/science.266.5191.1683.
[352] D. Golberg, Y. Bando, O. Stéphan, K. Kurashima, Octahedral boron nitride fullerenes formed by electron beam irradiation, Appl. Phys. Lett. 73 (1998) 2441–2443, https://doi.org/10.1063/1.122475.
[353] T. Oku, A. Nishiwaki, I. Narita, M. Gonda, Formation and structure of B24N24 clusters, Chem. Phys. Lett. 380 (2003) 620–623, https://doi.org/10.1016/j.cplett.2003.08.096.
[354] Y. Pan, K. Huo, Y. Hu, J. Fu, Y. Lu, Z. Dai, Z. Hu, Y. Chen, Boron nitride nanocages synthesized by a moderate thermochemical approach, Small 1 (2005) 1199–1203, https://doi.org/10.1002/smll.200500218.
[355] G. Lian, X. Zhang, S. Zhang, D. Liu, D. Cui, Q. Wang, Controlled fabrication of ultrathin-shell BN hollow spheres with excellent performance in hydrogen storage and wastewater treatment, Energy Environ. Sci. 5 (2012) 7072–7080, https://doi.org/10.1039/C2EE03240F.
[356] O.V. Pupysheva, A.A. Farajian, B.I. Yakobson, Fullerene nanocage capacity for hydrogen storage, Nano Lett. 8 (2008) 767–774, https://doi.org/10.1021/nl071436g.
[357] J. Beheshtian, M. Kamfiroozi, Z. Bagheri, A.A. Peyghan, B12N12 nano-cage as potential sensor for NO2 detection, Chinese J. Chem. Phys. 25 (2012) 60–64, https://doi.org/10.1088/1674-0068/25/01/60-64.
[358] T.S. Gee, K.-P. Yu, B.D. Clarkson, Treatment of adult acute leukemia with arabinosylcytosine and thioguanine, Cancer. 23 (1969) 1019–1032, https://doi.org/10.1002/1097-0142(196905)23:5<1019::AID-CNCR2820230506>3.0.CO;2-N.
[359] R.A. Gill, G.R. Onstad, J.M. Cardamone, D.C. Maneval, H.W. Sumner, Hepatic veno-occlusive disease caused by 6-thioguanine, Ann. Intern. Med. 96 (1982) 58–60, https://doi.org/10.7326/0003-4819-96-1-58.
[360] H.S. Zackheim, R.G. Glogau, D.A. Fisher, H.I. Maibach, 6-Thioguanine treatment of psoriasis: experience in 81 patients, J. Am. Acad. Dermatol. 30 (1994) 452–458, https://doi.org/10.1016/S0190-9622(94)70055-9.
[361] M. Noormohammadbeigi, S. Kamalinahad, F. Izadi, M. Adimi, A. Ghasemkhani, Theoretical investigation of thioguanine isomers anticancer drug adsorption treatment on B12N12 nanocage, Mater. Res. Express. 6 (2020) 1250g2, https://doi.org/10.1088/2053-1591/ab672a.
[362] W.P. Brade, K. Herdrich, M. Varini, Ifosfamide-pharmacology, safety and therapeutic potential, Cancer Treat. Rev. 12 (1985) 1–47, https://doi.org/10.1016/0305-7372(85)90011-8.
[363] J. Klastersky, Side effects of ifosfamide, Oncology 65 (Suppl. 2) (2003) 7–10, https://doi.org/10.1159/000073351.
[364] A. Soltani, E. Tazikeh-Lemeski, M.B. Javan, A comparative theoretical study on the interaction of pure and carbon atom substituted boron nitride fullerenes with ifosfamide drug, J. Mol. Liq. 297 (2020), 111894, https://doi.org/10.1016/j.molliq.2019.111894.
[365] S. Onsori, E. Alipour, A computational study on the cisplatin drug interaction with boron nitride nanocluster, J. Mol. Graph. Model. 79 (2018) 223–229, https://doi.org/10.1016/j.jmgm.2017.12.007.
[366] A. Hosseinian, E. Vessally, A. Bekhradnia, S. Ahmadi, P.D. Kheirollahi Nezhad, Interaction of α-cyano-4-hydroxycinnamic acid drug with inorganic BN nanocluster: a Density Functional Study, J. Inorg. Organomet. Polym. Mater. 28 (2018) 1422–1431, https://doi.org/10.1007/s10904-018-0778-y.
[367] N. Abdolahi, M. Aghaei, A. Soltani, Z. Azmoodeh, H. Balakheyli, F. Heidari, Adsorption of celecoxib on B12N12 fullerene: spectroscopic and DFT/TD-DFT study, Spectrochim. Acta Part A Mol. Biomol. Spectrosc. 204 (2018) 348–353, https://doi.org/10.1016/j.saa.2018.06.077.
[368] N.M. Davies, A.J. McLachlan, R.O. Day, K.M. Williams, Clinical pharmacokinetics and pharmacodynamics of celecoxib, Clin. Pharmacokinet. 38 (2000) 225–242, https://doi.org/10.2165/00003088-200038030-00003.
[369] P. Mantry, A. Shah, U. Sundaram, Celecoxib associated esophagitis: review of gastrointestinal side effects from cox-2 inhibitors, J. Clin. Gastroenterol. 37 (2003) https://journals.lww.com/jcge/Fulltext/2003/07000/Celecoxib_Associated_Esophagitis__Review_of.15.aspx.
[370] O.C. Trifan, W.F. Durham, V.S. Salazar, J. Horton, B.D. Levine, B.S. Zweifel, T.W. Davis, J.L. Masferrer, Cyclooxygenase-2 inhibition with celecoxib enhances antitumor efficacy and reduces diarrhea side effect of CPT-11, Cancer Res. 62 (2002) 5778 LP–5784http://cancerres.aacrjournals.org/content/62/20/5778.abstract.
[371] A.S. Ghasemi, M.R. Taghartapeh, A. Soltani, P.J. Mahon, Adsorption behavior of metformin drug on boron nitride fullerenes: thermodynamics and DFT studies, J. Mol. Liq. 275 (2019) 955–967, https://doi.org/10.1016/j.molliq.2018.11.124.
[372] E. Shakerzadeh, Quantum chemical assessment of the adsorption behavior of fluorouracil as an anticancer drug on the B36 nanosheet, J. Mol. Liq. 240 (2017) 682–693, https://doi.org/10.1016/j.molliq.2017.05.128.
[373] C. Xiao, K. Ma, G. Cai, X. Zhang, E. Vessally, Borophene as an electronic sensor for metronidazole drug: a computational study, J. Mol. Graph. Model. 96 (2020), 107539, https://doi.org/10.1016/j.jmgm.2020.107539.
[374] C.D. Freeman, N.E. Klutman, K.C. Lamp, Metronidazole, Drugs 54 (1997) 679–708, https://doi.org/10.2165/00003495-199754050-00003.
[375] L.H. Bernstein, M.S. Frank, L.J. Brandt, S.J. Boley, Healing of perineal Crohn's disease with metronidazole, Gastroenterology 79 (1980) 357–365, https://doi.org/10.1016/0016-5085(80)90155-9.

[376] A. Bendesky, D. Menéndez, P. Ostrosky-Wegman, Is metronidazole carcinogenic? Mutat. Res. Mutat. Res. 511 (2002) 133–144, https://doi.org/10.1016/S1383-5742(02)00007-8.
[377] A. Rastgou, H. Soleymanabadi, A. Bodaghi, DNA sequencing by borophene nanosheet via an electronic response: a theoretical study, Microelectron. Eng. 169 (2017) 9–15, https://doi.org/10.1016/j.mee.2016.11.012.
[378] Z. Noroozi, R. Rahimi, M. Solimannejad, A computational study for the B30 bowl-like nanostructure as a possible candidate for drug delivery system for amantadine, Comput. Theor. Chem. 1129 (2018) 9–15, https://doi.org/10.1016/j.comptc.2018.02.016.
[379] R.S. Schwab, A.C. England Jr., D.C. Poskanzer, R.R. Young, Amantadine in the treatment of Parkinson's disease, JAMA. 208 (1969) 1168–1170, https://doi.org/10.1001/jama.1969.03160070046011.
[380] L.V. Metman, P. Del Dotto, P. van den Munckhof, J. Fang, M.M. Mouradian, T.N. Chase, Amantadine as treatment for dyskinesias and motor fluctuations in Parkinson's disease, Neurology 50 (1998) 1323 LP–1326, https://doi.org/10.1212/WNL.50.5.1323.
[381] R.J. Sugrue, G. Bahadur, M.C. Zambon, M. Hall-Smith, A.R. Douglas, A.J. Hay, Specific structural alteration of the influenza haemagglutinin by amantadine, EMBO J. 9 (1990) 3469–3476, https://doi.org/10.1002/j.1460-2075.1990.tb07555.x.
[382] R. Khorram, H. Raissi, A. Morsali, M. Shahabi, The computational study of the γ-Fe2O3 nanoparticle as Carmustine drug delivery system: DFT approach, J. Biomol. Struct. Dyn. 37 (2019) 454–464, https://doi.org/10.1080/07391102.2018.1429312.
[383] S. Onsori, E. Alipour, A theoretical investigation on the adsorption of platinol drug on a ZnO nanocluster: solvent and density functional effect, J. Mol. Liq. 256 (2018) 558–564, https://doi.org/10.1016/j.molliq.2018.02.041.
[384] I. Ravaei, M. Haghighat, S.M. Azami, A DFT, AIM and NBO study of isoniazid drug delivery by MgO nanocage, Appl. Surf. Sci. 469 (2019) 103–112, https://doi.org/10.1016/j.apsusc.2018.11.005.
[385] M. Rezaei-Sameti, S.K. Abdoli, The capability of the pristine and (Sc, Ti) doped Be12O12 nanocluster to detect and adsorb of mercaptopyridine molecule: a first principle study, J. Mol. Struct. 1205 (2020), 127593, https://doi.org/10.1016/j.molstruc.2019.127593.
[386] P.S. Maddahi, N. Shahtahmassebi, M. Rezaee Roknabadi, F. Moosavi, Exploring the sensitivity of ZnO nanotubes to tyrosine nitration: ADFT approach, Phys. Lett. A 380 (2016) 2090–2097.
[387] M. Rezaei-Sameti, F. Moradi, Interaction of isoniazid drug with the pristine and Ni-doped of (4, 4) armchair GaNNTs: a first principle study, J. Incl. Phenom. Macrocycl. Chem. 88 (2017) 209–218, https://doi.org/10.1007/s10847-017-0720-x.
[388] S.A. Javarsineh, E. Vessally, A. Bekhradnia, A. Hosseinian, S. Ahmadi, A computational study on the purinethol drug adsorption on the AlN nanocone and nanocluster, J. Clust. Sci. 29 (2018) 767–775, https://doi.org/10.1007/s10876-018-1381-7.
[389] A. Hosseinian, E. Vessally, A. Bekhradnia, K. Nejati, G. Rahimpour, Benzoylethanamine drug interaction with the AlN nanosheet, nanotube and nanocage: density functional theory studies, Thin Solid Films 640 (2017) 93–98, https://doi.org/10.1016/j.tsf.2017.08.049.
[390] R. Moghadami, E. Vessally, M. Babazadeh, M. Es'haghi, A. Bekhradnia, Electronic and work function-based sensors for acetylsalicylic acid based on the AlN and BN nanoclusters: DFT studies, J. Clust. Sci. 30 (2019) 151–159, https://doi.org/10.1007/s10876-018-1466-3.
[391] R. Padash, A. Sobhani-Nasab, M. Rahimi-Nasrabadi, M. Mirmotahari, H. Ehrlich, A.S. Rad, M. Peyravi, Is it possible to use X12Y12 (X = Al, B, and Y = N, P) nanocages for drug-delivery systems? A DFT study on the adsorption property of 4-aminopyridine drug, Appl. Phys. A Mater. Sci. Process. 124 (2018) 582, https://doi.org/10.1007/s00339-018-1965-y.
[392] B. Khodashenas, M. Ardjmand, M.S. Baei, A.S. Rad, A.A. Khiyavi, Gelatin–gold nanoparticles as an ideal candidate for curcumin drug delivery: experimental and DFT studies, J. Inorg. Organomet. Polym. Mater. 29 (2019) 2186–2196, https://doi.org/10.1007/s10904-019-01178-0.
[393] L. Lennard, The clinical pharmacology of 6-mercaptopurine, Eur. J. Clin. Pharmacol. 43 (1992) 329–339, https://doi.org/10.1007/BF02220605.
[394] K. Geetha, T.N. Rekha, M. Umadevi, B.J.M. Rajkumar, G.V. Sathe, P. Vanelle, T. Terme, O. Khoumeri, DFT and SERS study of adsorption of 1,4-dimethoxy-2-nitro-3-methylanthracene-9,10-dione onto silver nanoparticles, Aust. J. Chem. 69 (2016) 76–84, https://doi.org/10.1071/CH15161.
[395] O. Khoumeri, M. Montana, T. Terme, P. Vanelle, First TDAE approach in quinonic series: synthesis of new 2-substituted 1,4-dimethoxy-9,10-anthraquinones, Tetrahedron 64 (2008) 11237–11242, https://doi.org/10.1016/j.tet.2008.09.046.
[396] M.B. Camarada, DFT investigation of the interaction of gold nanoclusters with poly (amidoamine) PAMAM G0 dendrimer, Chem. Phys. Lett. 654 (2016) 29–36, https://doi.org/10.1016/j.cplett.2016.05.007.
[397] D. Cortés-Arriagada, Phosphorene as a template material for physisorption of DNA/RNA nucleobases and resembling of base pairs: a cluster DFT study and comparisons with graphene, J. Phys. Chem. C 122 (2018) 4870–4880, https://doi.org/10.1021/acs.jpcc.7b11268.